REVERSE OSMOSIS TRANSPORT PHENOMENA IN THE PRESENCE OF STRONG SOLUTE-MEMBRANE AFFINITY

by

JAMES MORLEY DICKSON

Dissertation submitted to the Faculty of the
Virginia Polytechnic Institute and State University
in partial fulfillment of the requirements for the degree of
DOCTOR OF PHILOSOPHY
in
Chemical Engineering

APPROVED:

G.B. Wills, Chairman

D.R. Lloyd, Supervisor

G.H. Beyer

J.P. Wightman

H.M. McNair

April, 1985

Blacksburg, Virginia

REVERSE OSMOSIS TRANSPORT PHENOMENA IN THE PRESENCE OF STRONG SOLUTE-MEMBRANE AFFINITY

by

JAMES MORLEY DICKSON

(ABSTRACT)

The reverse osmosis performance of cellulose acetate membranes has been examined and analyzed for several aqueous systems where there is a strong attraction between the organic solute and the membrane material.

The systems investigated included the aromatic hydrocarbons benzene, toluene, and cumene in single-solute aqueous solutions. Six cellulose acetate membranes, modified by annealing at different temperatures, were studied.

Experiments were performed at four pressures (690, 1725, 3450, and 6900 kPa) and at several concentrations (in the range 5 to 260 ppm). The results were found to be markedly different than those observed in the absence of strong solute-membrane affinity. In particular, the solute-water separation decreased rather than increased with increasing pressure and the flux decreased with increasing concentration even though low concentrations, with low osmotic pressures, were studied. Qualitatively, the behavior was explained in terms of a porous membrane mechanism with both solute-membrane affinity and solute mobility varying as a function of solute position with respect to the membrane. The observed reduction in flux was expressed by an empirical equation as a function of concentration of solute in the boundary layer.

The experimental results were analyzed quantitatively by several transport models. The irreversible thermodynamics phenomenological transport, solution-diffusion imperfection and extended solution-diffusion relationships generated parameters that were inconsistent with the original formulations of the models. The irreversible thermodynamics Kedem-Spiegler model, solution-diffusion model, Kimura-Sourirajan analysis, and the three parameter finely-porous model were functionally unable to represent the data. Only the four parameter finely-porous model and the surface force-pore flow model were consistent with experimental results. From the finely-porous model the partition coefficient was found to be different on the high and low pressure sides of the membrane and this difference was a function of both pore size and solute. For the surface force-pore flow model, the agreement between the model and data was excellent. However, the surface force-pore flow model was considerably more difficult to use.

ACKNOWLEDGEMENTS

The research described in this dissertation has taken place over the past six years and over three university campuses. Therefore, many people and various funding agencies have had an influence on this project. I would like to thank all the people who have helped in this effort, in particular:

1. Dr. Sourirajan and Dr. Matsuura, who first introduced me to membranes and helped to develop my love for research.
2. Dr. Douglas Lloyd, my friend and research supervisor, who has guided me with patience and perspective throughout this project.
3. my friends and colleagues, and at Virginia Polytechnic Institute and State University, for their help and advice.
4. my friends and colleagues, and , and research technician at The University of Texas at Austin, for their help and advice.
5. and her staff in the Engineering Word Processing Centre, McMaster University, for typing this manuscript.
6. the various agencies that have supported this research, including: the American Institute of Chemical Engineering (Engineering Foundation grant RC-A-77-6E), the Office of Water Research and Technology (grant 14-34-0001-0522), the Natural Sciences and Engineering Research Council Canada for a post graduate scholarship, and the continuing support of NSERC (grant A5701).
7. last and certainly not least my wife for her technical help, emotional support and love.

Dedicated to the memory of my father.

TABLE OF CONTENTS

LIST OF TABLES

LIST OF TABLES IN APPENDICES

LIST OF FIGURES

Chapter 1

INTRODUCTION

This dissertation deals with mass transport across reverse osmosis membranes in the presence of strong solute-membrane affinity. In reverse osmosis, a feed solution is transported under pressure through a polymeric membrane. The rate at which individual solution components emerge in the permeate stream under specified operating conditions depends upon the morphology of the membrane and upon the nature and magnitude of interactions between solvent, solute, and membrane material. Either the solvent or the solute may exhibit strong affinity for the membrane. Depending on which affinity is greater, markedly different separation behavior may occur in the reverse osmosis process.

The specific systems studied were a series of three aromatic hydrocarbon solutes (benzene, toluene, and cumene) in single-solute aqueous solution with six cellulose acetate membranes with different flux and separation characteristics. The three aromatic hydrocarbon solutes exhibit strong affinity for cellulose acetate membranes due to various physicochemical characteristics, whereas the solvent, water, is less attracted to the surface of the membrane. These solutes represent a large number of organics which have industrial and environmental significance. Selection was based upon the range of nonpolar or dispersive character, solubility in water, and societal import. Cellulose acetate was chosen for the membrane material because its performance has been well characterized for many systems, and because many commercially available membranes are composed of this polymer.

Over the last 20 years, much effort has been spent in the investigation of the reverse osmosis membrane separation process as a practical unit operation in chemical engineering. One major result of these efforts was the emergence of several mathematical

models to describe transport in reverse osmosis membranes. Notwithstanding these efforts to understand and to apply reverse osmosis, the modelling of transport through reverse osmosis membranes is still controversial. Each of these models has been successful to some extent, even though the underlying premises of the models vary greatly. Agreement between data and each of these models has been demonstrated for inorganic solutes and many organic solutes in the absence of strong solute-membrane attraction. However, for organic solutes with strong solute-membrane attraction, the reverse osmosis behavior is significantly altered and no definitive model exists to describe this case. A primary goal of this research project was to evaluate the ability of existing models to describe the transport in the presence of strong solute-membrane affinity.

The difference in membrane performance between the case in which water-membrane affinity dominates and where solute-membrane affinity dominates are summarized below. In this work, separation is defined as:

$$f = \frac{m_{A1} - m_{A3}}{m_{A1}} \tag{1}$$

where m_{A1} and m_{A3} are the feed and permeate molalities, respectively. The case in which strong solvent-membrane affinity dominates includes most inorganic and many polar or ionized organic solutes with cellulose acetate membranes and the solvent water. These systems have been reported extensively in the literature (see for instance, (1)). Some general statements can be made concerning reverse osmosis transport:

1. Increasing the operating pressure usually increases separation.
2. The decrease in permeate flux with increasing feed concentration is due to the osmotic pressure effects.
3. Positive separation is observed.

However, when solute-membrane affinity dominates these statements do not hold true. Systems involving strong solute-membrane affinity (2) are characterized by:

1. Increasing the operating pressure tends to decrease separation.
2. The permeate flux is significantly less than the pure water permeation flux, even when osmotic pressure effects are negligible.
3. The separation may be positive, zero, or negative depending on the specific operating conditions.

Note that negative separation implies that the solute is enriched in the permeate stream.

The physicochemical criteria for the reverse osmosis separation of several classes of organic solutes in aqueous solutions using Loeb-Sourirajan type cellulose acetate membranes have been discussed extensively (1-3). Cellulose acetate membranes have both polar and nonpolar characteristics. The polar character of the membrane is attributed to the hydroxyl and ester groups present in the polymer, and the nonpolar character is due to the backbone carbon chain. Therefore, both the polar solvent (water) and nonpolar solute (hydrocarbon) can have affinity toward the membrane material. The relative affinity of the solute and solvent is important in determining the behavior of the system. The nonpolar or dispersive character of the aromatic hydrocarbon solute can be represented by Small's molar attraction constant (2,4). An increase in the dispersive character of a series of homologous compounds as indicated by an increase in the molar attraction constant results in an increase in the solute-membrane attractive forces. Values of the molar attraction constant and other data for the solutes under investigation are presented in Table 1.

Both a theoretical and an experimental approach to reverse osmosis transport are included in this study. A review of several existing transport models is presented with emphasis on the applicability of these models to systems involving strong solute-membrane

Table 1

Physicochemical Parameters for the Solutes Studied

	Benzene	Toluene	Cumene
Structure	C_6H_6	$C_6H_5-CH_3$	$C_6H_5-CH(CH_3)_2$
Molecular Mass, kg/kmol	78.11	92.15	120.20
Molar attraction constant[a], $(kJ\ m^3)^{1/2}/kmol$	53.4	61.4	77.1
Solubility in water[a], ppm	1780	515	50
Vapor Pressure[b], kPa	0.69	0.36	0.03
TLV[c], ppm of vapor in air	10	200	50
Molal Volume at the normal boiling point[d], $m^3/kmol$	0.0960	0.118	0.163
Partial Molar Volume[e], $m^3/kmol$	0.0889	0.106	0.140
Diffusivity in Water[f], m^2/s, x 10^9	1.096	0.968	0.799
Solute radius[g], m, x 10^{10}	2.23	2.53	3.06

a as reported in reference (2) at 25°C.
b as reported in reference (5) at 20°C.
c Threshold Limit Values (TLV) as reported in reference (5).
d as estimated by the method of LeBas (6).
e estimated from pure solute density as suggested by reference (7).
f estimated by the method of Wilke-Chang (8).
g calculated based on the Stokes-Einstein equation.

affinity. Papers in which authors have included solutes that exhibit strong solute-membrane attraction are discussed. The experimental data are presented and discussed. These data are correlated by a number of the available models and the results are interpreted based on the physical significance of the parameters generated. Finally, conclusions and recommendations for further study, based on the presented results, are made.

1.1 Historical Background

The purpose of this section is to provide the reader with some historical perspective on reverse osmosis systems involving strong solute-membrane attraction. Included are references in which data have been collected and interpreted qualitatively for these systems. A review of the work done on quantitative modelling of these systems is presented in the Theoretical Background section.

The first experimental evidence of unusual reverse osmosis behavior due to strong solute-membrane affinity was observed by Blunk (9) and by Keilin (10). Their results inspired Lonsdale et al. (7) to investigate the behavior of the phenol-water-cellulose acetate system in more detail. Lonsdale et al. (7) observed negative separation for phenol and noted that separation decreased with increasing pressure. These results are characteristic of systems with strong solute-membrane affinity. Equilibrium sorption and unsteady state diffusion experiments were conducted to determine the partition coefficient and the diffusion coefficient for phenol in the membrane material. The partition coefficient was large, 42 (kg phenol/m^3 cellulose acetate)/(kg phenol/m^3 solution), compared to 0.03 for sodium chloride. The diffusion coefficients for phenol and sodium chloride were both about 9.6×10^{-14} m^2/s. Subsequent work by Lonsdale and coworkers (7,11,12) confirmed the earlier results for phenol and attempted to analyze the data in terms of the solution-diffusion model and a frictional model. The negative separation of phenol was attributed to the large partition coefficient and

to "flow coupling" (in which the solute and solvent transport are linked rather than independent, as is usually assumed).

The separation of phenol-water solutions has dominated the literature on systems involving strong solute-membrane affinity, probably because this was the first system studied and because phenol-water separation is environmentally important. The early work by Lonsdale and coworkers has been repeated and re-analyzed by several authors including Matsuura and Sourirajan (13-15), Pusch and coworkers (16,17), Tone et al. (86, 87), and others (18-20). The qualitative features of the phenol-water-cellulose acetate system were similar in all these papers. Several of these authors also noted that the flux was reduced for their membranes in the presence of phenol compared to pure water flux. This effect is the same as the flux reduction effect mentioned above and is characteristic of systems with strong solute-membrane affinity. Notwithstanding the similarities in the data, interpretation of results was often different. Lonsdale and coworkers (7,12) favored a solution-diffusion approach, while Matsuura and Sourirajan (2,13,14) used a pore flow model with surface forces acting on the solute and solvent. Pusch and coworkers used the original (16) and a modified version of the solution-diffusion model, as well as irreversible thermodynamics (17) to describe their data. These models are discussed in more detail in the next section.

It was soon found that these results were not unique to the phenol-water-cellulose acetate system. Phenol derivatives, such as chlorophenols and nitrophenols, also exhibited strong affinity for cellulose acetate membranes (11,13,14,18,21). Although negative separation was usually observed, for some experimental conditions positive separations were reported (13,21). Hydrocarbon solutes, such as benzene and hexene, were also found to have strong affinity for the membrane material (2). For the hydrocarbon solutes, positive separations (2,22) were usually observed, but under certain experimental conditions, negative separations (23,24) occurred. Therefore, it became evident that strong solute-

membrane affinity was not restricted to phenol, or to cellulose acetate membranes, and positive, zero, or negative separation could be effected by experimental conditions.

The existence of solute-membrane attraction was also observed for other membrane materials. In particular for phenols and substituted phenols the characteristic behavior of strong solute-membrane affinity was found for aromatic polyamide (19,25), cellulose acetate butyrate, and North Star (NS-100) membranes (19,26). The NS-100 membrane is a polyethylenimine coated on a polysulfone support and cross-linked with toluene 2,4-diisocyanate. For a given solute and solvent, the strength and direction of the solute-membrane interaction is a function of the membrane material used. One example is the separation of p-chlorophenol-water with modified NS-100 membranes. The modified membrane (fabricated with twice the normal amount of cross-linking agent) exhibited an increase in p-chlorophenol-water separation with increasing pressure (26). But, for the unmodified NS-100 membrane it was observed that the p-chlorophenol-water separation decreased with increasing pressure (19). In this case, for the modified membrane the solvent-membrane attraction dominates and for the unmodified membrane the solute-membrane attraction dominates. Of course, doubling the amount of cross-linking agent changes the physical structure as well as the chemical nature of the membrane. However, it is primarily the chemical nature that determines the direction of change in separation as a function of increasing operating pressure. This example illustrates that even a relatively small change in membrane character can result in a large change in the nature of the solute-solvent-membrane interactions.

That the observed behavior for the phenol-water-cellulose acetate system is a result of the strong solute-membrane affinity is evidenced by the following experiment. When the pH of the solution is increased, phenol dissociates to a phenoxide anion. Experimental results (14,18) indicate that the phenol-water separation increases directly as

the degree of dissociation for phenol increases. Apparently, the phenoxide ion is repelled by the membrane. Therefore, it is only the neutral phenol molecule which experiences a strong attraction to the membrane material.

Strong solute-membrane attraction effects are important for many solutes and membrane materials. The strength of the interaction between solute and the membrane are important in determining the overall reverse osmosis performance. The application of these principles to the data in the literature for a number of quantitative transport models is discussed in the next section.

1.2 Theoretical Background

A number of models have been developed over the years to describe reverse osmosis transport. In most cases, these models have been developed to describe the transport of solvent and solute where the solute (usually NaCl) is repelled by the membrane material. Several papers published recently have reviewed these different models and have discussed the ability of these models to describe the transport for various inorganic and organic solutes (17,20,27,28). The following review focuses on how several of these models apply to solute systems involving strong solute-membrane attraction. The discussion will include a brief description of the basis, physical significance, and assumptions of each model as well as the final form of the equations. Instances where systems involving strong solute-membrane attraction have been modelled are reviewed.

1.2.1 General Considerations

Before the transport models are discussed, some general aspects of membrane transport will be discussed that are often considered to be independent of the particular membrane model under consideration.

Concentration Polarization. When solute is rejected by the membrane, the solute concentration near the membrane surface increases. The build-up in concentration in this boundary layer region is referred to as concentration polarization. In order to describe this concentration polarization, the film theory (29) is used. At steady state, the flux of solute to the membrane, $(C_A/C)(N_A + N_B)$, the flux of solute through the membrane, N_A, and the solute back diffusion, $-D_{AB}\,dC_A/dx$, are balanced as illustrated in Figure 1. Mathematically:

$$N_A = -D_{AB}\frac{dC_A}{dx} + \frac{C_A}{C}(N_A + N_B) \tag{2}$$

which is a form of Fick's first law (29). All symbols are defined in the NOMENCLATURE section. Solving this equation with appropriate boundary conditions (30b, 31) gives:

$$C_{A2} = C_{A3} + (C_{A1} - C_{A3})\exp(n_T/k\,C\,M_B) \tag{3}$$

where n_T is the mass flux through the membrane, and C_{A1}, C_{A2}, and C_{A3} are the feed, boundary layer, and permeate concentrations, respectively. As the mixing on the high pressure side of the membrane is increased, the mass transfer coefficient, k, increases and Equation (3) predicts that concentration polarization will decrease (C_{A2} decreases).

The mass transfer coefficient is a function of feed flow rate, cell geometry, and solute system. At fixed feed flow rate and cell geometry, k varies as a function of the diffusivity of the solute (32):

$$k \propto D_{AB}^{2/3} \tag{4}$$

That k varies as the 2/3 power of diffusivity comes from generalized correlations of mass transfer which have been proposed by several authors (30b,31-34). Equation (4) implies that $k/D_{AB}^{2/3}$ is a constant. Writing Equation (4) for a reference solute at the same experimental conditions and taking the ratio of the equations gives:

$$k = k_{ref}(D_{AB}/D_{AB,ref})^{2/3} \tag{5}$$

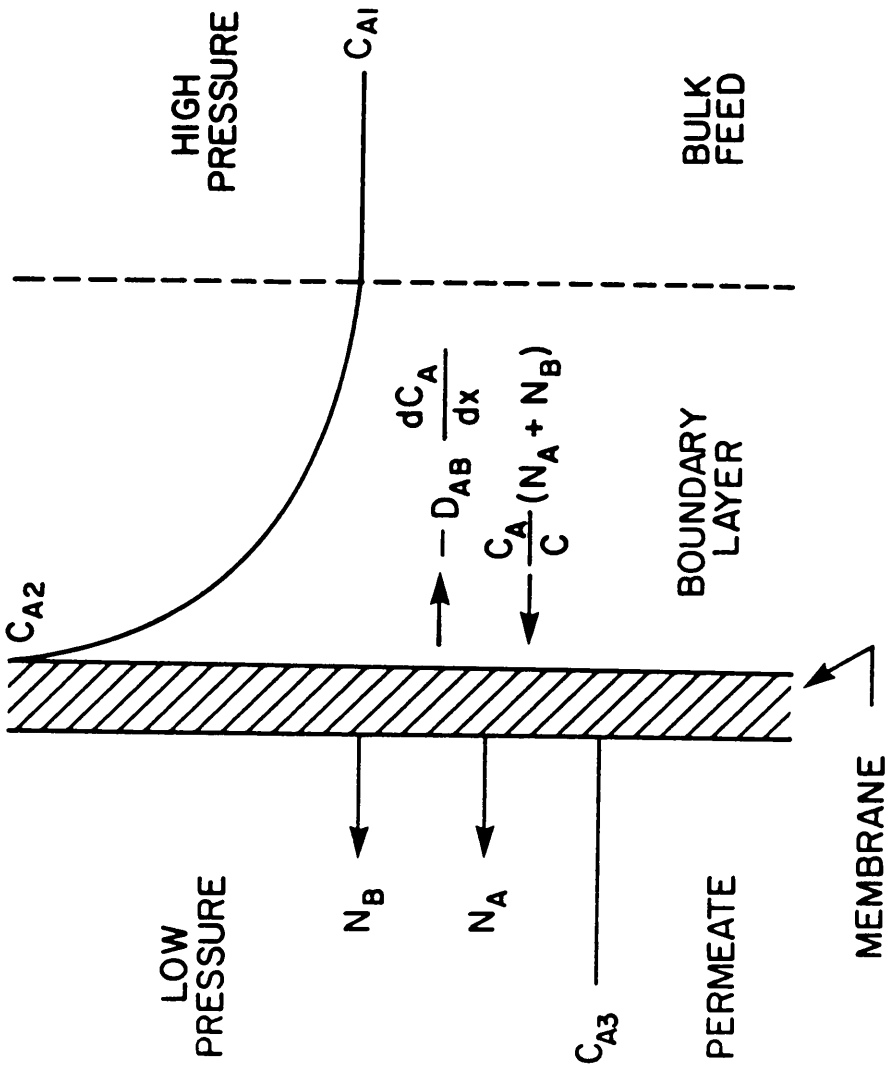

Figure 1. Concentration polarization at the high pressure surface of a reverse osmosis membrane.

If k is known for a reference solute, then k for any other solute can be estimated using Equation (5) if the diffusivities of the solute and reference solute are known.

Other approaches have been used to describe the concentration polarization layer more accurately (see for instance, (35)). However, for most practical purposes, Equation (3) is sufficiently accurate. For each of the models presented below, the original reference should be checked to determine how the authors modelled concentration polarization.

Definition of Separation. Separation, f, was defined above in terms of the feed and permeate molal concentrations, m_{A1} and m_{A3}, respectively:

$$f = (m_{A1} - m_{A3})/m_{A1} \tag{1}$$

For moderately dilute solutions, the molal concentration, m_{Ai}, can be approximated by the molar concentration, C_{Ai}, and Equation (1) can be rewritten as:

$$f = (C_{A1} - C_{A3})/C_{A1} \tag{6}$$

Alternatively, separation can be defined in terms of the concentration of the boundary solution near the membrane surface, C_{A2}, as calculated by Equation (3). The separation based on the boundary layer concentration, f', can be written as:

$$f' = (C_{A2} - C_{A3})/C_{A2} \tag{7}$$

The separation calculated in this manner represents the separation that would be measured with no concentration polarization (that is, $C_{A1} = C_{A2}$, and k = infinite). Some authors choose to ignore the difference between f and f' by claiming that if the mixing is sufficiently thorough, the boundary layer concentration will approach the bulk concentration. This may not be the case in large scale systems or even in many laboratory scale apparatus.

In reverse osmosis single-solute systems, the concentration of the solute in the permeate is related to the solvent and the solute fluxes by a simple material balance as:

$$X_{A3} = \frac{N_A}{N_A + N_B} \tag{8}$$

At moderately low concentrations, where $N_B >> N_A$ and the difference between molal and molar concentration may be ignored ($C_{Ai} = m_{Ai}$), Equations (7) and (8) can be combined to give:

$$f' = 1 - \frac{N_A}{C_{A2} J_v} = 1 - \frac{C N_A}{C_{A2} N_B} \tag{9}$$

where C is the molar density of water and J_v is the solvent volume flux. Equation (9) is used frequently in the derivation of the models discussed below

Osmotic Pressure Effects. When an ideal semi-permeable membrane (one that is permeable to solvent but not solute) is placed between two compartments, one containing pure solvent and the other containing a solution (solvent plus solute), the solvent will pass through the membrane to the solution side. This phenomenon is called osmosis. Transport occurs due to the chemical potential driving force which is caused by the presence of the solute. The exact pressure that must be applied to the solution side to stop the solvent flux is called the osmotic pressure. In reverse osmosis, a pressure greater than the osmotic pressure is applied to the solution to reverse the flow and drive solvent from the solution side to the pure solvent side; hence, the name reverse osmosis. To model the flux through a membrane, the influence of the osmotic pressure driving force must be considered. For a real membrane, some solute exists in the permeate and therefore the osmotic pressure of the solution on each side of the membrane must be considered. An effective pressure driving force across the membrane can be defined as the applied pressure difference minus the osmotic pressure difference. For most models, the water flux is considered to be proportional to the effective pressure driving force.

The manner in which each of the models to be discussed below handles the effect of osmotic pressure contributions varies. Each section briefly discusses the method used in that

particular model. Usually these equations take on the form shown here (written for volume flux, J_v, and for molar flux of solvent, N_B) so that the flux is directly proportional to the effective pressure driving force:

$$J_v = \ell_p (\Delta P - \Delta \pi) \tag{10}$$

$$N_B = A(\Delta P - \Delta \pi) \tag{11}$$

where ℓ_p and A are the appropriate proportionality constants. For the systems reported in this dissertation, the concentrations being considered are sufficiently low that osmotic pressure contributions are usually considered to be negligible.

For dilute systems, the osmotic pressure of a solution can be estimated by the van't Hoff equation (36) as:

$$\pi_i = C_{Ai} RT \tag{12}$$

Therefore, the osmotic pressure difference, $\Delta\pi$, across a membrane is related linearly to the concentration difference, $C_{A2} - C_{A3}$.

Membrane Structure. In order to facilitate the description of the various membrane models, a brief discussion of membrane structure is included here. The inquiry into the exact relationship between membrane structure and performance is an on-going concern (see for instance references (88, 89)) and the present discussion is limited to some of what is known about cellulose acetate membranes. The asymmetry of the membrane, the nature of the skin layer, and the influence of an annealing treatment are discussed.

The success of the reverse osmosis process is due in part to the development of the asymmetric membrane. An asymmetric membrane has a relatively dense surface layer supported by a porous layer underneath. Such a structure greatly reduces the resistance to flow through the membrane compared to a homogeneous dense membrane of the same overall thickness. For cellulose acetate membranes, such as those used in this study, the asymmetric

structure is a direct consequence of the casting procedure used. When a polymer solution is cast on a flat surface, the evaporation of the solvent produces a surface skin. Subsequent gelation in cold water fixes the structure; the porous substructure is formed by the replacement of solvent by the nonsolvent water. Scanning electron microscope examination of membranes made in this manner (37) indicates that three layers exist: a relatively dense surface skin, a transition layer, and an open porous support layer. The transition layer is intermediate in both density and position with respect to the other two layers. Most of the resistance to mass transfer through the membrane exists in the surface skin. Therefore, it may be assumed that the performance of the membrane is dependent primarily on the chemical nature, thickness, and structure of the surface skin.

For the skin layer, the basic question is whether it is porous. Membranes with pores sufficiently large that they can be seen with a scanning electron microscope are usually considered to be ultrafiltration membranes. These membranes are clearly porous. As the pore size becomes progressively smaller, there is no clear point at which the pores disappear. One possible definition of this point would be when the pore volume fraction becomes equivalent to the free volume of the polymer. This point is difficult to determine with a water-swollen polymer. The degree of crystallinity, for instance, will change the free volume. At what point does a void space in the polymer structure become a pore? With the technology available today, the existence of pores in the membranes such as those used in this study cannot be tested. Therefore, mechanism-independent models, nonporous models, and porous models have been included in the analysis of the data in this dissertation.

The performance of reverse osmosis membranes can be influenced by a thermal pretreatment (30a, 37). This annealing or shrinking step involves exposing the wet membrane to an elevated temperature for a short period of time (approximately 10 minutes), after which the membrane is cooled rapidly back to room temperature. Annealing has been

found to be effective at modifying the membrane performance, particularly for cellulose acetate membranes. The sodium chloride-water separation can be increased from less than 50% to more than 99%, with a corresponding decrease in permeate flux. Separation increases with increasing annealing temperature. Temperatures are typically in the range 60°C – 90°C. It is agreed generally that elevated temperatures increase the kinetic energy of the polymer molecules, allowing a rearrangement in the membrane structure to take place (37). The nature of the change depends on whether the membrane is considered to be nonporous or porous. If the membrane is nonporous, then the annealing step is a way of reducing any imperfections that may exist in the surface layer. In addition, the degree of cyrstallinity is increased, leading to relatively smaller amorphous regions through which transport can take place. Alternatively, if the membrane is porous, the annealing procedure shrinks the existing pores to a smaller size. It is not known which of these mechanisms is correct. However, annealing membranes at different temperatures does provide a convenient method for generating a series of membranes with gradated properties.

Membrane Pore Size. If the membranes are assumed porous, then it is desirable to have a measure of the pore size. Since, as discussed above, the pores cannot be seen, there is no direct way of measuring the size. An alternative is to use some relative measure of pore size based on experimental data. One such method has been suggested by Sourirajan and coworkers (38). They found that data for several single solute-water-cellulose acetate membranes, when water-membrane affinity dominates, could be correlated by the following equation:

$$\ln(D_{AM}K/\tau) = \ln C^{*}_{NaCl} + \Sigma(-\Delta\Delta G/RT)_i \qquad (13)$$

where $(D_{AM}K/\tau)$ is the solute transport parameter (discussed below), and $\Delta\Delta G$ is the free energy required to bring a solute molecule from free solution to the membrane surface. Free energy parameters, $(-\Delta\Delta G/RT)_i$, for various ions have been tabulated elsewhere (38). The

remaining term is interpreted as a membrane pore size parameter, $\ln C^*_{NaCl}$, which is constant for a given membrane sample. Substituting the known values of $(-\Delta\Delta G/RT)_i$ for the reference solute sodium chloride, Equation (13) may be rearranged as:

$$\ln C^*_{NaCl} = \ln(D_{AM}K/\tau \text{ cm/s}) - 1.37 \tag{14}$$

where $(D_{AM}K/\tau)$ must be in cgs units, to be consistent with the original paper, rather than in the SI units used in the rest of this dissertation.

The value of $\ln C^*_{NaCl}$ calculated by Equation (14) is a relative measure of the membrane pore size, based on experimental data for sodium chloride-water separation. As pore size increases, $\ln C^*_{NaCl}$ increases. This approach is consistent with other work published previously (3,21-24).

Membrane Compaction. Theoretically, when pressure is increased the pure water permeation flux increases proportionally. This behavior is predicted by Equation (11) (or equivalently by Equation (10)) for pure water in which case $\Delta\pi = 0$ and $N_B = A\,\Delta P$. However, at higher pressures the flux will usually be less than that prediced by Equation (10). The difference is attributed to compaction of the asymmetric membrane. One possible explanation of this phenomenon is as follows. The asymmetric membrane consists of three layers (a surface skin, a transition layer and a porous support) as discussed above. The primary resistance to flow is in the surface skin. When the operating pressure is increased the membrane is compressed by this force. The result is that some of the transition layer may be effectively incorporated into the dense surface skin. Therefore, the resistance to permeation is increased with increasing pressure as progressively more of the transition layer resistance is included in the overall membrane resistance. It is convenient to represent this compaction effect as a pressure dependence of the pure water permeability coefficient, A, by the empirical equation (30b):

$$A = A_0 \exp[-\gamma\,\Delta P] \tag{15}$$

Equation (15) suggests a linear relationship between A and ΔP on a semilog coordinate system.

1.2.2 Phenomenological Transport Models

In this section, models which are independent of the mechanism of transport will be discussed. These models are called phenomenological transport models and are based on the theory of irreversible thermodynamics.

Irreversible Thermodynamics Phenomenological Transport Relationship. In the absence of any knowledge of the mechanism of transport or the nature of the membrane structure, it is possible to apply the theory of irreversible thermodynamics (IT) to membrane systems (39). In IT, the membrane is treated as a "black box". Models stating the relationship between forces acting on the system and the flux of material through the membrane are formulated. For systems that are not far from equilibrium, IT suggests reasonable choices for forces and fluxes. The phenomenological relationships are manageable ways of expressing the relationships between the observed fluxes and the applied forces. Onsager (40) suggested that the fluxes and forces could be expressed by the following linear equations:

$$J_i = L_{ii} F_i + \sum_{j \neq i} L_{ij} F_j \quad \text{for } i = 1, \ldots, n \tag{16}$$

where the fluxes, J_i, are related to the forces, F_j, by the phenomenological coefficients, L_{ij}.

For membrane systems, the driving forces can be related to the pressure and concentration differences across the membrane, and the fluxes are solvent and solute permeate fluxes. This equation can be simplified by assuming that cross coefficients are equal, as first proposed by Onsager (40):

$$L_{ij} = L_{ji} \quad \text{for} \quad i \neq j \tag{17}$$

The above Onsager reciprocal relationship is valid when the system is close to equilibrium, the linear laws (Equation (16)) are valid, and the correct choice of fluxes and forces has been made. For systems that are far from equilibrium, as is often the case in reverse osmosis, Equation (17) may not be correct. The validity of the Onsager reciprocal relations has been discussed by Soltanieh and Gill (28).

Kedem and Katchalsky (39) used Equations (16) and (17) to derive what are known as the phenomenological transport equations (IT – PT):

$$J_v = \ell_p(\Delta P - \sigma\Delta\pi) \tag{18}$$

$$N_A = \omega\Delta\pi + (1 - \sigma)(C_{AM})_{ln} J_v \tag{19}$$

where the adjustable parameters ℓ_p, ω, and σ are simple functions of the original phenomenological coefficients, L_{ij}. $(C_{AM})_{ln}$ is the logarithmic mean solute concentration in the membrane. Equation (18) is similar to Equation (10) with the addition of the reflection coefficient, σ, as originally proposed by Staverman (41). Pusch (42) has shown that Equation (19) can be rewritten to relate separation, f', and flux, J_v, as:

$$\frac{1}{f'} = \frac{1}{\sigma} + \left(\frac{\ell_\pi}{\ell_p} - \sigma^2\right)(\ell_p/\sigma)\pi_2\left(\frac{1}{J_v}\right) \tag{20}$$

The above equation predicts a linear relationship between $1/f'$ and $1/J_v$. The osmotic permeability, ℓ_π, is related to ω as:

$$\omega = (\ell_\pi/\ell_p - \sigma^2)(C_{AM})_{ln}\,\ell_p \tag{21}$$

The parameters in the model are the solvent and osmotic permeabilities, ℓ_p and ℓ_π, and the reflection coefficient, σ. These parameters can be determined for a given solute and membrane by applying Equations (18) and (20) simultaneously using data collected at several different pressures and concentrations.

Jonsson (20) and Burghoff et al. (17) found this treatment to be satisfactory for describing the data for phenol-water separation for cellulose acetate membranes. These results seem promising; however, there are limitations. First, Equation (20) is only applicable when the linear laws apply across the whole membrane. For reverse osmosis systems, the concentration differences across the membrane are often large enough that the linear laws are not valid. As a result the L_{ij} coefficients will be concentration dependent to various extents (40). However, for many systems, the coefficients ℓ_p, σ, and ω are nearly constant provided that the concentration changes are not too great. This assumption is relaxed in the Kedem-Spiegler relationship, to be discussed next. Second, by considering the membrane as a "black box", the resulting analysis does not give any insight into the transport mechanism.

Irreversible Thermodynamics - Kedem Spiegler Relationship. One critical assumption in the IT – PT relationship is that the linear laws were assumed to apply over the whole thickness of the membrane. Spiegler and Kedem (43) resolved the problem by rewriting the original linear IT equations in differential form and then integrating them over the thickness of the membrane. The equations in differential form for the solvent and solute flux, respectively are:

$$J_v = p_B \left(\frac{dP}{dx} - \sigma \frac{d\pi}{dx}\right) \tag{22}$$

$$N_A = p_A \frac{d C_{AM}}{dx} + (1 - \sigma) C_{AM} J_v \tag{23}$$

where p_A is the solute permeability, p_B is the water permeability, and x is the coordinate direction perpendicular to the membrane.

If p_A, p_B, and σ are constant, Equation (22) can be integrated to give Equation (24) below and Equation (23) can be integrated and combined with Equation (9) to give (28,43) Equation (25):

$$J_v = (p_B/\Delta x)(\Delta p - \sigma \Delta \pi) \tag{24}$$

$$\frac{1}{f'} = \frac{1 - \sigma \exp[-(1-\sigma)(\Delta x/p_A) J_v]}{\sigma\{1 - \exp[-(1-\sigma)(\Delta x/p_A) J_v]\}} \tag{25}$$

where Δx is the membrane thickness. The result is a three-parameter model described by Equations (24) and (25), similar to the IT – PT relationship but which should have coefficients that are independent of concentration and pressure. The three parameters in the Kedem-Spiegler relationship (IT – KS) are $p_B/\Delta x$, $p_A/\Delta x$, and σ.

Similar to the IT – PT relationship, the IT – KS model was found by Burghoff et al. (17) and Jonsson (20) to describe negative separation for phenol-water-cellulose acetate systems. Again, this approach lends no insight into the mechanism of membrane transport.

1.2.3 Nonporous Membrane Transport Models

In this section, models in which it is specifically assumed that the membrane is nonporous are described. First, the solution-diffusion model and then two modifications of the solution-diffusion model are presented.

Solution-Diffusion Relationship. The solution-diffusion (SD) model was originally applied to reverse osmosis by Merten and coworkers (44,45). The membrane surface layer is considered to be homogeneous and nonporous. Transport of both solvent and solute occurs by the molecules dissolving in the membrane phase and then diffusing through the membrane. The permeability of a species is equal to the product of the solubility and the diffusivity for that species. Theoretically, the solubility and the diffusivity of the solute can be determined for a

membrane material by performing equilibrium sorption and unsteady state sorption/desorption studies, respectively. The water flux is proportional to the solvent chemical potential difference (usually expressed as the effective pressure difference across the membrane), and the solute flux is proportional to the solute chemical potential difference (usually given as the solute concentration difference across the membrane). The solvent and solute fluxes, respecitvely are:

$$J_v = \frac{D_{BM} C_{BM} V_B}{RT \Delta x} (\Delta P - \Delta \pi) \tag{26}$$

$$N_A = \frac{D_{AM} K}{\Delta x} (C_{A2} - C_{A3}) \tag{27}$$

Note that Equation (26) is identical to Equation (10), except that ℓ_p has been replaced by more physically meaningful terms. D_{AM} and D_{BM} are the diffusivities of the solute and the solvent in the membrane, respectively; C_{BM} is the membrane water content; V_B is the partial molar volume of water; R is the universal gas constant; T is the temperature; Δx is the actual thickness of the membrane skin; and K is the partition coefficient defined as follows:

$$K = \frac{\text{kg solute/m}^3 \text{ membrane}}{\text{kg solute/m}^3 \text{ solution}} \tag{28}$$

K is a measure of the relative solute affinity to ($K > 1.0$) or repulsion from ($K < 1.0$) the membrane material.

As illustrated by Pusch (42), Equations (26) and (27) may be combined with Equation (9) and rearranged to give:

$$\frac{1}{f'} = 1 + \frac{D_{AM} K}{\Delta x} \left(\frac{1}{J_v} \right) \tag{29}$$

Equation (29) predicts a linear relationship between $1/f'$ and $1/J_v$. Equations (26) and (29) can be fit to experimental data to generate the two parameters ($D_{BM} C_{BM} V_B/RT \Delta x$)

and ($D_{AM}K/\Delta x$), both of which are treated as single quantities. In order to resolve either of these terms into its component parts, it is necessary to have an independent measure of some of the terms (see for example reference (16) on how to measure D_{AM}, D_{BM}, and K, separately).

One restriction of the SD model is that the separation obtained at infinite flux is always equal to 1.0. However, this limit is not reached for many organic solutes; in particular, the model is not applicable to negative separation cases. Also, for negative separation, Equation (29) produces a negative value for (D_{AM} $K/\Delta x$), which is physically impossible, since none of the quantities in (D_{AM} $K/\Delta x$) can be negative. For these reasons, the SD model is inappropriate for systems involving strong solute-membrane attraction.

Two attempts to improve on this original model are the solution-diffusion imperfection model (SDI) and the extended solution-diffusion model (ESD).

Solution-Diffusion Imperfection Relationship. The solution-diffusion imperfection model (SDI), derived by Sherwood et al. (46), allows for small imperfections which can exist in the membrane surface. It was assumed that imperfections will transport solution from the boundary layer (C_{A2}) to the permeate side, without any change in concentration. Therefore, an additional term to both solvent and solute fluxes, that is proportional to the pressure driving force appears in the model as follows:

$$J_v = \kappa' (\Delta P - \Delta \pi) + \kappa''' \Delta P \tag{30}$$

$$N_A = \kappa'' \Delta \pi + \kappa''' \Delta P C_{A2} \tag{31}$$

As illustrated by Jonsson and Boesen (34), Equations (9), (30), and (31) can be rearranged to give:

$$\frac{1}{1-f'} = \frac{(\Delta P - \Delta\pi) + (\kappa'''/\kappa')\,\Delta P}{(\kappa''/\kappa')(\Delta\pi/C_{A2}) + (\kappa'''/\kappa')\,\Delta P} \tag{32}$$

For the particular case when $\Delta P >> \Delta\pi$ and solutions are dilute, then Equation (32) can be rearranged as:

$$\frac{1}{f'} = 1 + \frac{\kappa'''}{\kappa'} + \frac{\kappa''}{\kappa'}\left(\frac{RT}{\Delta P}\right) \tag{33}$$

which suggests a linear relationship between $1/f'$ and $1/\Delta P$. The derivation of Equation (33) from Equation (32) is presented in Appendix A. The SDI model has three adjustable parameters, κ', κ'', and κ'''. The κ' and κ'' are the transport parameters for diffusive water flux and diffusive solute flux, respectively. The κ''' transport parameter is for pore flow. Therefore, the ratio of κ''' to κ' is a measure of the relative contribution of pore flow compared to diffusive flow. The κ'' value is proportional to the product of the solute diffusivity in the membrane phase and the solute partition coefficient. Jonsson (20) found that this model failed in the negative separation region, which implies that the SDI model is not appropriate for handling the case of strong solute-membrane attraction.

Extended Solution-Diffusion Relationship. Burghoff et al. (17) and Jonsson (27) pointed out that in the original SD model, a pressure term in the solute chemical potential equation was neglected. The complete expression for chemical potential, including the pressure term is:

$$\Delta\mu_A = RT\ln(C_{A2}/C_{A3}) + V_A\,\Delta P \tag{34}$$

where $\Delta\mu_A$ is the solute chemical potential difference across the membrane and V_A is the solute partial molar volume. In general, to neglect the pressure term, $\ln(C_{A2}/C_{A3})$ must be significantly greater than $V_A\,\Delta P/RT$. For sodium chloride-water separation (where $V_A \simeq 0.02\ m^3/kmol$), as long as $\ln(C_{A2}/C_{A3}) >> 8.0 \times 10^{-6}\,\Delta P$ (with P in kPa), it is

acceptable to ignore the pressure term (17). For organic-water systems that exhibit lower separation, and for higher operating pressures, it is important to include the pressure term in the analysis.

Including the pressure term in the analysis leads to the following equation (17):

$$N_A = \frac{D_{AM}K}{\Delta x}(C_{A2} - C_{A3}) + \ell_{AP}\Delta P \tag{35}$$

where ℓ_{AP} is the pressure induced solute transport parameter. Equations (9), (10), and (35) can be combined (17) to give:

$$\frac{1}{f'}\{1 - \frac{\ell_{AP}}{C_{A2}\ell_p}\left(\frac{\Delta P}{\Delta P - \Delta\pi}\right)\} = 1 + \frac{D_{AM}K}{\Delta x}\left(\frac{1}{J_v}\right) \tag{36}$$

For the special case $\Delta P >> \Delta\pi$ then:

$$\frac{1}{f'} = \frac{1}{(1 - \ell_{AP}/C_{A2}\ell_p)} + \left(\frac{D_{AM}K}{\Delta x}\right)\frac{1}{(1-\ell_{AP}/C_{A2}\ell_p)}\left(\frac{1}{J_v}\right) \tag{37}$$

The three parameters in the model are ℓ_p, $(D_{AM}\,K/\Delta x)$, and ℓ_{AP}. Again, a linear relationship is predicted between $1/f'$ and $1/J_v$. Alternately, $1/(1-\ell_{AP}/C_{A2}\ell_p)$ may be used as a grouped parameter which may or may not be less dependent on the operating pressure and concentration. Burghoff et al. (17) found good agreement between the ESD model and the observed negative separation for phenol with cellulose acetate membranes. For this case, negative separation is attributed to a large pressure contribution to the flux of solute.

1.2.4 Porous Membrane Transport Models

In this section, transport models in which it is specifically assumed that the membrane is porous are presented.

Preferential Sorption-Capillary Flow Model. The preferential sorption-capillary flow model (PS-CF) was first proposed by Sourirajan (47). According to this model, the membrane surface is microporous. In addition to the number and size of pores, the membrane performance

depends on the chemical nature of the solute, solvent, and membrane material. In many applications, solvent-membrane attraction dominates; this situation is called water preferential sorption. A layer of almost pure water which exists at the membrane solution interface is continuously withdrawn through the membrane pores under the pressure driving force. The solute (for example, sodium chloride) is preferentially repelled. Only pores that have diameters larger than twice the thickness of the sorbed water layer allow solute to pass. On the other hand, for some solutes the solute-membrane attraction dominates over the water-membrane attraction. In this case it is possible to have preferential transport of the solute, leading to negative separation. Whether water-membrane or solute-membrane affinity dominates, the basic premise of the PS-CF model is that membrane performance can be described in terms of the number and size of pores and the physicochemical interactions between solute, solvent, and membrane.

The model provides a qualitative description of the reverse osmosis process. To be useful, the model must be translated into a quantitative transport relationship. Sourirajan and coworkers have proposed two transport models: the Kimura-Sourirajan analysis and the surface force-pore flow model. These two models are discussed in separate sections below.

Kimura-Sourirajan Analysis. The Kimura-Sourirajan analysis (KSA) (30b, 31) was developed from the PS-CF model to describe the transport through reverse osmosis membranes when solvent-membrane affinity dominates. According to the KSA relationship, the membrane surface is microporous and transport occurs only through the pores. The membrane has a preferential attraction for water and the resulting sorbed layer of almost pure water is forced through the membrane pores by pressure. The solvent flux is viscous in nature and therefore the driving force for solvent transport is given by the effective pressure as in Equation (11). The solute flux is diffusive in nature and is driven by the concentration

gradient:

$$N_A = \frac{D_{AM} K}{\tau} (C_2 X_{A2} - C_3 X_{A3}) \tag{38}$$

Equations (3), (8), (11), and (38) together make up the Kimura-Sourirajan analysis. For a pure water permeation experiment, $\pi_2 = \pi_3 = 0$, and A can be calculated directly from the pressure and observed flux using Equation (11). Feed and permeate concentrations and flux data obtained with solute present can then be used to determine the transport parameters using the KSA equations. Using physical data relating the osmotic pressure to solution concentration, Equation (11) can be used to calculate X_{A2}. This value of X_{A2} can be used in Equations (3) and (38) to calculate k and $(D_{AM}K/\tau)$, respectively. Therefore, the three transport parameters, A, $(D_{AM}K/\tau)$, and k, for a given solute and operating conditions, can be calculated from data obtained for a single experiment.

Equations (9), (11), and (38) can be combined to give the following relationship between f' and J_v:

$$\frac{1}{f'} = 1 + \frac{D_{AM} K}{\tau} \left(\frac{1}{J_v} \right) \tag{39}$$

Note that this equation is functionally the same as the SD model. The two parameters are A (from Equation (10)) and $(D_{AM}K/\tau)$. Even though Equation (39) is similar to Equation (29) for the solution-diffusion model, the coefficients are interpreted differently. In the KSA model, D_{AM} is the diffusivity of the solute in the membrane pore rather than in the polymer material; K is the partition coefficient defined based on the amount of solute in the pores rather than in the membrane material; and τ is the effective length of a pore, rather than the actual thickness of the membrane surface, Δx. As in the SD model, Equation (39) predicts that f' approaches 1.0 for infinite flux and $(D_{AM}K/\tau)$ is negative for negative separation cases. Neither of these characteristics of Equation (38) is realistic for the case of strong solute-membrane affinity.

Recently, attempts have been made to modify this approach to include cases involving strong solute-membrane attraction. For many solutes, it has been found that flux through the membrane is significantly decreased by the presence of solute in the feed solution. Several authors (2,21,22) have hypothesized that this decrease in flux is due to blocking of membrane pores by solute molecules. The "extent of pore blocking" (21) may be represented by $(1 - n_T/n_P)$. If $n_T = n_P$, no pore blocking has occurred and the extent of pore blocking is zero. If $n_T = 0$, the pores are totally blocked and the extent of pore blocking is 1.0. For the solutes p-chlorophenol (21), benzene, toluene, cumene (22), cyclohexane, cyclohexene, and 1,3-cyclohexadiene (23), the following empirical relationship was found to describe the extent of pore blocking as a function of concentration:

$$(1 - n_T/n_P) = Z\, X_{A2}^{\zeta} \tag{40}$$

The parameters Z and ζ, for a given solute and membrane, were found to be independent of pressure. For p-chlorophenol (21), the solute flux was found to be related to concentration and pressure as:

$$N_A = Z'\ X_{A2}^{\zeta} \Delta P^{\zeta'} \tag{41}$$

These relationships are potentially useful to describe a specific system. However, due to the empirical nature of Equations (40) and (41), it is not possible to extrapolate to other systems nor to interpret physically the parameters generated.

Finely-Porous Model. The finely-porous model (FPM), developed by Merten (45), is based on a balance of applied and frictional forces in a one-dimensional pore, as first proposed by Spiegler (48). A complete derivation of the model has been given by Jonsson and Boesen (34) and by Soltanieh and Gill (28). The general form of this model relates the volume flux, J_v, and the separation, f', as follows:

$$\frac{1}{1-f'} = \frac{b}{K_2} + \frac{K_3 - b}{K_2} \exp\{-(\frac{\tau}{\varepsilon}) \frac{J_v}{D_{AB}}\} \tag{42}$$

Algebraic rearrangement allows Equation (42) to be written in terms of 1/f' and J_v as:

$$\frac{1}{f'} = \frac{1-(1-K_3/b)\exp[-(\tau/\varepsilon D_{AB})J_v]}{(1-K_2/b)-(1-K_3/b)\exp[-(\tau/\varepsilon D_{AB})J_v]} \tag{43}$$

The solvent flux is represented by Equation (11). The parameters in the FPM relationship are the pure water permeability, A, the partition coefficients on the high and low pressures sides of the membrane, K_2 and K_3, respectively, the friction parameter, b, the effective membrane thickness, τ, and the fractional pore area of the membrane surface, ε. D_{AB} is the diffusivity of the solute in free solution.

The pure water permeability was discussed in Section 1.2.1. The partition coefficients, K_2 and K_3, are defined in a manner similar to that given earlier in Equation (28), with one difference. In this case, the concentration of solute in the membrane is interpreted as the concentration of solute in the membrane pore. The friction parameter, b, is defined (34) as:

$$b = (X_{AM} + X_{AB})/X_{AB} \tag{44}$$

where X_{AB} represents friction between the solute and solvent and X_{AM} represents friction between the solute and membrane material. Therefore, b can be thought of as the ratio of the total friction of the solvent plus membrane upon the solute to the friction between solute and solvent. The frictional forces can be represented (inversely) by the diffusivity of solute within the membrane phase, D_{AM}, and the diffusivity of the solute in the free solvent, D_{AB}, so that Equation (44) can be rewritten as:

$$b = D_{AB}/D_{AM} \tag{45}$$

A detailed discussion of the physical significance of b and how it can be estimated is given below in Section 1.2.5. The effective thickness of the membrane, τ, is a product of the actual thickness of the membrane surface layer (membrane "skin" layer) multiplied by the

tortuosity of the membrane pore. The tortuosity factor corrects the actual membrane skin thickness to an effective thickness that includes the nonlinearity of the pore geometry. ε is the fractional pore area of the membrane surface. For an asymmetric membrane, the value of ε will be much less than that calculated from the water content of the whole membrane.

The FPM relationship, as represented by Equations (11) and (43), is a four parameter model (referred to as FPM-4). The four grouped parameters are A, b/K_2, K_3/K_2, and ι/ε, which can be obtained by fitting experimental reverse osmosis data to the model. The individual parameters, b, K_2, K_3, ι, and ε cannot be obtained unless independent information is available for some of them. The parameter ratio, ι/ε, is a measure of the size and number of pores only, and should be a constant for a given membrane sample.

In principle, K_2 and K_3 may be different, but it is often assumed (16,17,34) that $K_2 = K_3 = K$. In order for this to be true, K should be independent of concentration, pressure, and membrane structure. Whether K is constant should be determined for each new system studied. When the above assumption is made, Equation (43) reduces to:

$$\frac{1}{f'} = \frac{1-(1-K/b)\exp[-(\iota/\varepsilon D_{AB})J_v]}{(1-K/b)\{1-\exp[-(\iota/\varepsilon D_{AB})J_v]\}} \tag{46}$$

which is a three-parameter model (referred to as FPM-3). The three parameters are A, b/K, and ι/ε.

Several authors (17,20,34,45) have successfully used this model (in the FPM-3 form) to describe the transport of various electrolyte and nonelectrolyte solutes through reverse osmosis membranes. Few cases involving strong solute-membrane attraction have been examined and analyzed by the FPM relationships. Most notable were the efforts by Jonsson (20,27) and by Burghoff et al. (17). Jonsson (20) examined three solutes (phenol, octanol, and hexanol) in which the nature of the strong solute-membrane attraction produced negative separation. The data for the solutes phenol and octanol were well fitted by the model.

However, the hexanol data were not represented well in that the parameter estimation routine did not converge. The b/K terms for phenol and octanol were found to be less than 1.0, which reflects the large value of K that is associated with strong solute-membrane attraction. Burghoff et al. (17) reported similar results for phenol and once again the FPM-3 relationship did a good job of describing the observed results. By independently measuring the K value (using equilibrium sorption experiments), values of b were calculated to be in the range 25 to 35 (indicating that the diffusivity of phenol in the pore is about 1/30th of the free solution diffusivity). More recently (90) the FPM-4 model was used to describe the decrease in flux as a function of concentration for cyclic hydrocarbon solutes in water with cellulose acetate membranes.

Surface Force-Pore Flow Model. The surface force-pore flow (SF-PF) model has been proposed recently by Matsuura and Sourirajan (49,50). This model mathematically extends the physical concepts of the preferential sorption-capillary flow mechanism. The flow of solute and solvent takes place through pores which are modelled as perfect cylinders of radius R_W and length ι. Similar to the FPM relationships, a balance of applied and frictional forces is made on the solute in the pore. However, this balance is written as a function of both radial and axial positions in the pore. In the FPM relationship, only the axial dependence is considered. The two-dimensional description makes it possible to include a surface potential function which represents the attraction (or repulsion) of the solute by the membrane material as a function of radial position. The resulting equations are shown below.

The following dimensionless quantities are defined (49,50) as:

$$\rho = r/R_e \tag{47}$$

$$\alpha(\rho) = u_B(\rho)\, \iota/D_{AB} \tag{48}$$

$$C_A(\rho) = C_{A3}(\rho)/C_{A2} \tag{49}$$

$$\beta_1 = \eta D_{AB}/RT C_{A2} R^2_e \tag{50}$$

$$\beta_2 = \Delta P/RT C_{A2} \tag{51}$$

where r is the radial position in the pore, u_B is the solvent velocity at position ρ, and η is the solution viscosity. The dimensionless symbols defined have meanings as follows: ρ is the dimensionless radial position, α(ρ) is the dimensionless solvent velocity, $C_A(\rho)$ is the dimensionless concentration at the pore exit, β_1 is a dimensionless ratio of physical constants for a solute-solvent-membrane system, and recognizing that $RT C_{A2} = \pi_2$ (from Equation (12)), β_2 is the ratio of the applied pressure to the osmotic pressure at the pore entrance. The effective pore radius, R_e, is related to the actual pore radius, R_W, as follows:

$$R_e = R_W - R_B \tag{52}$$

Using the effective pore radius takes into account the finite size of a water molecule. The water molecule can get no closer than within one molecular radius of the pore wall. Therefore, flow through the pore should be calculated based on R_e rather than R_W.

The performance of a membrane can be represented by the pure water mass flux, n_P, the solution mass flux, n_T, and the separation, f'. For the SF-PF model, the pure water flux is represented by Equation (11), and:

$$N_B = n_P/M_B \tag{53}$$

The solution mass flux, n_T, and the separation, f', are given by the following two equations:

$$(1 - \frac{n_T}{n_P}) = 1 - 16 \frac{\beta_1}{\beta_2} \int_0^1 \alpha(\rho)\, \rho\, d\rho \tag{54}$$

$$f' = 1 - \frac{\int_0^1 C_A(\rho)\, \alpha(\rho)\, \rho\, d\rho}{\int_0^1 \alpha(\rho)\, \rho\, d\rho} \tag{55}$$

$C_A(\rho)$ and α(ρ) are determined as a function of ρ by solving the following differential equation:

$$\frac{d^2\alpha(\rho)}{d\rho^2} + \frac{1}{\rho}\frac{d\,\alpha(\rho)}{d\rho} + \frac{\beta_2}{\beta_1} + \frac{1}{\beta_1}(1 - \exp(-\phi(\rho))(C_A(\rho) - 1)$$

$$- \frac{1}{\beta_1}(b(\rho) - 1)\,\alpha(\rho)\,C_A(\rho) = 0 \tag{56}$$

where

$$C_A(\rho) = \frac{\exp(\alpha(\rho))}{1 + \dfrac{b(\rho)}{\exp(-\phi(\rho))}(\exp(\alpha(\rho) - 1)} \tag{57}$$

with boundary conditions:

$$\frac{d\,\alpha(\rho)}{d\,\rho} = 0 \qquad \text{when } \rho = 0 \tag{58}$$

and

$$\alpha(\rho) = 0 \qquad \text{when } \rho = 1 \tag{59}$$

In the above equations, the form of the potential function $\phi(\rho)$ is different for ionized inorganic and nonionized organic solutes. For inorganic solutes:

$$\phi(\rho) = \frac{\mathbf{A}}{d(\rho)} \tag{60}$$

and for organic solutes:

$$\phi(\rho) = \begin{cases} 10 & \text{when } d(\rho) \le \mathbf{D} \\ \dfrac{\mathbf{B}}{d(\rho)^3} & \text{when } d(\rho) > \mathbf{D} \end{cases} \tag{61}$$

where the distance from the pore wall $d(\rho)$ is given by:

$$d(\rho) = R_B + R_e(1 - \rho) \tag{62}$$

The parameters in the model are the pure water permeability coefficient, A, the pore radius, R_W, the solute-membrane interaction parameter, **B** (or **A** for inorganics), the steric repulsion parameter, **D**, and the friction parameter, b. The significance of the pure water permeability coefficient was discussed in the section on osmotic pressure effects. Pores on the surface are

different in size and shape so that R_W is an effective average pore radius. The potential function, $\phi(\rho)$, is a Sutherland-type function (51), represented by Equation (61) and illustrated in Figure 2. **B** and **D** are characteristic parameters describing the potential function. As a solute molecule approaches the membrane surface (decreasing d), attraction between solute and membrane increases (negative ϕ, corresponding to attractive forces) until a minimum at d = **D** is reached. At d = **D**, solute is repelled strongly by steric forces. As a first approximation, **D** can be set equal to the solute radius, R_A. The solute-membrane friction parameter b (defined the same as in the FPM relationship) may be written as a function of radial position. A more detailed description of the friction parameter is presented below in Section 1.2.5.

Therefore, the SF-PF relationship is a five-parameter model. The parameters are Λ, **A** or **B**, **D**, R_W and b. In principle, according to the original authors (49), data for several membranes of different pore size are analyzed together for a reference solute, such as NaCl, which does not involve strong solute-membrane attraction. The values of **A** (for NaCl), **D**, and R_W are determined simultaneously by fitting the data using a nonlinear least squares analysis. The known pore sizes can then be applied to data for an attracting solute (such as toluene) to determine the **B** and **D** parameters for that solute.

The SF-PF model has been applied successfully to the solutes p-chlorophenol, benzene, and cumene (49) with cellulose acetate membranes. It would be expected that the model should work well for the similar solute systems under consideration in this dissertation. One problem with the SF-PF model approach is that it is considerably more complex than the other models discussed here. It is essential to have good numerical routines to solve the equations accurately to provide meaningful results.

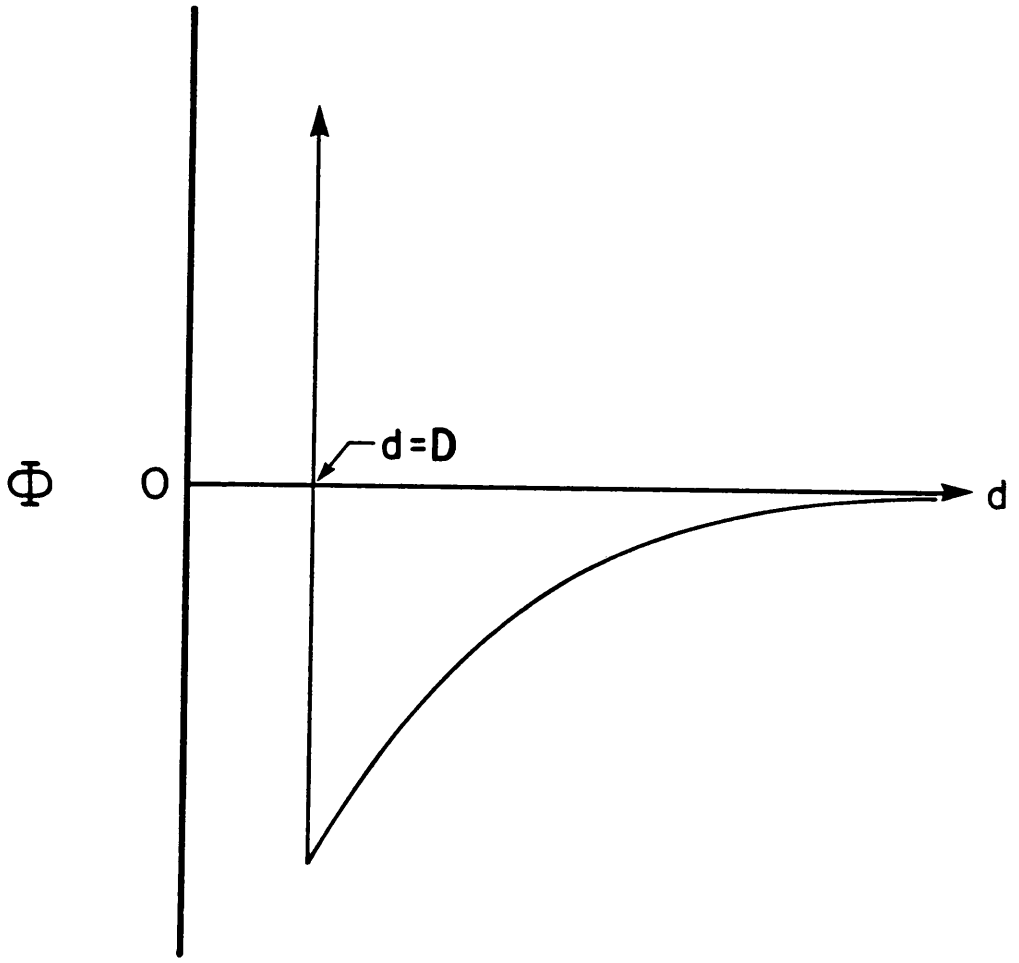

Figure 2. A Sutherland potential function

1.2.5 Restricted Diffusion in Pores

The functions b and b(ρ), which appear in the FPM and the SF-PF relationships, respectively, describe friction between the solute molecule and the pore wall. In free solution, friction between solute and solvent is represented by the diffusivity. However, in a pore, there is additional friction between the solute and pore wall. As presented in the section on the FPM relationship, b is equal to D_{AB}/D_{AM}. For relatively large pores, this ratio is 1.0. As the pore size gets progressively smaller, the size of the solute becomes significant compared to the size of the pore and friction becomes a function of the ratio of the solute radius to pore radius, λ (where $\lambda = R_A/R_W$). This situation can be compared to the hydrodynamic problem of describing a sphere moving in a narrow cylinder. What is needed is a mathematical model which describes the drag exerted on the sphere by the wall as a function of position in the cylinder. Since solute molecules are seldom spherical and pores are usually not cylindrical it is also desirable to account for the shape of the solute and the pore.

Faxen originally approached the problem of flow past a sphere in a narrow cylinder in 1923 (52). The analytical solution obtained for the particular case in which the sphere is on the center line of the cylinder is:

$$1/b = 1 - 2.104\,\lambda + 2.09\,\lambda^3 - 0.95\,\lambda^5 \qquad (63)$$

This problem was reanalyzed by Bohlin in 1959 (53), and again by Faxen in 1959 (54).

The idea of applying the Faxen equation to describe the friction of a solute in a cylindrical pore immediately suggests itself. Lane and Riggle (55) successfully used the Faxen equation to describe the restricted diffusion of solutes in dialysis membranes. Bean (56) utilized the Faxen equation in his elaborate work on the physics of porous membranes. Jonsson and Boesen (34) applied the Faxen equation to data for transport of single solute aqueous solutions (solutes: raffinose, sucrose, glucose, pentaerythritol, glycerol, and urea) across two cellulose acetate membranes. They found that variation in separation as a function

of solute size was well represented by the Faxen equation for the larger pore membrane. However, the pore radius, estimated by the Faxen equation for the smaller pore membrane, was significantly too small based on the solvent permeability.

The Faxen equation is simple in form and hence easy to use. However, it would be more correct to allow the solute to achieve any radial position when calculating the solute-membrane friction. Bean (56) pointed out that there is no analytical solution for the equations describing the drag exerted on a sphere by the wall of a cylinder except the center line solution given by Faxen. The radial dependence of the friction function b was estimated numerically by Bean (56), based on the work of Famularo (57). Figure 3, reproduced from Bean's paper (56), illustrates how the drag coefficient and hence the friction function, b, increases as the sphere approaches the cylinder wall. An average b can be obtained by integrating b(ρ) as a function of ρ. The average values of b were found to be significantly higher than those calculated based on the Faxen equation alone.

Satterfield et al. (58) have also reviewed this problem. They found that the Faxen Equation (63) was not adequate to fit their experimental data for effective diffusion coefficients in silica-alumina catalyst beads for a variety of binary systems of aromatic and paraffinic hydrocarbons and with aqueous solutions of sugars and salts. Instead, they arrived at the empirical correlation:

$$\log_{10}(1/b) = -0.37 - 2.0\,\lambda \tag{64}$$

Why the Faxen equation was unsuccessful is discussed in the Satterfield paper; however, the problem is not resolved.

More recently, Anderson and Quinn (59) have reexamined the problem of restricted diffusion in pores. The conditions necessary in order to assume a one-dimensional flow model are reviewed. They strongly endorse the position of Bean (56) that the radial dependence of b should be taken into account, using a two-dimensional flow model.

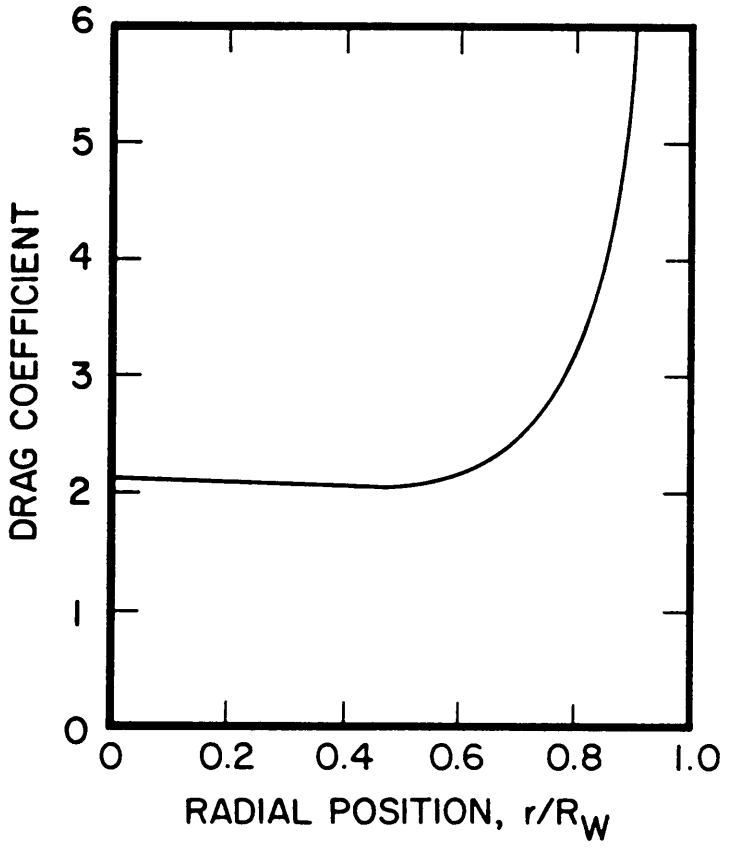

Figure 3. Drag coefficient as a function of the radial position in a pore (adapted from reference (56)). The friction function, b(ρ), increases with the drag coefficient as the solute approaches the pore wall.

Matsuura and Sourirajan have discussed the applicability of the Faxen equation to describing the b parameter in the SF-PF model. The approach they suggested in their first paper was modified in subsequent papers. In the first paper (49), the friction is a function of the radial position in the pore. As discussed by Anderson and Quinn (59), from a theoretical point of view this approach is probably better than using an average value over the whole pore radius. The friction function is given as:

$$b(\rho) = \begin{cases} \exp(10) & \text{when } d(\rho) \le \mathbf{D} \\ \exp(\mathbf{E}/d(\rho)) & \text{when } d(\rho) > \mathbf{D} \end{cases} \tag{65}$$

so that the friction decreased as an inverse function of distance, $d(\rho)$, from the membrane, where **E** is an adjustable parameter and $d(\rho)$ is given by Equation (62). However, it is simpler to use a constant b value (essentially a b value averaged, in some manner, over the pore radius). Also, most other authors have treated b as a constant value. Therefore, in subsequent papers (50,60) they used an average b value. They reasoned that for relatively larger pores (small λ), the Faxen equation would be sufficient. But for relatively smaller pores (larger λ), a different value would be necessary. An empirical equation was determined by finding the b values that best fit the reverse osmosis data for each of several solutes with the SF-PF model and then these b values were correlated with the known λ values (50,60). As illustrated below, the Faxen equation was used for λ values less than 0.22 and the empirical equation for values above λ of 0.22:

$$1/b = \begin{cases} 1 - 2.104\lambda + 2.09\,\lambda^3 - 0.95\,\lambda^5 & \text{when } \lambda \le 0.22 \\ 1/(44.57 - 416.2\,\lambda + 934.9\,\lambda^2 + 302.4\,\lambda^3) & \text{when } \lambda > 0.22 \end{cases} \tag{66}$$

In order to keep the two equations consistent with each other at the transition point, it was necessary to use a value of $\lambda = 0.227531$, which was the calculated intersection of the two curves. The form of the function is consistent (50) with the data obtained by Satterfield (58). More recent results published by Deen et al. (61) for Ficoll solute (Ficoll is a cross-linked

polymer of sucrose and epichlorohydrin) in polycarbonate track-etched membranes closely follow Equation (66) (see Figure 5 in Deen's paper).

In addition to the radial dependence of the friction parameter, it is also possible to adjust the model to account for different pore and solute geometries. These effects can include any of: nonspherical solute, noncylindrical pore, pore size distribution, and nonrigid solute. Including these factors can make the model more realistic but also much more complicated. For the aromatic solutes under consideration in this work it is reasonable to assume that they can be characterized as rigid spheres. For the membranes used, no firm information is available on pore shape or pore size distribution, so that uniform rigid cylinders are a reasonable first choice. Therefore, to include the above additional factors for the particular case under consideration could not be justified based on the physical knowledge of the system. Some of the work done in this area is referenced here for future use. The effect of solute shape has been considered by Anderson and Quinn (59) and by Deen et al. (61). The choice of pore shape was examined by Bean (56) and by Beck and Schultz (62). Both Beck and Schultz (62) and Matsuura and Sourirajan (49) have examined the influence of pore size distributions on membrane performance. Munch et al. (63) have compared the results for rigid and nonrigid macrosolutes in membranes of well characterized pore size. These modifications to the porous model are usually only justifiable when there is physical evidence for a particular system that such effects are important.

Out of this review of the literature on restricted diffusion in pores, several significant pieces of information arise. The problem of modelling the friction as a function of radial position in the pore is a formidable one that has been an issue in the literature for more than 50 years. The temptation to use an average b value should be resisted until it is determined that it is not possible to find a reasonable representation of the radial variation of the friction function. In light of the results of Satterfield discussed above, it may be that the Faxen

equation will not work in the present case at all. It is possible to account for different solute and pore geometries, but the analysis is more complex.

Steric Exclusion. In addition to friction between solute and the membrane pore, steric exclusion of solute from pores may influence membrane transport. Since the solute radius is of the same order of magnitude as the pore radius, there is significant exclusion just due to the size of the solute. By simple geometric arguments, the reduction in effective diffusivity in the pore by steric exclusion is given by $(1 - \lambda)^2$. This idea was first proposed by Ferry (64) and has been discussed more recently by Ackers (65) and Beck and Schultz (62). The nature of this exclusion is similar to that proposed as the separation mechanism in size exclusion chromatography. The coupling of the steric exclusion with the frictional drag (given by the Faxen equation) leads to the following equation:

$$1/b = (1 - \lambda)^2 (1 - 2.104\lambda + 2.09\,\lambda^3 - 0.95\,\lambda^5) \qquad (67)$$

which was first given by Renkin (66). Thus, Equation (67) is known as the Ferry-Faxen equation or the Renkin equation. This equation was determined by Beck and Schultz (62) to be consistent with their experimental results on diffusion in track-etched mica membranes. Bean (56) also uses the additional $(1 - \lambda)^2$ term as in Equation (67) to account for the exclusion or as he calls it, the steric restrictions. Figure 4, reproduced from Bean's paper (56), illustrates the trends for the case of (a) steric exclusion alone, (b) steric exclusion and frictional drag from Equation (67), and (c) with the radial variation of frictional drag included. When the solute is small compared to the pore size, $\lambda = 0$, and all three cases predict no restricted diffusion, $b = 1.0$. As λ increases, $1/b$ decreases, corresponding to increasing friction. Adding frictional drag (curve (b)) and radial variation of the frictional drag (curve (c)) to the model compared to the case of steric exclusion alone (curve (a)) results in the

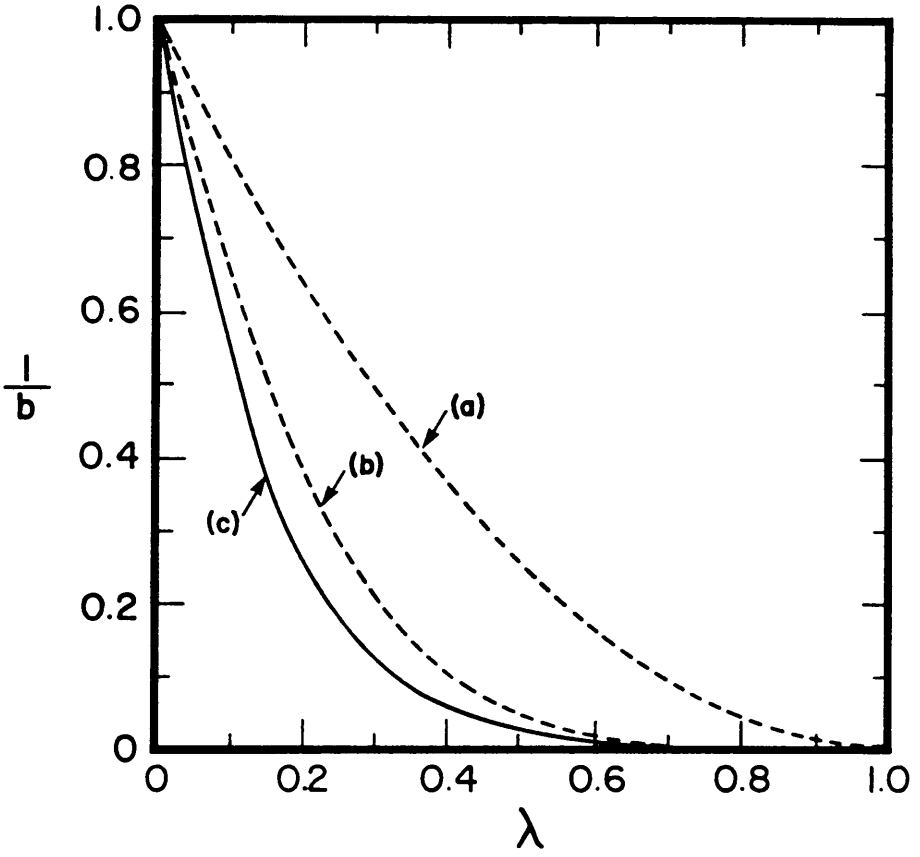

Figure 4. Restricted diffusion as a function of ratio of solute radius to pore radius (adapted from reference (56)). Curve a) illustrates the influence of steric exclusion alone. Curve b) illustrates the effect of steric exclusion plus frictional drag calculated based on the center line value from the Faxen equation. Curve c) is a numerical approximation including both steric exclusion and the radial variation of the frictional drag.

prediction of a larger friction parameter. Therefore, when solute size is relatively large then it is important to include the influence of steric exclusion and restricted diffusion in the model. Jonsson and Boesen (34) have successfully used the Ferry-Faxen equation in combination with the FPM-3 relationship to model the behavior of organic solute-water-cellulose acetate systems.

1.2.6 Summary and Comparison of Transport Models

In the preceding sections, several models which can be used to represent reverse osmosis transport have been presented. At this point, the models will be summarized and compared to each other. Table 2 furnishes a summary of the models and the appropriate equations and parameters. As indicated in Table 2, knowledge of the mass transfer coefficient, k, or some other means of representing concentration polarization is also required. The calculation of k and the modelling of the concentration polarization are discussed in Section 1.2.1.

Although the models presented have been developed based on different conceptual points of view, the final models are in some cases similar in mathematical form. This is particularly true of the relationship between J_v (or ΔP) and f' predicted by each model. With the exception of the SF-PF model, all of the models may be written in one of the following forms:

Form a)

$$\frac{1}{f'} = E_0 + E_1\left(\frac{1}{J_v}\right) \tag{68}$$

Form b)

$$\frac{1}{f'} = \frac{1 - E_0 \exp(-E_1 J_v)}{E_0[1 - \exp(-E_1 J_v)]} \tag{69}$$

Form c)

$$\frac{1}{f'} = E_0 + E_1\left(\frac{RT}{\Delta P}\right) \tag{70}$$

Table 2

Summary of Several Reverse Osmosis Transport Models

Model	Equation Number	Number of Parameters [a]	Parameters
Phenomenological			
IT-PT	18, 20	3	ℓ_p, ℓ_π, σ
IT-KS	24, 25	3	$p_B/\Delta x$, $p_A/\Delta x$, σ
Nonporous			
SD	26, 29	2	ℓ_p, $(D_{AM}\, K/\Delta x)$
SDI	30, 33	3	κ', κ'', κ'''
ESD	10, 37	3	ℓ_p, ℓ_{AP}, $(D_{AM}\, K/\Delta x)$
Porous			
KSA	11, 39	2	A, $(D_{AM} K/\tau)$
FPM-3	11, 46	3	A, b/K, τ/ε
FPM-4	11, 43	4	A, b/K_2, K_3/K_2, τ/ε
SF-PF	11, 54-57	5	A, R_W, B, D, b

[a] In calculating the number of parameters, it has been assumed that the mass transfer coefficient, k, is known.

Form d)

$$\frac{1}{f'} = \frac{1 - E_o \exp(-E_2 J_v)}{E_1 - E_o \exp(-E_2 J_v)} \tag{71}$$

Form c) is similar to Form a), the difference being that f' is related to J_v in Form a) and to ΔP in Form c). Also, Form b) and d) are similar. If $E_0 = E_1$ in Form d), then Form b) and d) are identical.

The E_i coefficients are generalized coefficients. Coefficients with the same E_i symbol are not the same from one equation to the next. The values of E_i for each of the appropriate models are summarized in Table 3. Four of the models, IT-PT, SD, ESD, and KSA, predict a linear relationship between 1/f' and $1/J_v$, as in Equation (68). Both the SD and KSA relationships predict that E_0 should be 1.0, while for the IT-PT and ESD models E_0 is not necessarily 1.0. The significance of E_0 in Equation (68) is that at infinite flux through the membrane, 1/f' should approach E_0. For the SD, ESD, and KSA models, the E_1 parameter should be relatively concentration independent. However, for the IT-PT relationship, the E_1 parameter contains a π_2 term, which implies a concentration dependence.

Both the IT-KS and FPM-3 relationships can be represented by Form b). This similarity has been noted previously by several authors (28,34). This result is significant in that a connection can be made between the phenomenological coefficients of the IT-KS model and the physical parameters of the FPM-3 model.

The FPM-4 relationship is represented by Form d). As pointed out above, when the simplification that $K_2 = K_3 = K$ is imposed upon the FPM-4 model, it reduces to the FPM-3 model. The above simplification corresponds to Form d) reducing to Form b). The SF-PF model does bear some resemblance to the FPM-3 relationship. Equation (46) in the FPM-3 relationship can be arranged as (34):

$$\frac{C_{A3}}{C_{A2}} = \frac{\exp[(\upsilon/\varepsilon D_{AB}) J_v]}{1 + (b/K)\{\exp[(\upsilon/\varepsilon D_{AB}) J_v] - 1\}} \tag{72}$$

Table 3

Comparison of the Form of Several Reverse Osmosis Transport Models

Form (a) $$\frac{1}{f'} = E_0 + E_1\left(\frac{1}{J_v}\right)$$

Form (b) $$\frac{1}{f'} = \frac{1 - E_0 \exp(-E_1 J_v)}{E_0[1 - \exp(-E_1 J_v)]}$$

Form (c) $$\frac{1}{f'} = E_0 + E_1 (RT/\Delta P)$$

Form (d) $$\frac{1}{f'} = \frac{1 - E_0 \exp(-E_2 J_v)}{E_1 - E_0 \exp(-E_2 J_v)]}$$

Model	Form	E_0	E_1	E_2
Phenomenological				
IT – PT	a	$1/\sigma$	$(\ell_\pi/\ell_p - \sigma^2)(\ell_p/\sigma)\,\pi_2$	–
IT – KS	b	σ	$(1-\sigma)\,(\Delta x/p_A)$	–
Nonporous				
SD	a	1	$(D_{AM}K/\Delta x)$	–
SDI	c	$1+\kappa'''/\kappa'$	κ''/κ'	–
ESD	a	$1/(1-\ell_{AP}/C_{A2}\ell_p)$	$(D_{AM}K/\Delta x)\,E_0$	–
Porous				
KSA	a	1	$(D_{AM}K/\tau)$	–
FPM-3	b	$(1 - K/b)$	$(\tau/\varepsilon\, D_{AB})$	–
FPM-4	d	$(1 - K_3/b)$	$(1 - K_2/b)$	$(\tau/\varepsilon\, D_{AB})$

which has the same form as Equation (57) in the SF-PF relationship. The main differences are that the SF-PF model applies over an annular region, between ρ and $(\rho + d\rho)$, and therefore is written as a function of ρ, and the K term is explicitly replaced as a function of the potential function, $\phi(\rho)$. The similarity in form of the SF-PF and FPM-3 models is due to the parallelism in the initial assumption of the models.

Table 3 provides a summary of all but one of the models discussed. One conclusion which can be drawn from Table 3 is that simple agreement between the experimental data and a model does not necessarily mean that the model is conceptually correct, since several of the models have the same mathematical form (28). How well these models performed at fitting the data obtained in the current work is presented in the RESULTS AND DISCUSSION section.

1.2.7 Physicochemical Nature of the Solutes Studied

The solutes which were chosen for study are the three aromatic hydrocarbons benzene, toluene, and cumene. As discussed above, these solutes were selected on the bases of range of nonpolar character, solubility in water, and societal impact. The structure of the solutes and some relevent physicochemical data are illustrated in Table 1. Most of the information in Table 1 is self-explanatory. Vapor pressure values for these solutes are significant which indicates that care should be exercised in handling samples so that little solute is lost by evaporation. The Threshold Limit Value (TLV) indicates that care should be taken so that the vapors are not inhaled. The vapor pressure and TLV values were obtained from reference (5).

Previous work by Matsuura and Sourirajan (2) indicated that the qualitative behavior of hydrocarbon-water separation could be expressed by the nonpolar character of the solute. For the purpose of defining a nonpolar parameter, Matsuura and Sourirajan (2) used

the molar attraction constant defined by Small (4). Experimental data was collected for several different classes of hydrocarbon solutes including aliphatic, alicyclic, and aromatic hydrocarbons. They found that separation could be related to the molar attraction constant for a given class of hydrocarbon. However, the correlation of separation versus molar attraction constant resulted in a different line for each class of solute. This result is less than optimal. It would be better ultimately to find one parameter that would correlate all the data.

It is important to examine exactly what is meant by the nonpolar character of the solute. This term refers to the dispersive character of the solute, which is related to the London dispersion forces (67). London dispersion forces are the result of induced dipole moments which can be represented by the polarizability of the solute (67). Polarizability, P, can be calculated by the Lorentz-Lorenz equation (68):

$$P = \frac{n^2-1}{n^2+2}\,\frac{M_A}{g}\,\frac{3}{4\pi N_0} \tag{73}$$

where n is the refractive index, g is the density, and N_0 is Avogadro's number. Refractive index values were obtained from reference (69). For the 12 aromatic hydrocarbons listed in Table 4 the polarizability was calculated and compared to the molar attraction constant as reported by Matsuura and Sourirajan (2). That the molar attraction constant is related to the polarizability is illustrated in Figure 5. Therefore, when the term "nonpolar character of the solute" is used in this work, it refers to the dispersive character or polarizability of the solute.

Table 4

Relationship between Polarizability and Modified Small's Number for Some Aromatic Hydrocarbon Solutes

Solute	Molecular Weight[a] kg/kmol	Solute Density[a] kg/m^3	Refractive Index[a]	Polarizability[b] x 10^{30} m^3	Molar Attraction Constant[c]
Benzene	78.11	879	1.5011	10.38	53.4
Toluene	92.15	867	1.4961	12.31	61.4
Ethylbenzene	106.17	867	1.4959	14.18	70.0
o-Xylene	106.17	880	1.5055	14.19	70.3
m-Xylene	106.17	864	1.4972	14.26	70.3
p-Xylene	106.17	861	1.4958	14.27	70.3
Cumene	120.20	862	1.4915	16.03	77.1
Propylbenzene	120.20	862	1.4920	16.04	78.6
Mesitylene	120.20	865	1.4994	16.18	79.1
t-Butylbenzene	134.22	867	1.4927	17.84	83.1
s-Butylbenzene	134.22	862	1.4920	17.90	85.7
i-Butylbenzene	134.22	853	1.4866	17.92	85.7

[a] Values obtained from reference (69).

[b] Polarizability calculated from Equation (72).

[c] Molar attraction constants have units of (kJ m^3)$^{1/2}$/kmol which were converted from the values in reference (2).

Figure 5. The relationship between polarizability and the molar attraction constant for several aromatic hydrocarbons.

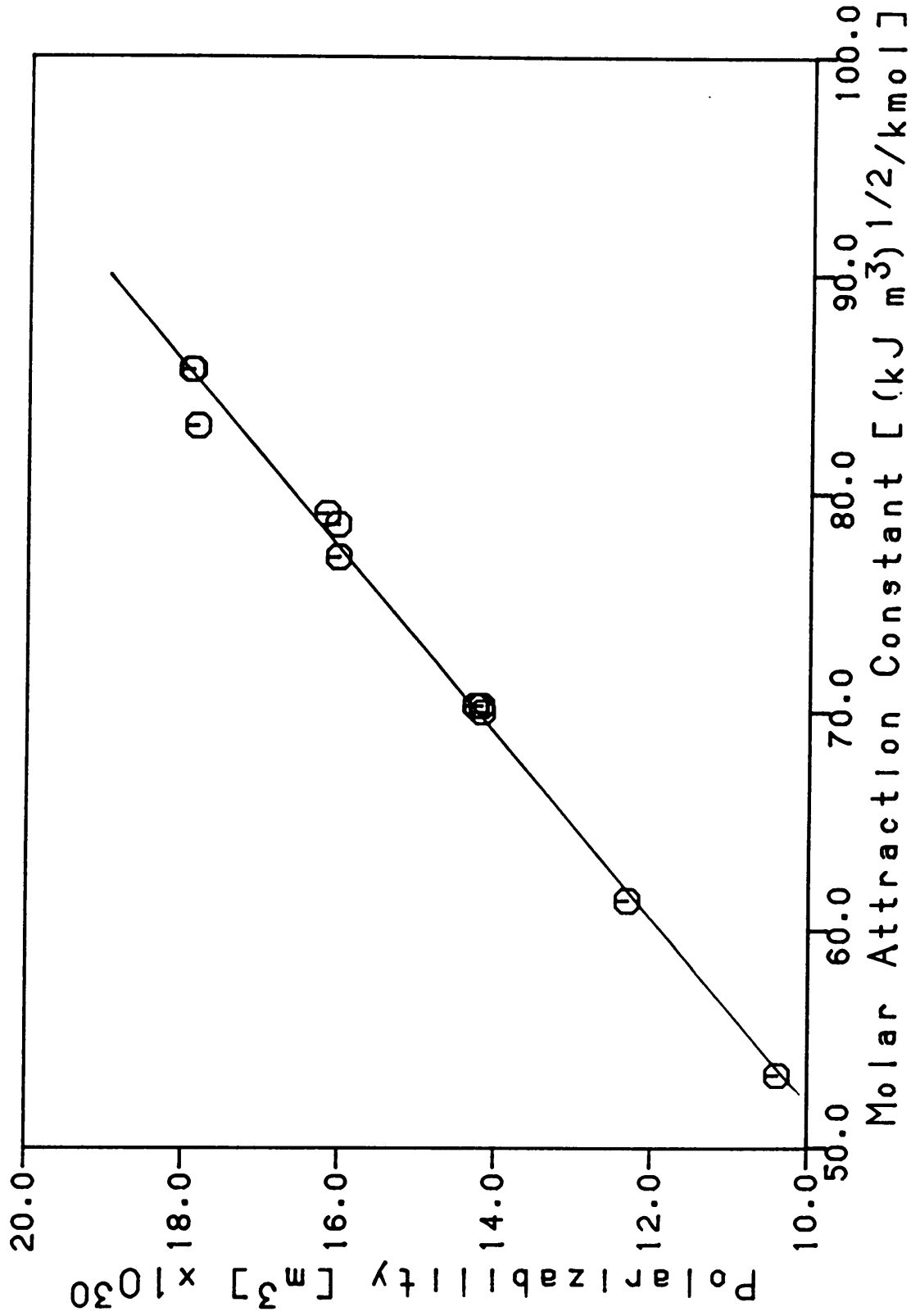
Polarizability [m^3] x 10^{30}
20.0
18.0
16.0
14.0
12.0
10.0
50.0
60.0
70.0
80.0
90.0
100.0
Molar Attraction Constant [(kJ m^3)$^{1/2}$/kmol]

Chapter 2

EXPERIMENTAL

This section briefly describes the experimental methods used in this study. More details of membrane making and experimental procedures have been given elsewhere (30a,22-24,70-73). The methods used here have been adopted from those sources. The chemicals and equipment used are listed separately. The reverse osmosis flow cell equipment list is given in the laboratory equipment operating manual (72).

2.1 Membrane Fabrication

In this study, Loeb-Sourirajan type cellulose acetate membranes (30a,71) were fabricated. Briefly, the casting solution composition was 17.0 wt-% cellulose acetate, 69.2 wt.-% acetone, 12.35 wt.-% water, and 1.45 wt.-% magnesium perchlorate (73). The casting solution was cooled to 0°C and then cast, with a Gardner Knife, on a glass plate at room temperature (25°C). An evaporation period of 1.0 minute was allowed before the membrane was gelled by immersing it in ice water (0°C). After one hour, the membrane sheet was removed from the glass plate and cut into circles of the appropriate diameter for mounting in the reverse osmosis cell. Prior to mounting in the flow cell, the membrane was annealed in water for 10 minutes. The annealing step has been shown to increase the separation and reduce the flux of the membrane. The higher the annealing temperature used, the greater the increase in separation. The temperatures used were 68.0, 72.0, 75.0, 79.0, 82.0, and 85.0°C. This method produced a series of 6 membranes with gradated morphological properties. After mounting the membranes in the cells, they were pressurized at 12,000 kPa for two hours to stabilize the behavior (30a,73).

2.2 Reverse Osmosis Experiments

The apparatus is illustrated schematically in Figure 6. A schematic of a radial flow cell is presented in Figure 7. A detailed description of the equipment and operating procedures is given in reference (72). Briefly, the system consists of six radial flow cells connected in series, a high pressure diaphragm metering pump, a bladder accumulator, a back pressure regulator, and a pressure gauge. The feed solution was pumped through the six cells, and after passing through the regulator, it was returned to the feed solution. The membrane permeate for each cell was collected separately, weighed, and analyzed to give the flux and permeate concentration. The feed concentration remained approximately constant during the course of the experiment since the volume removed through each membrane was small compared to the total feed solution volume. The cells were placed in a constant temperature chamber in order that the temperature could be held constant at 25 ± 1°C. The apparatus allows the feed flow rate, feed concentration, and operating pressure to be controlled independently. By using the six cells, different membranes could be studied under the same experimental conditions.

Experiments were performed at the following conditions. The temperature and feed flow rate were fixed at 25 ± 1°C and 400 ± 20 mℓ/min., respectively for all experiments. The operating pressures used were 690, 1725, 3450, and 6900 kPa gauge (gauge pressures are used throughout this dissertation). At each pressure, experiments were repeated at four or more concentrations for each of the three aromatic hydrocarbon solutes. The range of the feed concentrations for the organic solutes was from 5 to 260 ppm, depending on the solubility limit and the sensitivity of the chemical analysis. Data were collected for each of the six cellulose acetate membranes which had been previously annealed at different temperatures. The range of sodium chloride-water separation was from 58% to 98%. Thus the effects of changing operating pressure, feed concentration, solute, and membrane were studied.

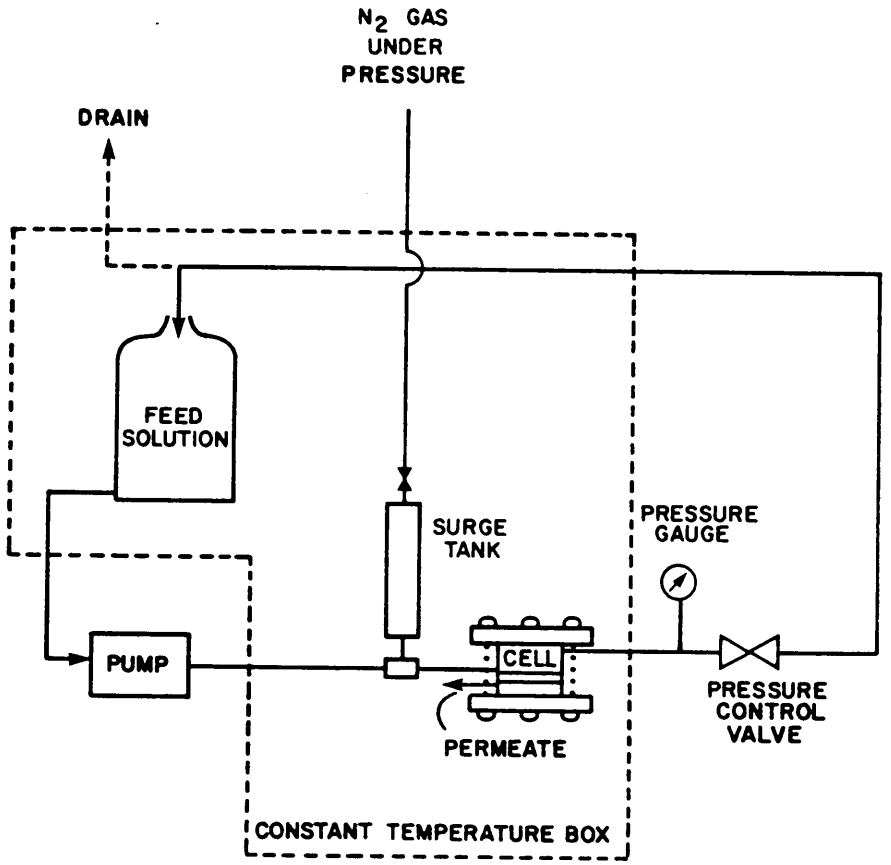

Figure 6. A schematic of the reverse osmosis test equipment. In the actual equipment, six cells were connected with the feed streams in series.

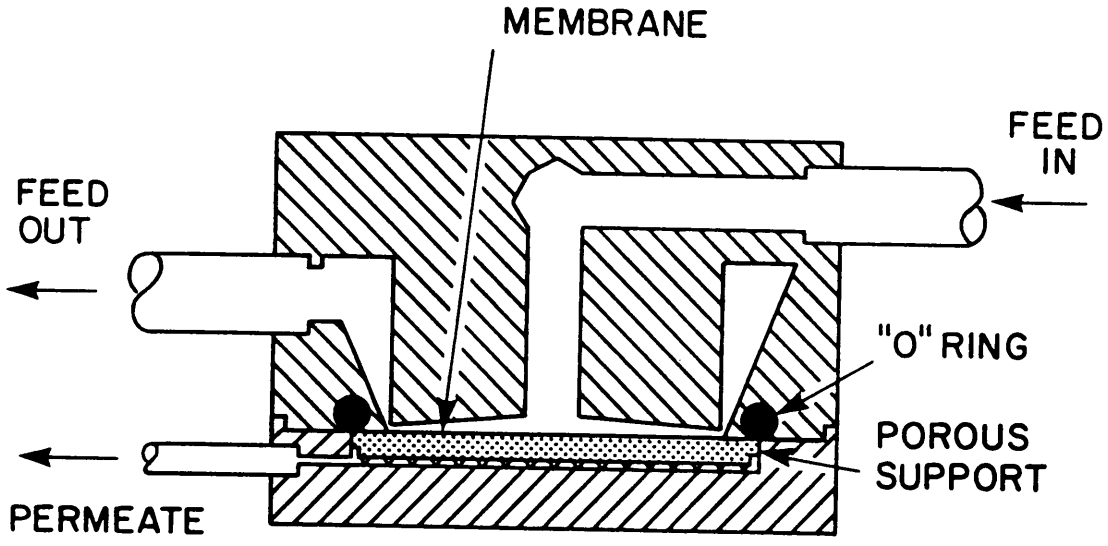

Figure 7. A schematic of a radial flow test cell (cross section).

Each experiment consisted of the following steps. First, the pure water permeability of the six membranes was measured by using a pure water feed, under a given set of operating conditions (feed flow rate, pressure, and temperature). Then the feed was switched to a feed solution of specified concentration. After the system reached steady state, the permeate flux and permeate concentration for each cell were measured. This step corresponds to measuring the quantities n_P, n_T and X_{A3} at a given ΔP, X_{A1}, and temperature, T. Steady state was insured by allowing at least 10 mL of permeate to pass through the membrane. Previous studies (2,22,30a) have indicated that this procedure was sufficient.

Sodium chloride-water experiments were repeated periodically to characterize the membranes and to monitor any changes in the membrane performance. These experiments were performed at 6900 kPa operating pressure and a feed concentration of 10 000 ppm NaCℓ.

2.3 Chemical Analysis

Sodium chloride concentrations were measured using a YSI Model 31 Conductivity Meter. A calibration curve of conductance, in μmhos, versus sodium chloride concentration, in parts per million (ppm), was constructed over the range of 0.5 ppm to 12,000 ppm. All samples were analyzed at 25(±0.5)°C. Details of the analysis and the calibration data are given in reference (70).

The organic solutes were analyzed using an Oceanography International Corporation Total Carbon System, Model 524C. This instrument allowed the dilute organic in water samples to be sealed into glass ampules for later analysis. Immediately sealing the samples reduced the loss of solute by evaporation. The sealed ampules, which contained potassium persulphate as an oxidating agent, were heated in an autoclave to oxidize all the carbon to CO_2. The ampules were broken in the analyzer and purged with nitrogen gas. The purging gas carried the CO_2 to an infrared gas analyzer. Output from the gas analyzer was

integrated and peak areas were used to determine the carbon concentration in the sample. Details of the calibration and many precautions employed in the analysis are given in reference (70).

2.4 Chemicals

The chemicals used in this project are as follows:

1. Acetone (C_3H_6O); M_A = 58.08; Fisher Scientific (A-18); Certified ACS; Lot unknown.
2. Benzene (C_6H_6); M_A = 78.12; Fisher Scientific (B-245); Certified ACS; Lot 773729.
3. Cellulose Acetate; 39.8 wt.-% acetyl content; ASTM viscosity 3; Eastman Chemical (E398-3); Lot A6F.
4. Cumene (C_9H_{12}); M_A = 120.20; Fisher Scientific (O-2065); Certified; Lot 781931.
5. Glycerol ($C_3H_8O_3$); M_A = 92.10; Matheson, Coleman and Bell (GX-185); Reagent ACS; Lot A 4N28.
6. Magnesium Perchlorate ($Mg(ClO_4)_2$); M_A = 223.23; Fisher Scientific (M-54); Reagent; Lot B106.
7. Potassium Persulphate ($K_2S_2O_8$); M_A = 270.33; Matheson, Coleman and Bell (PX-1560); Reagent ACS; Lot E8M04.
8. Sodium Chloride (NaCl); M_A = 58.45; Fisher Scientific; Certified ACS; Lot 791337.
9. Toluene (C_7H_8); M_A = 92.14; Fisher Scientific (T-324); Certified ACS; Lot 70287.

2.5 Equipment

The equipment used in this project is documented in detail in reference (72). Other equipment is as follows:

1. Analytical Balance; Mettler AK160; 4 decimal digit accuracy.

2. Carbon Analyzer; Oceanography International Corporation; Model 524C.

3. Conductivity Meter; YSI; Model 31.

4. Pipetman; Gilson H-79-13637; Models P1000 and P5000.

Chapter 3

RESULTS AND DISCUSSION

In this chapter, the experimental results obtained are presented and discussed. The results for the sodium chloride-water system are used to characterize the test cells and the membrane samples. The data for the three aromatic hydrocarbon solutes are presented and then interpreted in a qualitative manner. A description of the compaction analysis and the numerical parameter estimation methods is given. Finally, a quantitative description of the hydrocarbon solute data, using the models presented in the INTRODUCTION, is presented and the applicability of the various models is discussed. The models investigated include the phenomenological transport models of irreversible thermodynamics, the nonporous membrane transport models based on a solution-diffusion approach and the porous membrane transport models.

The exact structure of the membrane surface layer is unknown. The question of whether the membrane surface is porous has not been resolved. However, in order to discuss the data in Sections 3.1-3.3, it has been assumed for the moment that the membranes are porous. This assumption allows a qualitative explanation of the data to be made, with pore size as one of the parameters. The data and most of the discussion in Sections 3.1-3.3 have been published previously (23). Subsequent work with cyclic hydrocarbon solutes was found to be qualitatively similar (24).

The raw data are tabulated in the Appendices. Appendix B summarizes the NaCl-water performance data and Appendix C summarizes similar information for the aromatic hydrocarbon solutes.

3.1 Membrane and Cell Characterization

The six cells and corresponding cellulose acetate membranes were characterized by pure water and sodium chloride-water performance. The data are summarized in Table 5. Characterization experiments were repeated at regular intervals to monitor membrane change, and the tabulated data represent the average of 17 tests.

The pure water permeability coefficient (a measure of the overall membrane porosity (30b)) decreased over the period of several experiments. The decrease, which is attributed to membrane compaction, varied from 10% for the most permeable membrane to 5% for the least permeable membrane. The rate of membrane compaction during exposure to the hydrocarbon solutions was slightly higher than is usually observed for salt solution experiments at similar pressures. When cellulose acetate is exposed to a high concentration of an organic solute the polymer can swell or dissolve. Swelling the polymer would lead to an increased rate of creep of the membrane structure which would be observed as an increased rate of compaction. For the dilute solutions used in this study no such detrimental effect was expected. However, repeated exposure to the relatively high interfacial concentrations may have caused a slight swelling of the polymer, which ultimately increased the rate of compaction.

The original membrane in cell 6 was damaged during the course of study and was replaced by a membrane annealed at the same temperature. Since these two membranes were similar in performance, they were treated as one membrane (membrane 6) in all analyses.

The average separation and the mass flux for pure water and for aqueous NaCl solutions measured under the indicated conditions are listed in Table 5. The six membrane samples covered the range of sodium chloride-water separation from 58 to 98%

Table 5

Characterization and Performance
of the Cellulose Acetate Membranes and of the Radial Flow Cells[a]

	Film and Cell Number					
	1	2	3	4	5	6
Annealing temperature, T, °C	85.0	82.0	79.0	75.0	72.0	68.0
Hydraulic permeability, ℓ_p, x 10^9, m/s kPa	1.277	1.560	2.193	3.285	4.014	4.421
Pure water permeability coefficient, A, x 10^7, kmol/m^2s kPa	0.7068	0.8635	1.214	1.818	2.222	2.447
NaCl – Water separation[b], f, %	97.9	97.3	96.0	91.1	78.9	58.5
Total solution mass flux, n_T, x 10^3, kg/m^2 s	7.57	9.25	12.84	19.06	23.48	24.88
Solute transport parameter, $(D_{AM}K/t)_{NaCl}$, x 10^7, m/s	1.388	2.157	4.166	12.87	39.05	63.94
$\ln C^*_{NaCl}$	−12.555	−12.114	−11.456	−10.328	−9.218	−8.725
Mass transfer coefficient, k, x 10^6, m/s	43.0[c]	50.9[c]	49.9[c]	51.8[c]	49.5[c]	25.6[d]

[a] Film area, 1.443 x 10^{-3} m^2; operating pressure, 6900 kPa; feed concentration, 10 000 ppm NaCl; temperature, 25°C; feed flow rate 400 ml/min. The experimental results reported are the average of 17 tests.

[b] Separation is calculated based on the feed concentration, $f = (C_{A1} - C_{A3})/C_{A1}$.

[c] An average value of k = 49.0 x 10^{-6} m/s is used.

[d] A value of k = 25.0 x 10^{-6} m/s is used.

(corresponding to a range of the pore size parameter, ln C^*_{NaCl}, from -8.7 to -12.5) measured at 6900 kPa operating pressure and 10 000 ppm feed concentration. To determine the pore size parameter, the sodium chloride-water data were analyzed by the Kimura-Sourirajan Analysis. The solute transport parameter, $D_{AM}K/t$, and the mass transfer coefficient, k, were calculated from the experimental data for each sodium chloride-water experiment using Equations (3), (8), (11), and (38) and the osmotic pressure data tabulated in Appendix II of reference (30). The ln C^*_{NaCl} values were calculated using Equation (14). Average values of D_{AM} K/t, k, and ln C^*_{NaCl} are listed in Table 5. The solute transport parameter for sodium chloride, and hence ln C^*_{NaCl}, remained essentially constant over the experimental time period. When A decreases and ln C^*_{NaCl} remains constant as a function of time, this indicates that the effective pore diameter has remained constant and the effective pore length has increased (30b). Since the separation is primarily determined by the effective pore diameter the results from early and later experiments can still be compared.

Values of the sodium chloride mass transfer coefficient listed in Table 5 are reasonably constant and an average value of $k = 49 \times 10^{-6}$ m/s was used for cells 1 to 5. However, cell 6 had a marginally larger flow channel for feed which resulted in lower feed solution velocities and a lower k value, 25×10^{-6} m/s.

3.2 Hydrocarbon-Water-Cellulose Acetate Reverse Osmosis System

The experimentally determined performance for the separation of benzene and water at four different pressures is illustrated in Figure 8. The data obtained at each operating pressure indicate that as pore size increases the benzene-water separation decreases, reaches a minimum, and then increases. For each pressure, the separation was shown via an analysis of covariance (70, 74) to have no concentration dependence at a 0.99

Figure 8. Effect of feed concentration on the reverse osmosis performance for the benzene-water system at four different pressures. membrane material = cellulose acetate; ln C^*_{NaCl} obtained at 6900 kPa; feed flow rate = 400 mL/min; temperature = 25°C.

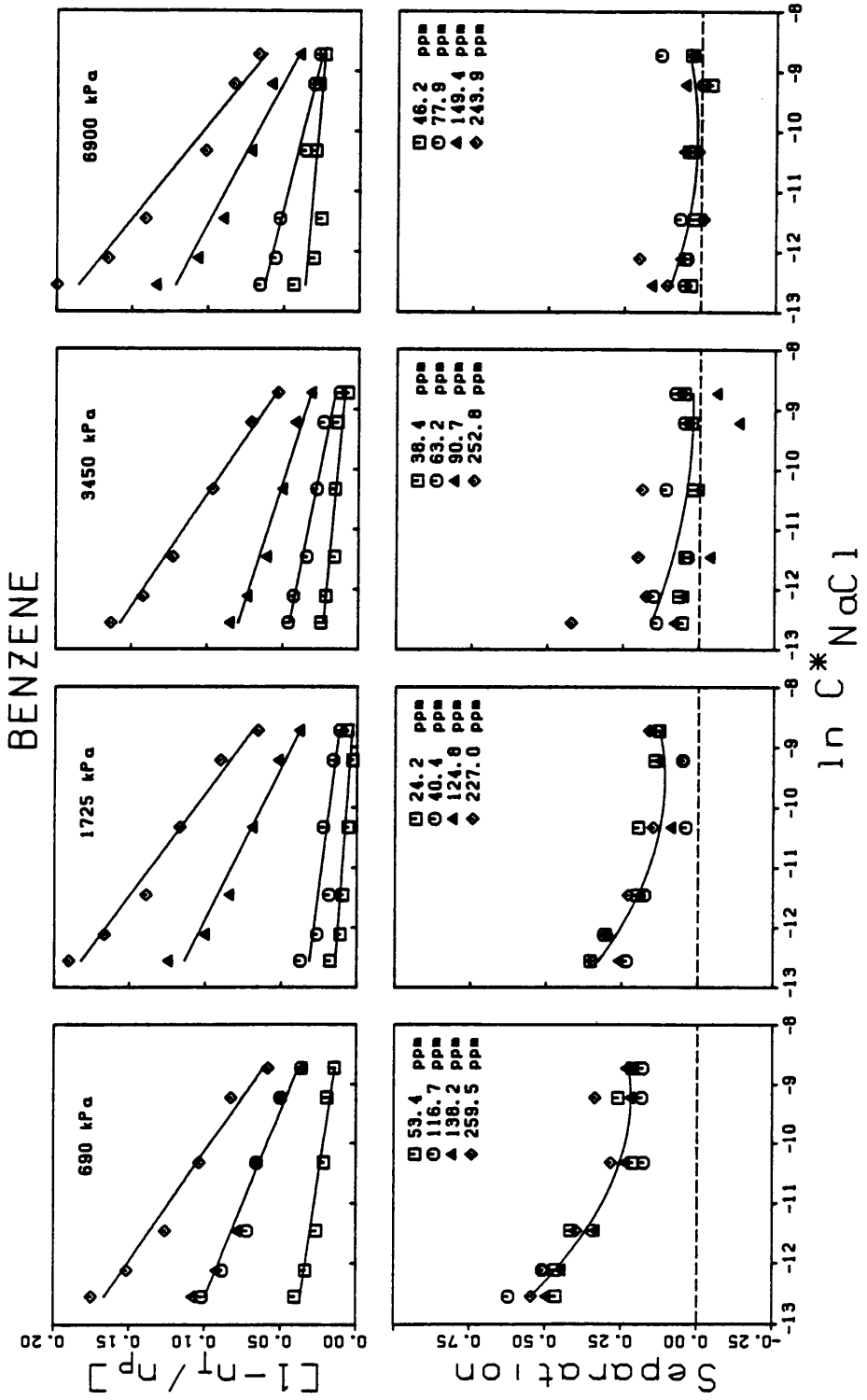
BENZENE
690 kPa
1725 kPa
3450 kPa
6900 kPa
[1−nt/np]
Separation
ln C*NaCl
53.4 ppm
116.7 ppm
138.2 ppm
259.5 ppm
24.2 ppm
40.4 ppm
124.8 ppm
227.0 ppm
38.4 ppm
63.2 ppm
90.7 ppm
252.8 ppm
46.2 ppm
77.9 ppm
149.4 ppm
243.9 ppm

Figure 9. Effect of feed concentration on the reverse osmosis performance for the toluene-water system at four different pressures. membrane material = cellulose acetate; ln C^*_{NaCl} obtained at 6900 kPa; feed flow rate = 400 mL/min; temperature = 25°C.

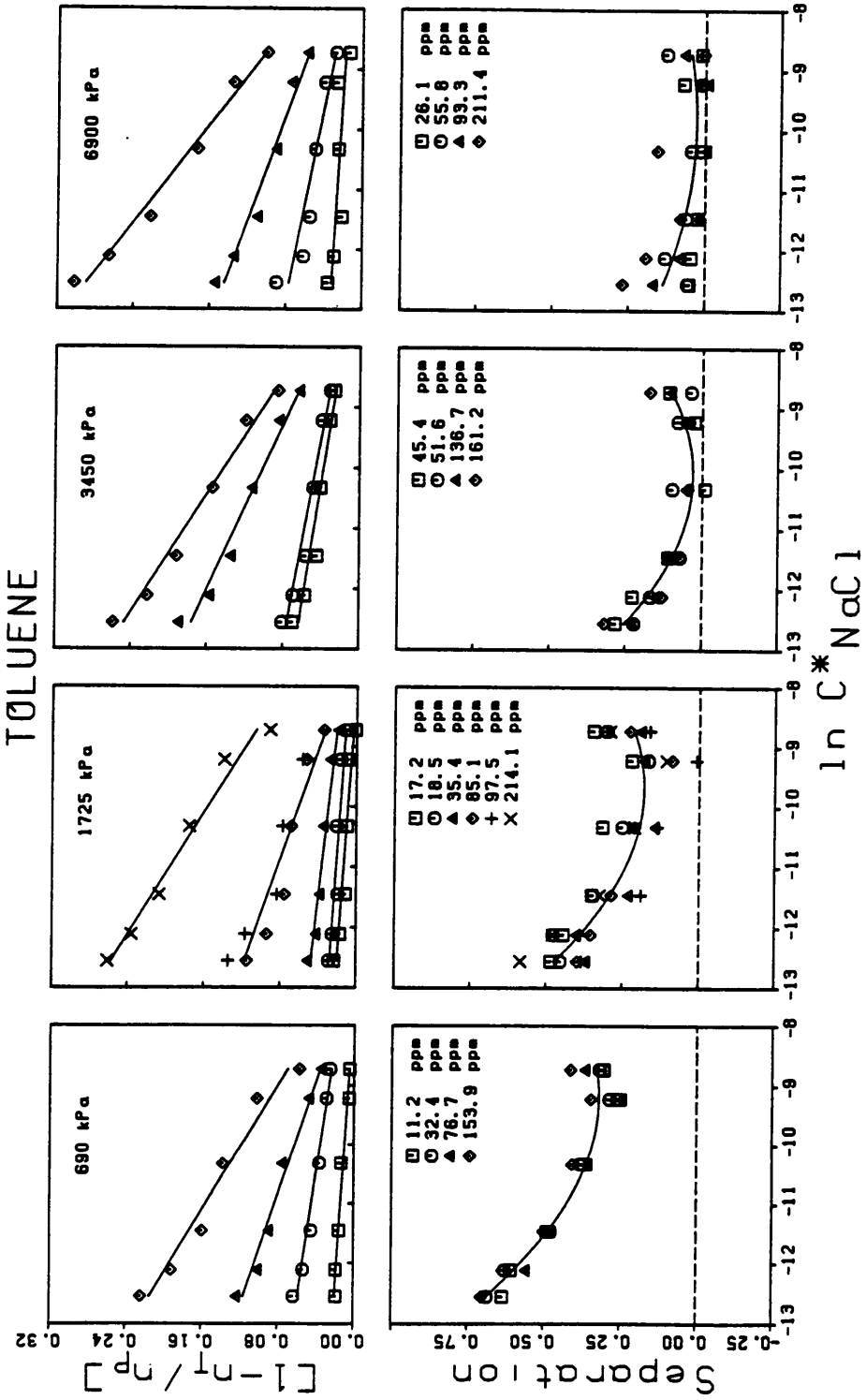
TOLUENE
690 kPa
1725 kPa
3450 kPa
6900 kPa
[1−nt/np]
Separation
ln C*NaCl
11.2 ppm
32.4 ppm
76.7 ppm
153.9 ppm
17.2 ppm
18.5 ppm
35.4 ppm
85.1 ppm
97.5 ppm
214.1 ppm
45.4 ppm
51.6 ppm
138.7 ppm
161.2 ppm
26.1 ppm
55.8 ppm
93.3 ppm
211.4 ppm

Figure 10. Effect of feed concentration on the reverse osmosis performance for the cumene-water system at four different pressures. membrane material = cellulose acetate; ln C^*_{NaCl} obtained at 6900 kPa; feed flow rate = 400 mL/min; temperature = 25°C.

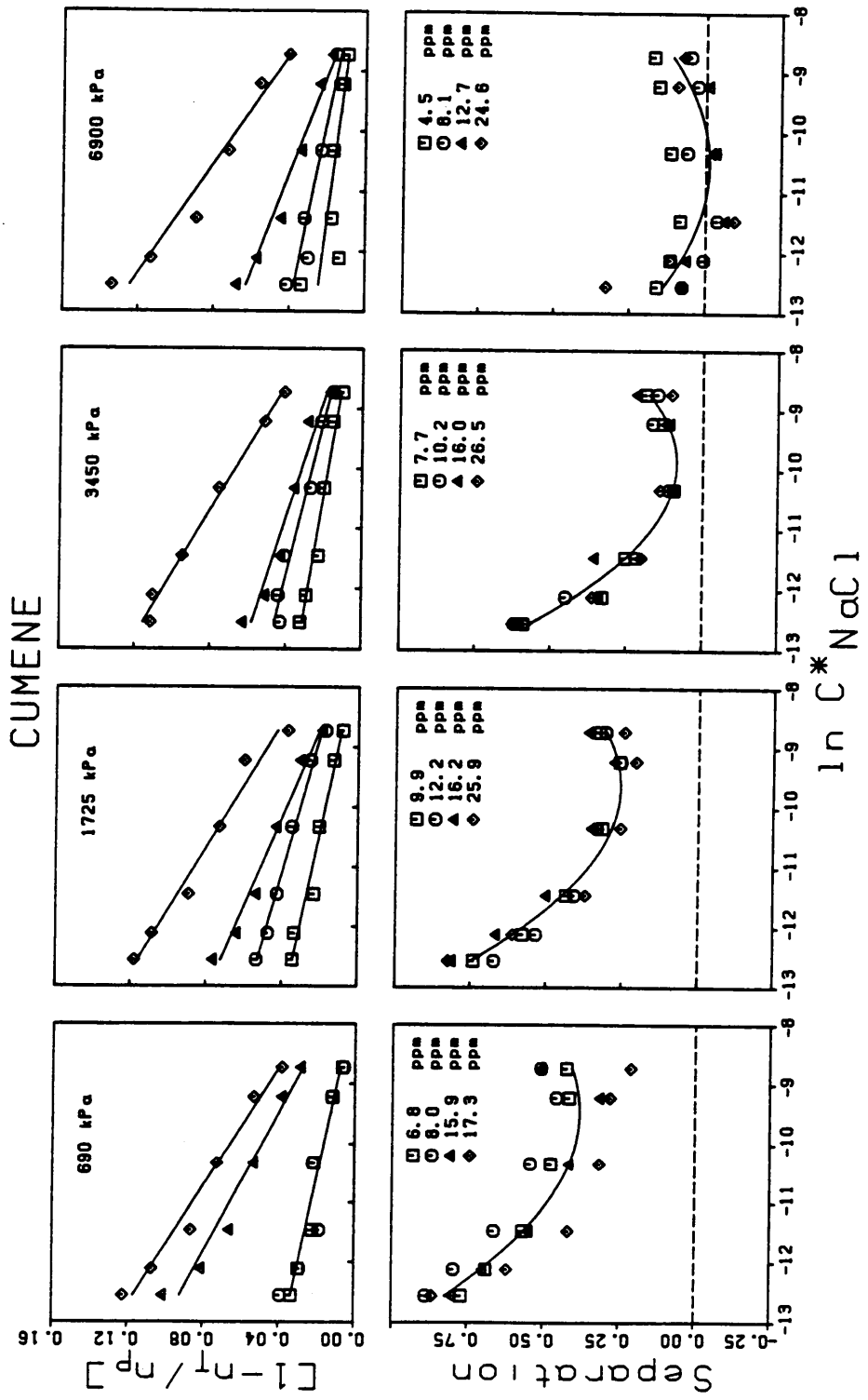
CUMENE
690 kPa
1725 kPa
3450 kPa
6900 kPa
[1-nt/np]
Separation
ln C*NaCl
6.8 ppm
8.0 ppm
15.9 ppm
17.3 ppm
9.9 ppm
12.2 ppm
16.2 ppm
25.9 ppm
7.7 ppm
10.2 ppm
16.0 ppm
26.5 ppm
4.5 ppm
8.1 ppm
12.7 ppm
24.6 ppm

confidence level. Comparing separation data over the range of pressures studied, it is observed that as the operating pressure increases the separation decreases.

At each pressure and for each concentration, as the pore size increases the extent of pore blocking decreases. The data have been fit to a first order (linear) relationship. A number of points are worthy of note. For any given operating pressure, the slope increases with increasing feed concentration. This observation is in contrast to the previously stated apparent concentration independence of separation. The effect of operating pressure on the extent of pore blocking is not immediately evident from Figure 8, due to the additional influence of concentration. The influence of pressure on extent of pore blocking is discussed below. By way of comparison, if a plot of $(1-n_T/n_P)$ versus ln C^*_{NaCl} were made for sodium chloride-water systems in the concentration range discussed here, the result would be a horizontal line at $(1-n_T/n_P)$ equals zero. At higher concentrations of sodium chloride in water, there would be a reduction in the ratio n_T/n_P due to osmotic pressure effects rather than the blocking of pores by solute molecules. However, the results would not necessarily follow a simple relationship such as that shown in Figure 8.

The data for the single-solute systems of toluene-water and cumene-water are illustrated in Figures 9 and 10, respectively. These results are similar to those for the benzene-water system. The shape and direction of the separation curves as a function of the pore size parameter ln C^*_{NaCl} are similar to those for benzene. Separation again decreases with increasing pressure and remains independent of concentration. Similarly, the decrease in extent of pore blocking with both increasing pore size and decreasing concentration are observed. Since cumene is much less soluble in water than either toluene or benzene (see Table 1), the concentrations of cumene were much lower. Even when these concentration differences are taken into consideration, differences are observed between the three solute-water systems. For any given pressure, concentration, and membrane, the separation

observed for the benzene-water system is less than that of the toluene-water system, which is less than the corresponding value for cumene-water. For similar molar concentrations, the extent of pore blocking increases in the order benzene < toluene < cumene, and the slope of the $(1 - n_T/n_p)$ versus ln C^*_{NaCl} plot increases in the same order.

For all three solutes there is a minimum in the separation versus ln C^*_{NaCl} curves. This minimum appears to occur, within experimental error, at an ln C^*_{NaCl} value of -9.75 for all solutes. The rate at which separation decreases and then increases with increasing pore size once again is ordered benzene < toluene < cumene.

By taking the concentration-independent average separation obtained for a given solute and membrane, it is possible to plot the data for all membranes and solutes as a function of pressure. These plots are illustrated in Figure 11. Note that the curves for membranes 3 to 6 are similar. Membranes 1 and 2 exhibit the same trend as the other membranes although the position of the curves are different. In particular, the curve for cumene-water with membrane 1 is concave downward whereas all the other curves are concave upward. The actual lines given in Figure 11 are third order curves which have been hand fit to emphasize the parallelism in the data and are not best-fit curves through the data points. Each data point in Figure 11, represents the average of several points (either 4 or 6 points) at different concentrations. For the three solutes, all membranes exhibit a decrease in separation as pressure is increased. As discussed in the INTRODUCTION, this decrease in separation with increasing pressure is characteristic of strong solute-membrane attraction. From a practical point of view, it is desirable to operate at low pressures to increase the separation; however, this decrease in pressure will also result in a decrease in flux.

The blocking of the pores on the membrane surface by sorbed solute can be treated in a more quantitative manner than presented above. The appropriate k value for the

Figure 11. Effect of operating pressure on the separation of benzene (□), toluene (O), and cumene (Δ) in single solute aqueous systems for the six cellulose acetate membranes annealed at different temperatures.

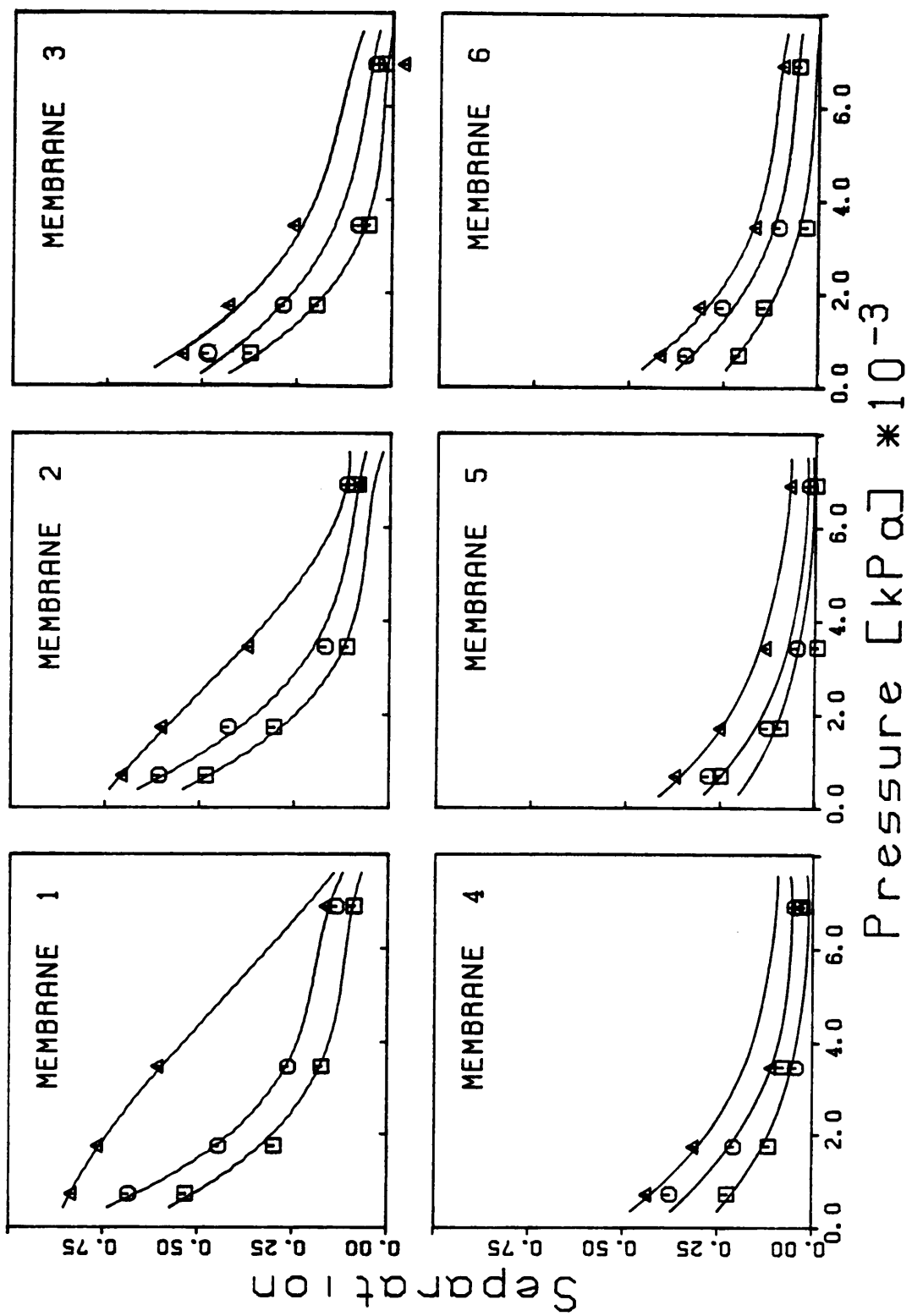
MEMBRANE 1
MEMBRANE 2
MEMBRANE 3
MEMBRANE 4
MEMBRANE 5
MEMBRANE 6
Separation
0.00
0.25
0.50
0.75
0.0
2.0
4.0
6.0
Pressure [kPa] *10-3

particular solute of interest was estimated for each cell (32) using Equation (5) and the known value of k for NaCl listed in Table 5. The values of D_{AB} for the three organic solutes were estimated by the method of Wilke and Chang (8). For the Wilke-Chang method it was necessary to estimate the molal volume of the solute at the normal boiling point, V_A, using the method of LeBas as outlined in reference (6). The diffusivity of sodium chloride in water is 1.61×10^{-9} m^2/s as reported in reference (15). Calculated values of V_A and D_{AB} are listed in Table 1. The boundary layer concentration, C_{A2}, and hence X_{A2}, were calculated from Equation (3) for each experiment.

For membranes 1 and 6, the extent of pore blocking versus X_{A2} is illustrated in Figures 12-14 for the three hydrocarbon solutes. These figures illustrate that extent of pore blocking is independent of pressure. Similar results were obtained for the other four membranes. Thus, pressure changes effect the same relative change both in solution flux and in pure water flux. Figures 12-14 suggest that a more quantitative treatment of the pore blocking data is possible. As stated in the INTRODUCTION and in previous publications (21-24), it is possible to relate the extent of pore blocking to the boundary concentration by Equation (40). This equation, which has the form of the Freundlich sorption isotherm, is consistent with the sorption phenomenon taking place between the solute and the membrane surface. By taking the natural logarithm of both sides of Equation (40), a linear equation is produced. Using a linear least-squares fit, the coefficients Z and ζ were calculated. The ζ values were all reasonably close to 1.0 (the average ζ is 1.035 ± 0.043 (95% confidence) based on 18 estimates), so the Z values were recalculated with ζ set equal to 1.0. Setting $\zeta = 1.0$ is equivalent to saying that the $(1-n_T/n_p)$ versus X_{A2} relationship can be represented by a straight line through the origin as indicated in Figures 12-14. These new Z values for all membranes are given in Table 6. The data in Table 6 demonstrate not only the dependence of Z on the average pore size but also the dependence of Z on the nonpolar or dispersive

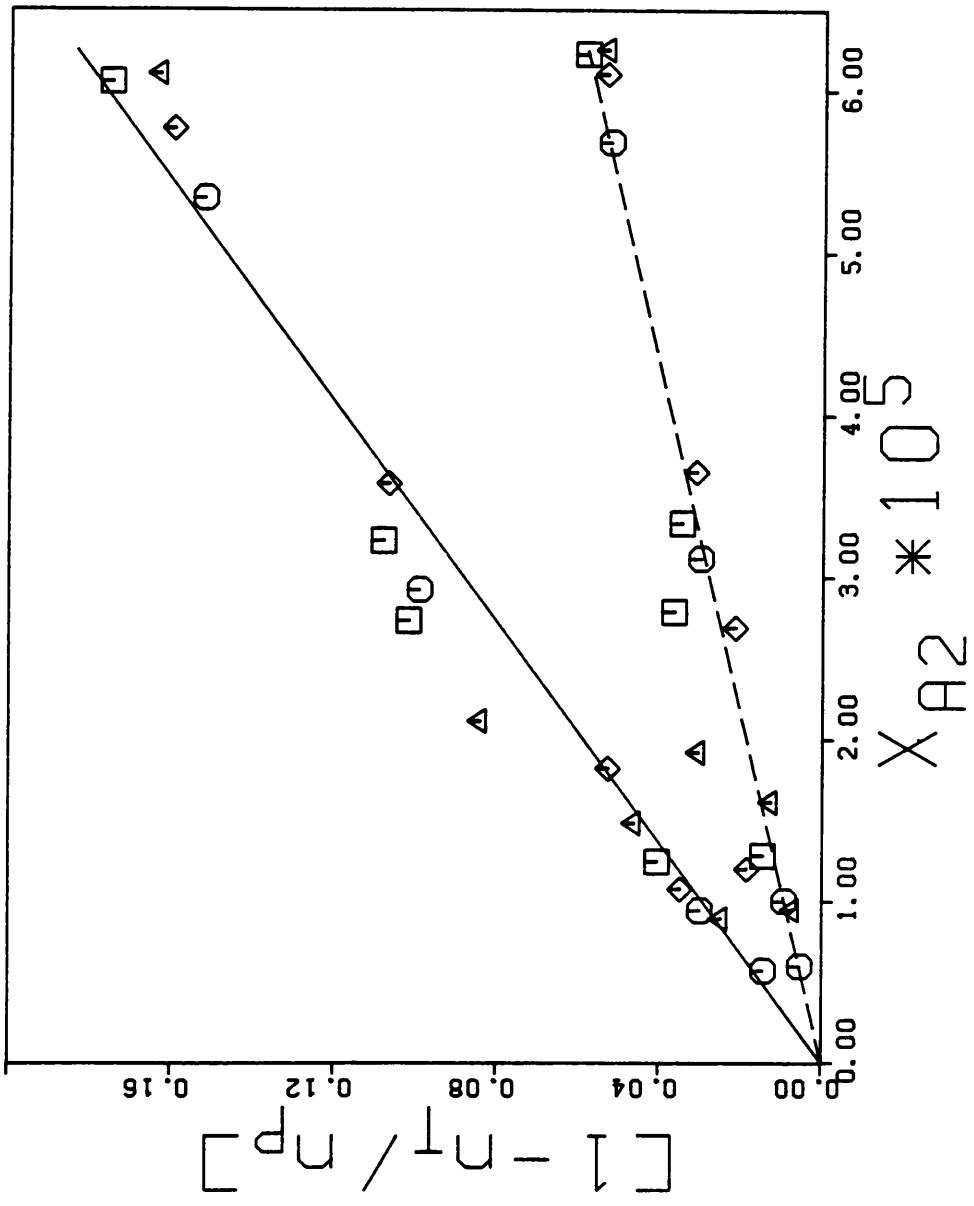

Figure 12. Correlation of extent of pore blocking, $(1 - n_T/n_P)$, and boundary layer concentration of benzene, X_{A2}, for two representative membranes of different pore size: (□) 690 kPa; (O) 1725 kPa, (Δ) 3450 kPa, (◇) 6900 kPa; (—) membrane 1; (---) membrane 6.

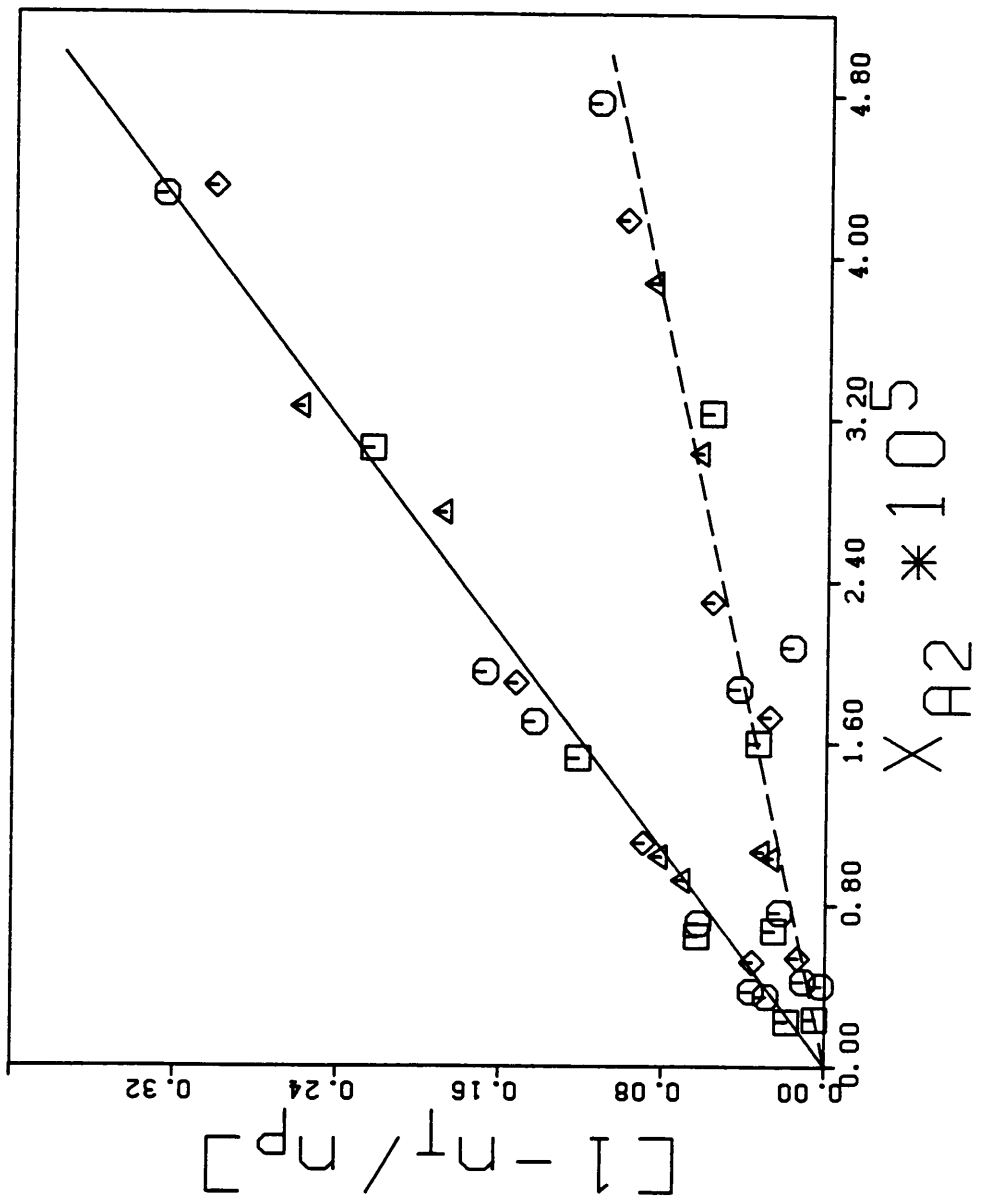

Figure 13. Correlation of extent of pore blocking, $(1 - n_T/n_P)$, and boundary layer concentration of toluene, X_{A2}, for two representative membranes of different pore size: (□) 690 kPa; (O) 1725 kPa, (Δ) 3450 kPa, (◇) 6900 kPa; (–) membrane 1; (---) membrane 6.

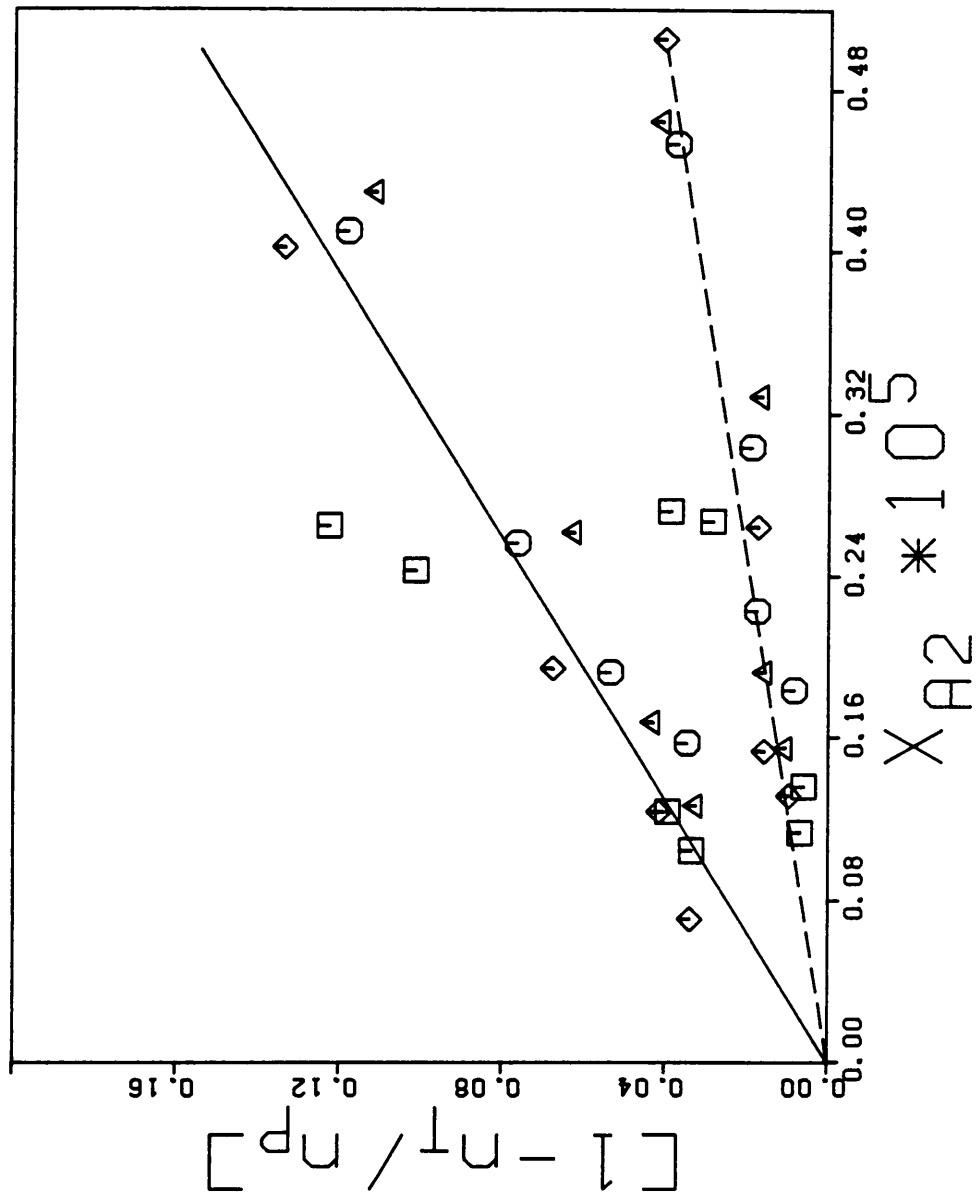

Figure 14. Correlation of extent of pore blocking, $(1 - n_T/n_P)$, and boundary layer concentration of cumene, X_{A2}, for two representative membranes of different pore size: (□) 690 kPa; (O) 1725 kPa, (Δ) 3450 kPa, (◇) 6900 kPa; (–) membrane 1; (---) membrane 6.

Table 6

Proportionality Constants from the Correlation of X_{A2} and the Extent of Pore Blocking

	Z		
Membrane	Benzene	Toluene	Cumene
1	2944	7538	30895
2	2501	6535	27566
3	2122	5525	23120
4	1696	4527	18721
5	1348	3592	13403
6	935	2183	8072

character of the solute. With the limited amount of data available, it is not possible to speculate on the exact nature of the relationship between Z and the dispersive character other than to state that Z increases with increasing solute dispersive character. The physical interpretation of this trend is that at identical molar concentrations benzene blocks the pore the least while cumene has the greatest ability to block the pore.

There are sufficient data to obtain the functionality between Z and ln C^*_{NaCl}. In Figure 15, this functionality is shown to be adequately represented by a linear relationship on a semi-logarithmic basis. Within experimental error, the slopes of these three lines appear to be identical. Figure 15 may be used to predict Z from the experimental ln C^*_{NaCl} data for any of the three solutes studied. Subsequent work with cyclic hydrocarbon solutes also followed Equation (40) with ζ equal to 1.0. The cyclic hydrocarbon data when plotted as in Figure 15 produced lines parallel to the aromatic hydrocarbon data (24). Therefore, in spite of the empirical nature of the treatment, Figure 15 and Equation (40) can be used to predict the extent of pore blocking when the solute is strongly attracted to the membrane material.

3.3 Interpretation of the Hydrocarbon Solute Data

The results presented above can be interpreted qualitatively based on a modified version of the preferential sorption-capillary flow model (2, 30b). The membranes are assumed to be porous. The flux and separation are determined by the number and size of pores, by the interactions between solute, solvent, and membrane, and by the relative mobility of solute and solvent in pores.

The trends in Figures 8-11 are consistent with the qualitative features of strong solute-membrane attraction. The solution flux is lower than the pure water flux due to pore blocking rather than to any significant osmotic pressure effects (the maximum osmotic pressure difference across the membrane in any of the experiments was about 3.5 kPa, which

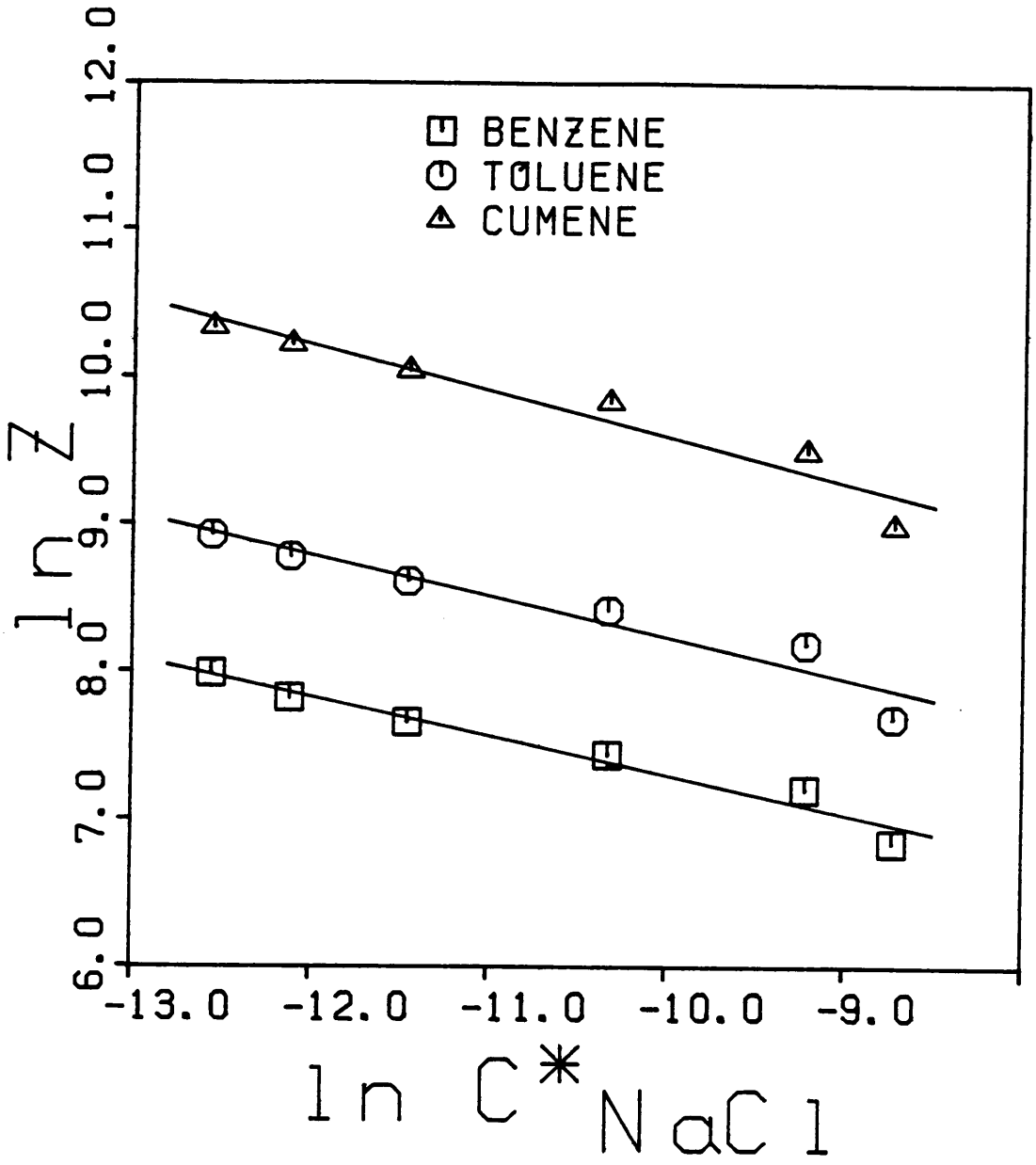

Figure 15. Correlation of proportionality constant, Z, and pore size parameter ln C^*_{NaCl}.

is much lower than the lowest operating pressure of 690 kPa). This effect is enhanced either by decreasing the pore size or by increasing the feed concentration. Both of these factors lead to a relative increase in the solute content in the pore and thus to a restricted solution transport through the pore.

In the highly concentrated region of solution near the membrane surface (referred to here as the interfacial region), the solute-membrane attraction forces decrease with distance from the membrane surface. Thus, solute mobility increases and solute concentration decreases with increasing distance from the membrane surface. In the limit, a point is reached at which solute mobility and concentration can be considered to be no longer under the influence of interfacial attractive forces. When a portion of this interfacial layer is transported through the pores of a membrane, the average solute mobility and the average solute concentration of the transported portion determine the flux and separation. If the average pore on the membrane surface is extremely small, the portion of solution transported is that region of high concentration and low mobility. As the average pore size is increased, the portion of the interfacial layer being transported increases to include less concentrated but more mobile solution. Thus, the average concentration in the pore decreases and the average solute mobility increases. Decreasing average concentration of the transported solution indicates increasing separation. Increasing solute mobility of the transported solution indicates decreasing separation. These two factors present opposing influences on separation as a function of pore size. Note that the solute in the region near the membrane is strongly attracted to the membrane and is relatively immobilized while the water remains relatively mobile. However, the velocity of the solution passing through the pore creates a shear force which strips the sorbed solute molecules from the surface and transports them.

The factors discussed above can be used to explain the results observed in the present study. The opposing factors of decreasing concentration and increasing mobility with

increasing distance from the surface suggest that separation as a function of pore size can exhibit a local minimum as observed in Figures 8-10. The initial section of decreasing separation with increasing pore size represents the transport of the lower portions of the interfacial layer. In this region, the mobility of the solute is a stronger function of distance than is the concentration; thus, solute mobility determines the separation. The section of the curve with increasing separation as pore size increases represents the transport of a larger portion of the interfacial layer. In this region, the solute concentration is a stronger function of distance than is the mobility; thus, the average solute concentration in the pore determines the separation. Between these two sections of the curves there is a minimum where the two opposing factors cancel.

For a membrane with a given average porosity, increasing the pressure increases the velocity of the solution through the pore, resulting in an increased flux. The increased velocity causes increased solute mobility due to shear of the concentrated interfacial layer; thus, separation decreases with increasing pressure as observed in Figures 8-11. The solute-water separation may be positive, negative, or zero depending upon the system and specific operating conditions. When these factors are such that the solute-membrane interaction is relatively strong, the solute is immobilized and the permeating water leads to positive separation. When these factors are such that the solute-membrane interactions are relatively weak, the solute enriched solution in the interfacial region is carried through the pore with less resistance, resulting in negative separation. Balancing these two factors produces zero separation. The solution flux is significantly less than the pure water flux because the solute molecules sorbed to the pore wall tend to decrease the effective pore diameter. This phenomenon is known as the pore blocking effect.

In comparing the present work to aromatic hydrocarbon-water-cellulose acetate studies reported in the literature (2), a number of points are of interest. The present findings

are in agreement with the previously reported results in that for any given system the separation is pressure dependent. However, Matsuura and Sourirajan (2) also report a pressure dependence of the extent of pore blocking; in the present study no such pressure dependence was found (see Figures 12-14). Instead, the extent of pore blocking was found to be concentration dependent (see Figures 8-10). The discrepancy can be explained by the fact that Matsuura and Sourirajan treated a range of feed concentrations (36 to 64 ppm benzene, 19 to 53 ppm cumene) as one concentration. Evidently, a different concentration was used for each pressure study; thus, the concentration effect was incorrectly interpreted as a pressure effect. The present study demonstrates the significant role that concentration plays in determining membrane performance in systems showing strong solute-membrane affinity. Since the extent of pore blocking is primarily a function of the physicochemical interaction of the solute and the membrane, it is more logical that the extent of pore blocking be concentration dependent as reported here rather than pressure dependent as reported earlier (2).

The dependence of the extent of pore blocking on the physicochemical nature of the solute is evident when Figures 12-14 are compared. All other parameters being equal, the extent of pore blocking is least with the more mobile solute (benzene) and greatest with the least mobile solute (cumene).

In comparing the results in previous sections, certain differences in behavior were noted for the three solutes. The order of these differences is always benzene < toluene < cumene. This order is the same as the order of the dispersive character of the solute and, therefore, the order of solute-membrane affinity. Thus, the dispersive character of the solute provides a rough guide for predicting the reverse osmosis performance of the aromatic hydrocarbon-water-cellulose acetate membrane system. In order to obtain a more

quantitative relationship between performance and dispersive character, data for more solutes are required.

3.4 Membrane Compaction Analysis

The dependence of the pure water permeability coefficient, A, on the operating pressure is illustrated in Figure 16 for each of the membranes. As predicted by Equation (15), a linear semilogarithmic relationship is obtained. Each point on the graph represents the average value of several data obtained at different times under the same conditions. Ranging from 1.2×10^{-5} to $3.8 \times 10^{-5}\,kPa^{-1}$, the values of γ obtained are comparable with those reported in the literature by Sourirajan (30b) which ranged from 3.0×10^{-5} to $6.0 \times 10^{-5}\,kPa^{-1}$. Therefore, Equation (15) appears to be valid for the cellulose acetate membranes used in this study.

Some of the models examined in this study make the assumption that no membrane compaction is occurring. Over the range of pressures studied, the A values decreased between 5% for the least permeable and 10% for the most permeable membrane. It is clear that A is not independent of pressure for the membranes used in this study.

3.5 Parameter Estimation Methods

Before discussing the details of the transport analysis, some general information is given here about the parameter estimation methods. For the majority of the models, the International Mathematics and Statistical Library (75) IMSL routine ZXSSQ has been used to estimate the unknown parameters. This routine is an unconstrained non-linear parameter estimation routine which uses a modified Levenberg-Marquardt algorithm (76, 77) that does not require the user to supply explicit partial derivatives. In all cases the routine acts to minimize the sum of the square error between f′ calculated and f′ experimental by adjusting

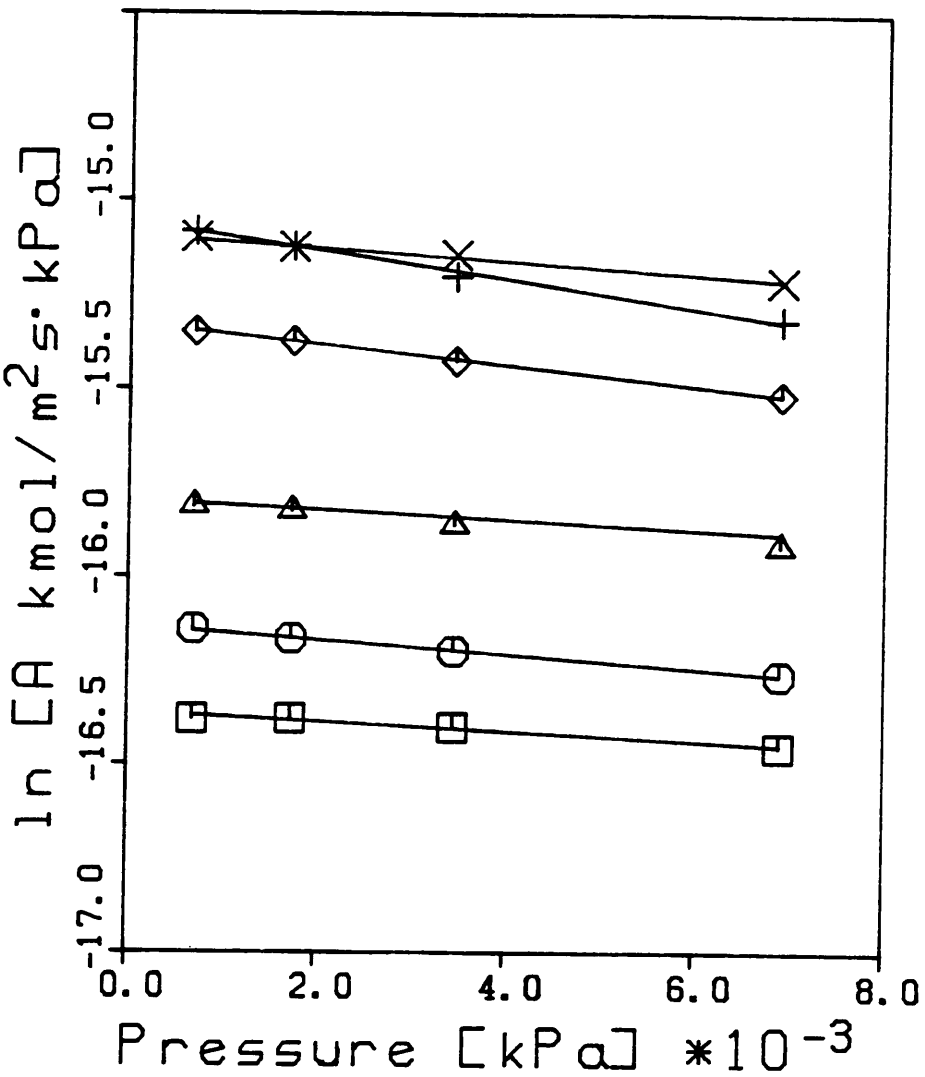

Figure 16. Membrane compaction as represented by the decrease in the pure water permeability coefficient, A, as a function of increasing operating pressure for the six cellulose acetate membranes.

(□) membrane 1; (O) membrane 2; (Δ) membrane 3; (◇) membrane 4; (+) membrane 5; (X) membrane 6.

the model parameters. For specific models, the dependence of f′ on system parameters is written as 1/f′, but the program always uses the error in f′ for the minimization so that all the models can be compared equally. The standard deviation of the error was calculated (74) as:

$$s = (\Sigma (f' - f'_{cal})^2/d.f.)^{1/2} \tag{74}$$

where d.f. is the number of degrees of freedom, which is given by the number of data minus the number of parameters estimated.

Due to the sensitivity of the surface force-pore flow model to the adjustable parameters, an unconstrained optimization code was found to be undesirable. Therefore, a constrained optimization code called GRG2 (78) was used. This algorithm uses a Generalized Reduced Gradient method (79) which allows equality and inequality constraints to be incorporated into the optimization. Supplying partial derivatives is optional in this program. With GRG2, the adjustable parameters could be bound to reasonable limits in order to prevent the algorithm from choosing unreasonably small or large values.

3.6 Phenomenological Transport Models

In this section the results of analyzing the aromatic hydrocarbon data by phenomenological transport models of irreversible thermodynamics are discussed.

3.6.1 Irreversible Thermodynamics - Phenomenological Transport Relationship

The form of the irreversible thermodynamics-phenomenological transport relationship (IT-PT) as discussed in Section 1.2.2 is:

$$\frac{1}{f'} = \frac{1}{\sigma} + \left(\frac{\ell_\pi}{\ell_p} - \sigma^2 \right) \left(\frac{\ell_p}{\sigma} \right) \pi_2 \left(\frac{1}{J_v} \right) \tag{20}$$

The three parameters in the model are ℓ_p, σ, and ℓ_π. The model is of Form a) as represented by Equation (68), which suggests a linear relationship between $1/f'$ and $1/J_v$ at constant concentration (actually constant π_2). For the aromatic hydrocarbon data it was difficult to maintain a constant concentration for different experiments. Therefore, it was necessary to take the concentration into account when analyzing the aromatic hydrocarbon data. The data were analyzed by three different but related methods. In the first method, any possible concentration dependence was ignored and the separation f' and the volume flux J_v were correlated by Equation (68) with constant coefficients. In the second approach, the π_2 term was accounted for explicitly. Finally, in the third method, the concentration dependence of ℓ_p was taken into account. These three methods are discussed below separately.

For all of the phenomenological transport models, the ℓ_p parameter was estimated from the pure water data. For this purpose Equation (18), or equivalently for dilute solution Equation (10), was used. The results are listed in Table 5 for each of the six cellulose acetate membranes.

Method A. When the linear relationship between $1/f'$ and $1/J_v$ is assumed with constant E_0 and E_1 coefficients, the model is designated as the IT-PT-A model. The values of E_0, E_1, and s estimated for each solute and membrane are summarized in Table 7. The shape of the curves thus calculated can be compared to the experimental data on a f' versus J_v plot in Figures 17-19 for the three solutes. The model appears to do a reasonable job of representing the data. The σ values presented in Table 7 are an estimate of the separation at infinite flux for each solute and membrane. The σ values increase, for the different solutes, in the order benzene $<$ toluene $<$ cumene, which is the order of increasing nonpolar or dispersive character for the solutes (23). For a given solute, σ increases with increasing annealing temperature, except for membrane 6. The σ values for membrane 6 are larger than would be expected based on the

Table 7

Parameters for the Phenomenological Transport (IT-PT-A) and Extended Solution-Diffusion (ESD) Models

Film	Solute	E_0	$E_1 \times 10^6$	s	$\sigma = 1/E_0$	$\ell_\pi^a \times 10^7$	$\ell_{AP}^b \times 10^{12}$	$\frac{D_{AM}K}{\Delta x} \times 10^6$
			m/s			(m/s kPa)	$\left(\frac{\text{kmol}}{\text{m}^2\text{s kPa}}\right)$	m/s
					(IT – PT – A)	(IT – PT – A)	(ESD)	(ESD)
1	Benzene	5.626	−3.128	0.114	0.1777	−1.444	1.632	−0.5560
1	Toluene	3.550	−1.745	0.120	0.2817	−2.164	0.8407	−0.4915
1	Cumene	2.131	−0.8624	0.215	0.4693	−14.15	0.07826	−0.4045
2	Benzene	6.215	−4.517	0.090	0.1609	−1.887	2.035	−0.7268
2	Toluene	4.120	−2.686	0.120	0.2427	−2.871	1.083	−0.6519
2	Cumene	3.073	−1.934	0.184	0.3254	−22.00	0.1215	−0.6294
3	Benzene	10.33	−11.56	0.093	0.0968	−2.906	3.079	−1.119
3	Toluene	6.295	−6.683	0.103	0.1589	−4.676	1.691	−1.062
3	Cumene	4.845	−4.489	0.202	0.2064	−34.99	0.2010	−1.001
4	Benzene	12.42	−20.26	0.071	0.0805	−4.237	4.695	−1.631
4	Toluene	8.249	−14.42	0.098	0.1212	−7.700	2.646	−1.748
4	Cumene	6.262	−10.32	0.135	0.1597	−57.62	0.3187	−1.648
5	Benzene	29.84	−84.10	0.095	0.0034	−7.320	6.030	−2.818
5	Toluene	12.88	−32.57	0.075	0.0776	−11.14	3.393	−2.529
5	Cumene	5.609	−10.31	0.098	0.1783	−64.27	0.3809	−1.838
6	Benzene	7.538	−11.63	0.116	0.1327	−4.007	5.960	−1.543
6	Toluene	4.372	−5.876	0.119	0.2287	−5.918	3.125	−1.344
6	Cumene	2.796	−2.299	0.110	0.3577	−28.74	0.3279	−0.8222

a ℓ_π has been calculated assuming an average value of π_2 = 3.85, 2.27, and 0.286 kPa for benzene, toluene, and cumene, respectively.

b ℓ_{AP} has been calculated assuming an average value of $C_{A2} = 1.55 \times 10^{-3}$, 0.916×10^{-3}, and 0.115×10^{-3} kmol/m^3 for benzene, toluene, and cumene, respectively.

Figure 17. The effect of volume flux on separation for the benzene-water-cellulose acetate system at 25°C. (□) experimental points; (—) irreversible thermodynamics-phenomenological transport model (IT-PT-A) and the extended solution-diffusion model (ESD); (— · — ·) irreversible thermodynamics - Kedem Spiegler model (IT-KS) and the three parameter finely-porous model (FPM-3); (---) solution-diffusion model (SD) and the Kimura-Sourirajan analysis model (KSA).

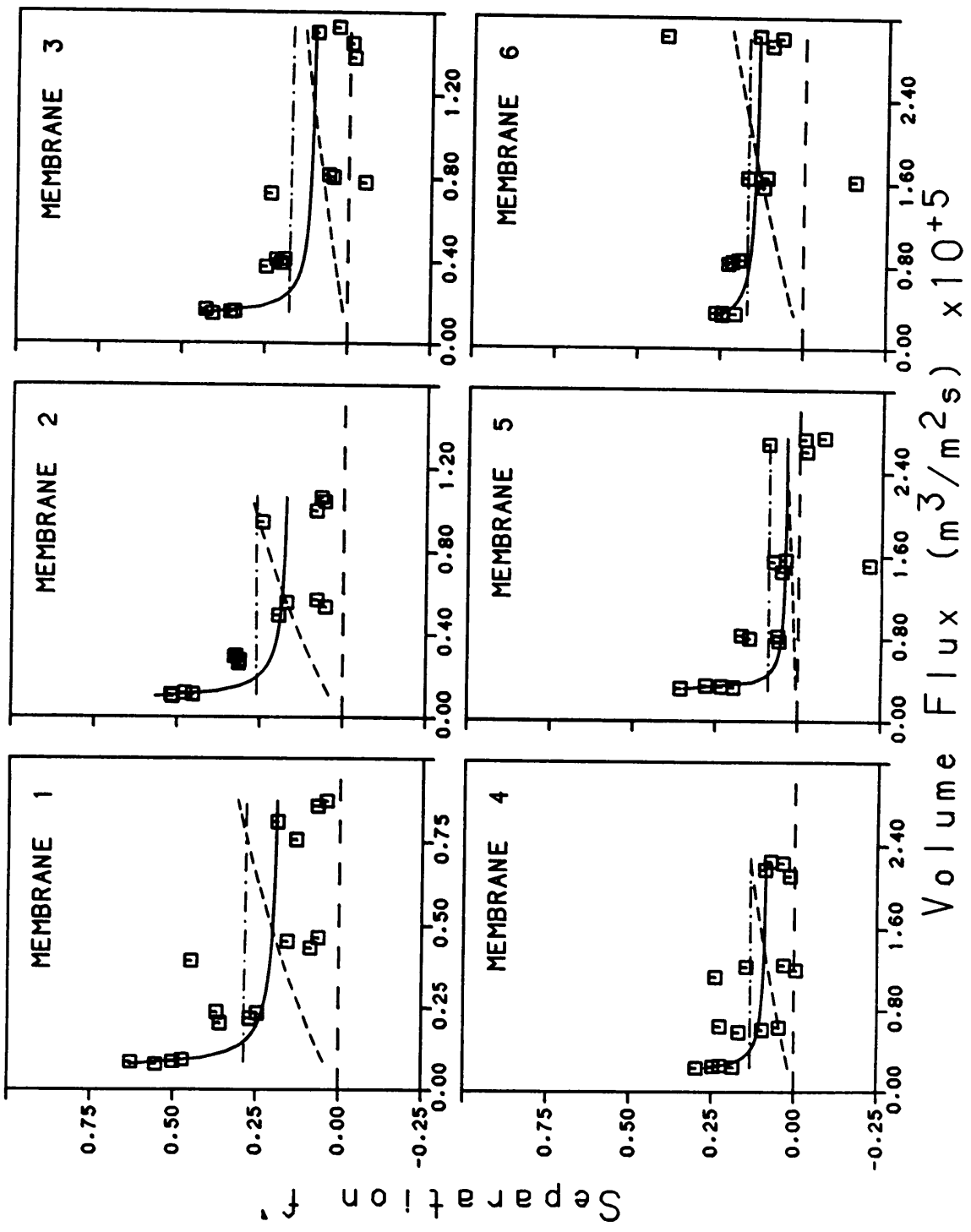
MEMBRANE 1
MEMBRANE 2
MEMBRANE 3
MEMBRANE 4
MEMBRANE 5
MEMBRANE 6
Separation f'
Volume Flux (m3/m2s) x10+5
0.75
0.50
0.25
0.00
-0.25
0.00
0.25
0.50
0.75
0.40
0.80
1.20
1.60
2.40

Figure 18. The effect of volume flux on separation for the toluene-water-cellulose acetate system at 25°C. (□) experimental points; (—) irreversible thermodynamics-phenomenological transport model (IT-PT-A) and the extended solution-diffusion model (ESD); (— · — ·) irreversible thermodynamics - Kedem Spiegler model (IT-KS) and the three parameter finely-porous model (FPM-3); (---) solution-diffusion model (SD) and the Kimura-Sourirajan analysis model (KSA).

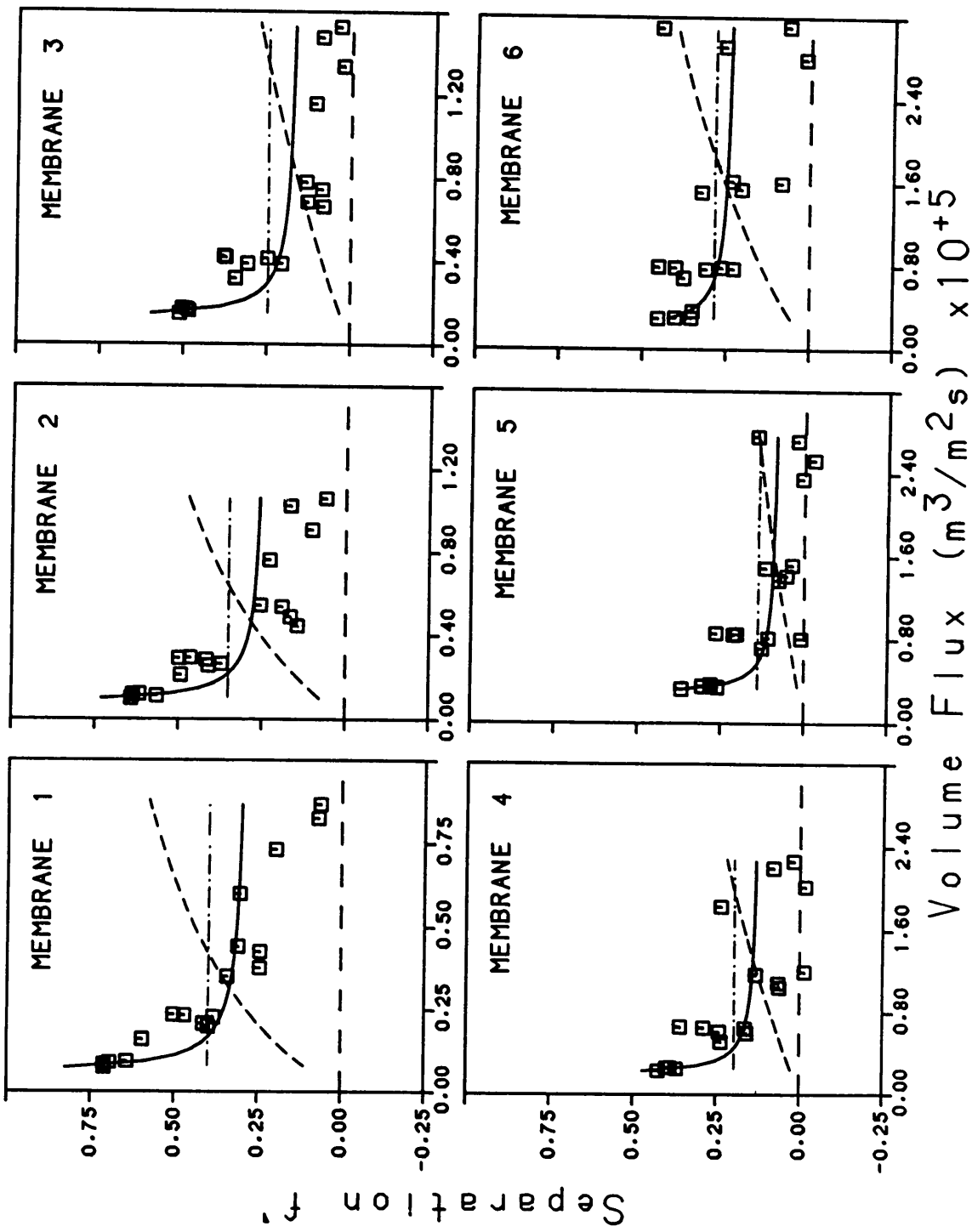
MEMBRANE 1
MEMBRANE 2
MEMBRANE 3
MEMBRANE 4
MEMBRANE 5
MEMBRANE 6
Separation f'
Volume Flux (m3/m2s) x10+5
0.75
0.50
0.25
0.00
-0.25
0.00
0.25
0.50
0.75
0.40
0.80
1.20
1.60
2.40

Figure 19. The effect of volume flux on separation for the cumene-water-cellulose acetate system at 25°C. (□) experimental points; (—) irreversible thermodynamics-phenomenological transport model (IT-PT-A) and the extended solution-diffusion model (ESD); (— · — ·) irreversible thermodynamics - Kedem Spiegler model (IT-KS) and the three parameter finely-porous model (FPM-3); (---) solution-diffusion model (SD) and the Kimura-Sourirajan analysis model (KSA).

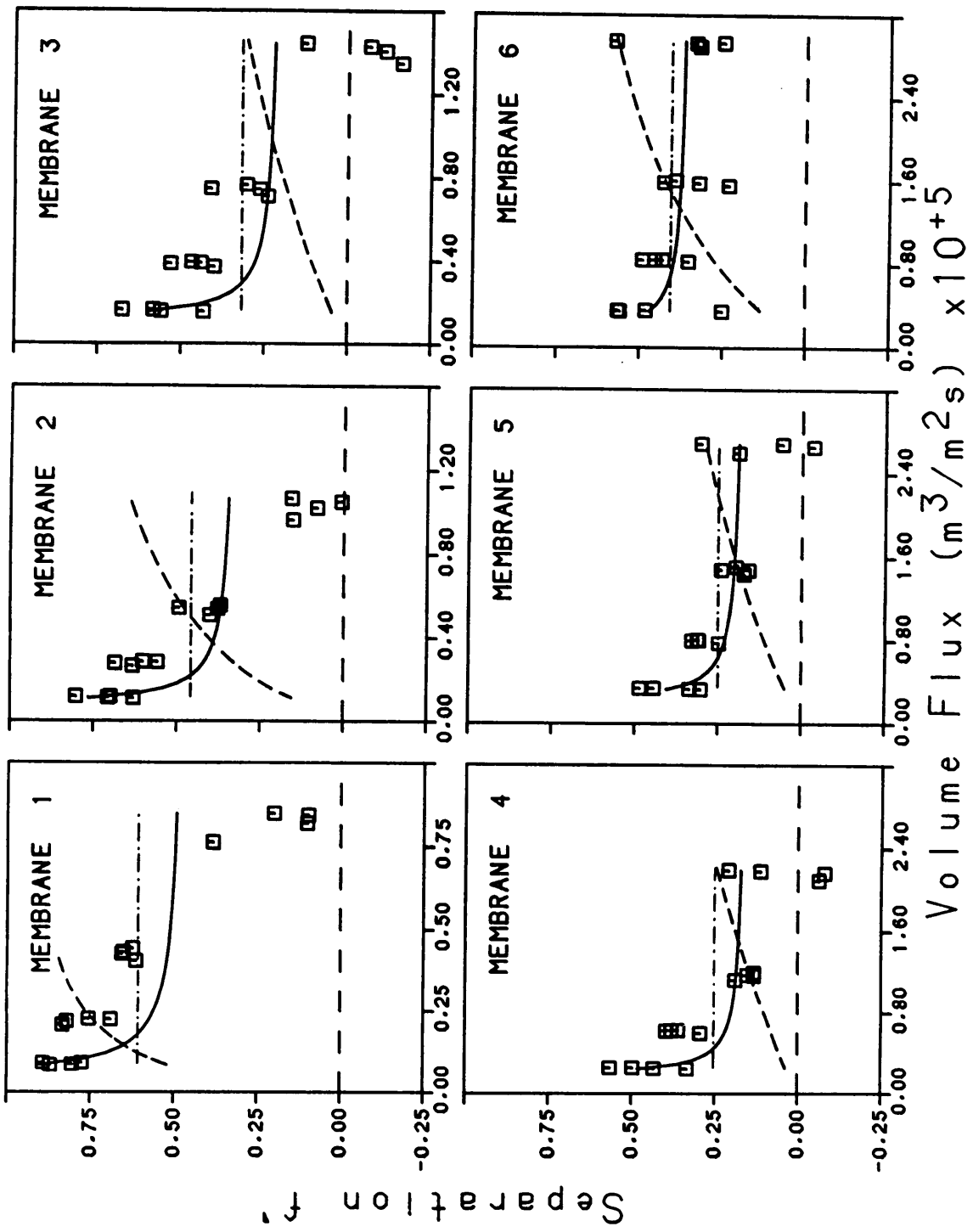
MEMBRANE 1
MEMBRANE 2
MEMBRANE 3
MEMBRANE 4
MEMBRANE 5
MEMBRANE 6
Separation f'
Volume Flux (m3/m2s) x10+5
0.75
0.50
0.25
0.00
-0.25
0.00
0.25
0.50
0.75
0.40
0.80
1.20
1.60
2.40

trend observed for the other membranes. It is not known if the results for membrane 6 represents a trend or if there is some other reason for the observed results. Further work is required to clarify this point. If the experiments had been performed such that C_{A2}, and hence π_2, were constant for all the experiments for each solute, then ℓ_π could be calculated from the known ℓ_p, σ, and $E_1 = (\ell_\pi/\ell_p - \sigma^2)(\ell_p/\sigma)\pi_2$ values. Due to the difficulty of making up and maintaining a predetermined concentration of these solutions, it was not feasible to do several experiments at the same concentration. Even if sufficient means were employed to ensure that the same feed concentration was used for experiments at different operating conditions, this effort would not guarantee a constant boundary layer concentration. Therefore, strictly speaking, π_2 cannot be assumed to be constant. However, for the purpose of estimating ℓ_π for the IT-PT-A model, it was assumed that π_2 was constant for each solute. The value of π_2 used was the arithmetic average of the π_2 values calculated for all the experiments for each solute. Calculated ℓ_π values, listed in Table 7, are all negative. The absolute value of ℓ_π increases in the order benzene < toluene < cumene and decreases with increasing annealing temperature (again membrane 6 is an exception). According to the original definition of the IT model, it is impossible for the ℓ_π coefficient to be negative (28, 40). Negative ℓ_π values imply that solute is being driven against the concentration gradient. Since this result contradicts the original assumptions of the model, it casts doubt on the interpretation of the results by the IT-PT-A model. Changing the value of π_2 used to estimate ℓ_π only changes the magnitude and not the sign of the ℓ_π parameter. Therefore, the conclusions drawn are not influenced by the assumption that π_2 is constant.

Method B. A more logical approach to the application of the IT-PT model is to remove the concentration effect of the π_2 term and group it with J_v. Therefore, a plot of f' versus (J_v/π_2) is

suggested with the three parameters ℓ_p, σ, and $(\ell_\pi/\ell_p - \sigma^2)(\ell_p/\sigma)$. This approach is designated as the IT-PT-B model.

The results for the IT-PT-B model, summarized in Table 8, are somewhat similar to those obtained for the IT-PT-A model. The data plotted in Figures 20-22 as f' versus J_v/π_2 are similar to Figures 17-19 for the IT-PT-A model. Comparing the plots for the IT-PT-A and IT-PT-B models, it may be stated that there is considerably more scatter in the data for the IT-PT-B model. In fact, the scatter in the plots for the IT-PT-B model is large enough that it is questionable whether a line should even be drawn through the data. The σ parameters are marginally larger and follow the same trends as the values obtained for the IT-PT-A model. The ℓ_π values calculated for the IT-PT-A and IT-PT-B models are different but follow the same trends. In this case, it is not necessary to assume that either C_{A2} or π_2 is constant since the effect of varying π_2 is included in the (J_v/π_2) term. The s values are larger for the IT-PT-B model than they are for the IT-PT-A model, which is expected based on the scatter in the data for the IT-PT-B model. This result implies that the grouped parameter $(\ell_\pi/\ell_p - \sigma^2)(\ell_p/\sigma)\,\pi_2$ is less concentration dependent than $(\ell_\pi/\ell_p - \sigma^2)(\ell_p/\sigma)$. Otherwise, the σ and ℓ_π values are similar for the IT-PT-A and IT-PT-B model and the general conclusions are the same. The negative ℓ_π values are inconsistent with the basic assumptions of the model.

It is apparent that neither the IT-PT-A nor the IT-PT-B model is satisfactory because of the negative ℓ_π parameters calculated. In the estimation of the parameters it has been implicitly assumed that the parameters are all constant, independent of operating pressure and concentration. In fact, one might suspect that ℓ_p should decrease with increasing concentration as indicated by the lowered flux in the presence of the solute. The next section presents the results obtained when the concentration influence on ℓ_p is included in the model.

Table 8

Parameters for the Irreversible Thermodynamics - Phenomenological Transport (IT-PT-E) Model

Film	Solute	E_0	$E_1 \times 10^6$ (m/s kPa)	s	$\sigma = 1/E_0$	$\ell_{II} \times 10^7$ (m/s kPa)
1	Benzene	4.113	−0.2332	0.163	0.2431	−0.5657
1	Toluene	2.871	−0.2784	0.180	0.3483	−0.9666
1	Cumene	2.002	−2.250	0.227	0.4995	−11.24
2	Benzene	4.532	−0.3373	0.141	0.2207	−0.7427
2	Toluene	3.272	−0.4109	0.178	0.3056	−1.254
2	Cumene	2.720	−4.310	0.214	0.3676	−15.84
3	Benzene	6.971	−0.8082	0.134	0.1435	−1.159
3	Toluene	4.755	−0.9857	0.159	0.2103	−2.073
3	Cumene	4.011	−9.519	0.235	0.2493	−23.73
4	Benzene	9.234	−1.693	0.080	0.1083	−1.833
4	Toluene	6.072	−2.081	0.137	0.1647	−3.426
4	Cumene	5.019	−18.65	0.172	0.1992	−37.16
5	Benzene	15.15	−4.582	0.120	0.0660	−3.024
5	Toluene	9.010	−4.671	0.108	0.1110	−5.184
5	Cumene	4.686	−17.42	0.125	0.2134	−37.17
6	Benzene	6.494	−1.093	0.120	0.1540	−1.682
6	Toluene	3.893	−1.165	0.127	0.2569	−2.989
6	Cumene	2.557	−1.724	0.117	0.3911	−6.735

Figure 20. The effect of the volume flux to osmotic pressure ratio, J_v/π_2, on separation for the benzene-water-cellulose acetate system at 25°C. (□) experimental points; (—) irreversible thermodynamics-phenomenological transport model (IT-PT-B).

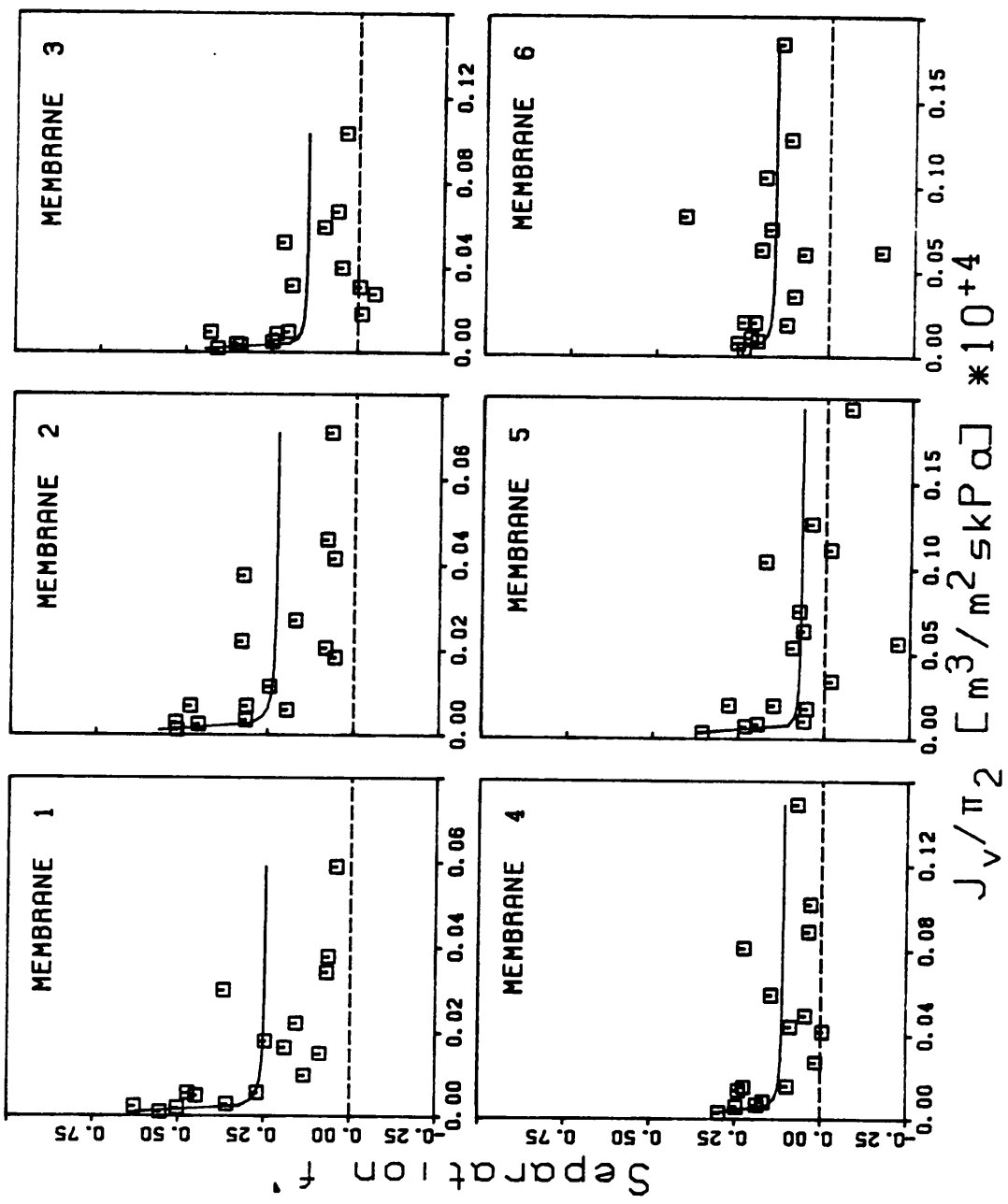
MEMBRANE 1
MEMBRANE 2
MEMBRANE 3
MEMBRANE 4
MEMBRANE 5
MEMBRANE 6
Separation f
J_v/π_2 [$m^3/m^2 s kPa$] *10+4

Figure 21. The effect of the volume flux to osmotic pressure ratio, J_v/π_2, on separation for the toluene-water-cellulose acetate system at 25°C. (□) experimental points; (—) irreversible thermodynamics-phenomenological transport model (IT-PT-B).

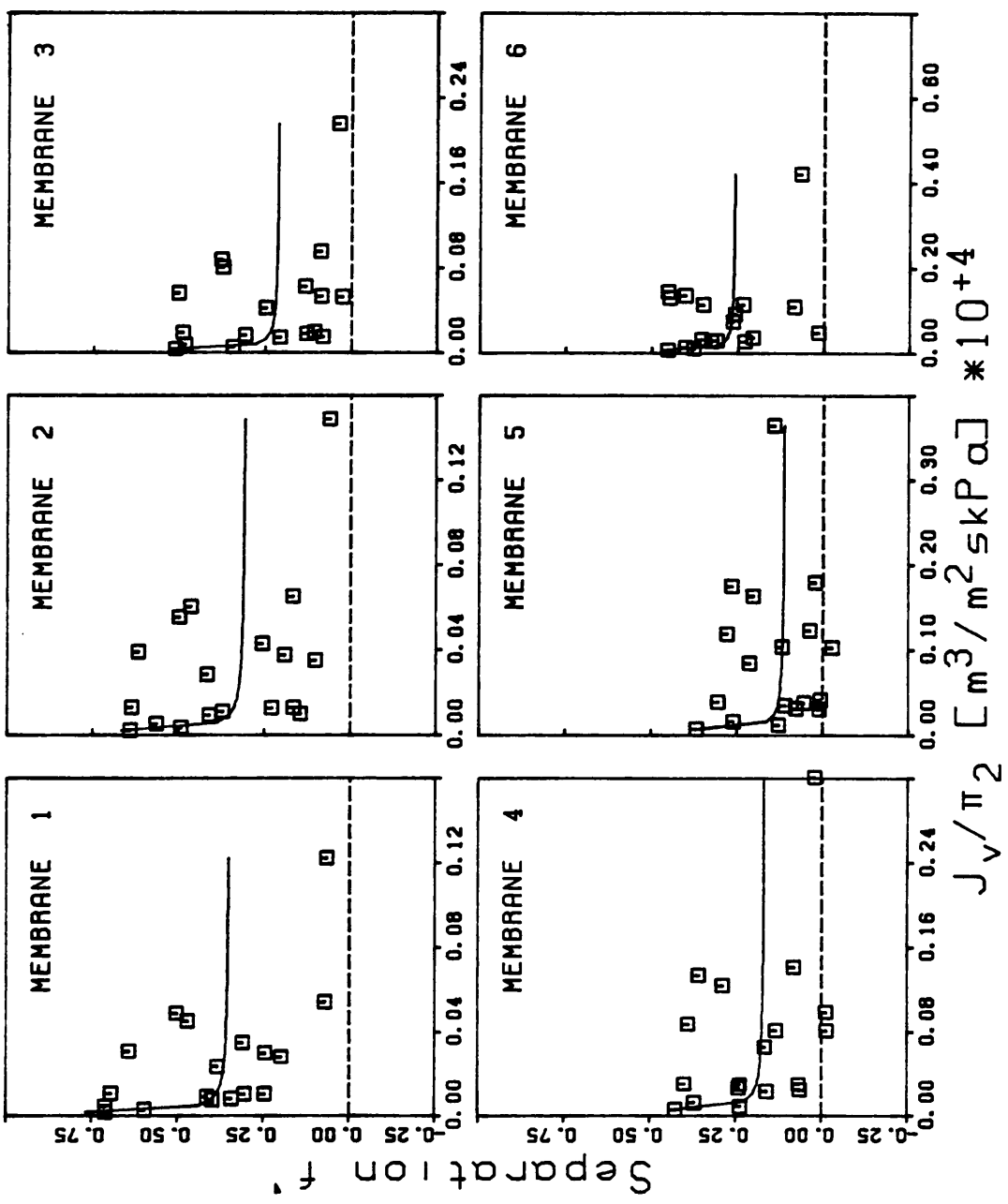
MEMBRANE 1
MEMBRANE 2
MEMBRANE 3
MEMBRANE 4
MEMBRANE 5
MEMBRANE 6
Separation f'
J_v/π_2 [$m^3/m^2 s kPa$] *10^{+4}

Figure 22. The effect of the volume flux to osmotic pressure ratio, J_v/π_2, on separation for the cumene-water-cellulose acetate system at 25°C. (□) experimental points; (—) irreversible thermodynamics-phenomenological transport model (IT-PT-B).

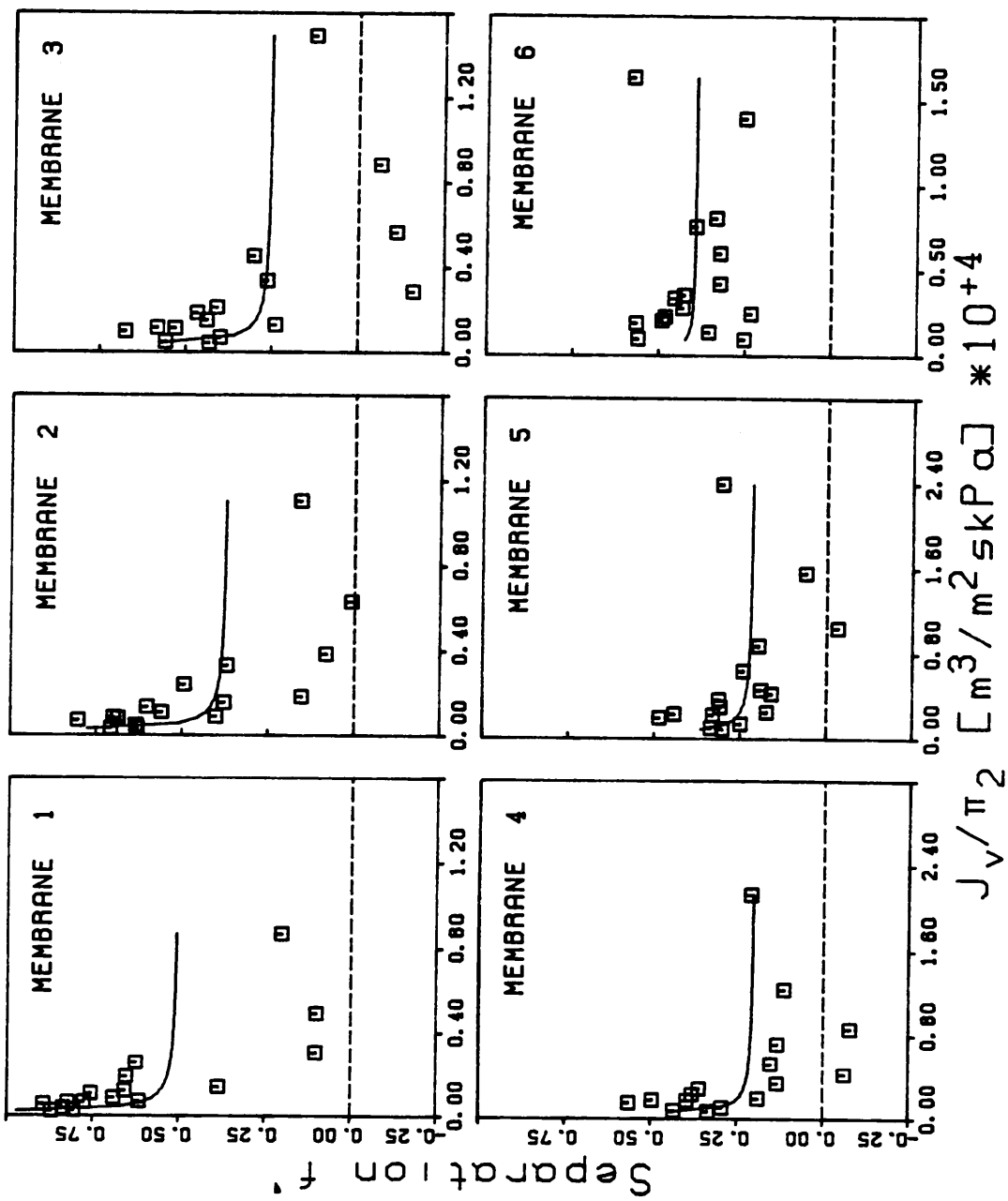
MEMBRANE 1
MEMBRANE 2
MEMBRANE 3
MEMBRANE 4
MEMBRANE 5
MEMBRANE 6
Separation f
J_v/π_2 [$m^3/m^2 s kPa$] *10+4

Method C. In order to investigate the possibility of incorporating a concentration dependent ℓ_p parameter into the IT-PT model, a further re-arrangement of the model was made. This approach is designated as the IT-PT-C model. In the present case, $\Delta\pi$ and f' values are such that $\Delta P >> \sigma\Delta\pi$ (note that theoretically σ is less than or equal to 1 (41)) and Equation (18) can be rewritten as:

$$J_v = \ell_p \Delta P \tag{75}$$

By substituting for ℓ_p in Equation (20) using Equation (75), the ℓ_p parameter can be removed from the model. The resulting equation is:

$$\begin{aligned} 1/f' &= 1/\sigma + (\ell_\pi \Delta P/J_v - \sigma^2)(J_v \pi_2/\sigma \Delta P)(1/J_v) \\ &= 1/\sigma - \sigma(\pi_2/\Delta P) + (\ell_\pi/\sigma)(\pi_2/J_v) \end{aligned} \tag{76}$$

Data for f', J_v, ΔP, and π_2 may be used to estimate the two remaining parameters σ and ℓ_π. In essence, the experimental value for ℓ_p (approximated by $J_v/\Delta P$) is used for each experiment. Any concentration dependence that ℓ_p may have is accounted for explicitly.

The data for each solute and membrane were fit to Equation (76). The results obtained were the same as the results for the IT-PT-B model within 3 digits accuracy. This result occurs because the magnitude of the ℓ_π and $\sigma^2\ell_p$ terms in Equation (19) are such that:

$$\ell_\pi >> \sigma^2 \ell_p \tag{77}$$

Because of the dominance of the ℓ_π parameter, the ℓ_p term (or equivalently $J_v/\Delta P$ term) has little influence on the model. This means that including a description of the concentration dependence of ℓ_p will not improve the ability of the model to describe the aromatic hydrocarbon data.

As mentioned in the INTRODUCTION the IT-PT relationship contains the assumption that the linear laws of IT may be applied across the thickness of the membrane. This assumption may not be valid for reverse osmosis type membranes where there are large

concentration gradients across the membrane. The model discussed in the next section avoids this problem.

3.6.2 Irreversible Thermodynamics - Kedem Spiegler Relationship

When the linear equations of IT are written for a differential element of membrane thickness and then integrated over the total membrane thickness, the equations known as the Kedem-Spiegler model result. The relationship between f' and J_v predicted by the IT-KS model is:

$$\frac{1}{f'} = \frac{1 - \sigma \exp[-(1-\sigma)(\Delta x/p_A) J_v]}{\sigma\{1 - \exp[-(1-\sigma)(\Delta x/p_A) J_v]\}} \tag{25}$$

which is of Form b) represented by Equation (69). The three adjustable parameters in the model are ℓ_p, σ, and $\Delta x/p_A$.

The IT-KS model was found to be unable to describe functionally the reverse osmosis data for aromatic hydrocarbon solutes. When the separation, f', is positive, the model always predicts f' will increase with increasing J_v as shown by Equation (25). However, the data indicate that f' decreases with increasing J_v. When the data are fit to the IT-KS model, a large value of $\Delta x/p_A$ is predicted such that the exponential terms in the model approach zero. The calculated value of σ is then just an average value of f'. The σ values and the standard deviations, s, are listed in Table 9 for the IT-KS model. Similar to the IT-PT models, σ is found to increase in the order benzene < toluene < cumene and increases with increasing annealing temperature (except for membrane 6). The average f' values calculated are illustrated in Figures 17-19 for comparison. Therefore, the IT-KS relationship must be rejected as a possible method of describing the aromatic hydrocarbon-water-cellulose acetate data.

Table 9

Parameters for the Irreversible Thermodynamics Kedem-Spiegler[a] (IT-KS) and the Three Parameter Finely-Porous Model[b] (FPM-3) Relationships

Film	Solute	E_0	s	σ (IT-KS)	b/K (FPM-3)
1	Benzene	0.2857	0.199	0.2857	1.400
1	Toluene	0.4048	0.212	0.4048	1.680
1	Cumene	0.6104	0.278	0.6104	2.567
2	Benzene	0.2612	0.174	0.2612	1.354
2	Toluene	0.3566	0.202	0.3566	1.554
2	Cumene	0.4593	0.258	0.4593	1.850
3	Benzene	0.1738	0.161	0.1738	1.210
3	Toluene	0.2518	0.180	0.2518	1.337
3	Cumene	0.3178	0.263	0.3178	1.466
4	Benzene	0.1318	0.100	0.1318	1.152
4	Toluene	0.1993	0.153	0.1993	1.249
4	Cumene	0.2528	0.193	0.2528	1.338
5	Benzene	0.0893	0.146	0.0893	1.098
5	Toluene	0.1421	0.122	0.1421	1.166
5	Cumene	0.2538	0.135	0.2538	1.340
6	Benzene	0.1727	0.125	0.1727	1.142
6	Toluene	0.2902	0.138	0.2902	1.409
6	Cumene	0.4023	0.118	0.4023	1.673

[a] All of the $\Delta x/p_A$ parameters for the IT-KS model are infinity.

[b] All of the τ/ε parameters for the FPM-3 model are infinity.

3.6.3 Interpretation of the Results for the Phenomenological Transport Models

These results presented above for the phenomenological transport models may be explained in the following manner. In order to estimate the transport parameters for any of the IT models, it is necessary that all adjustable parameters remain constant over the range of operating conditions studied. For the present case, at least one of the transport parameters appears to be changing as a function of the operating conditions. The possibility that ℓ_p may be a function of concentration was investigated. It was determined that including a concentration dependence in the ℓ_p term for the IT-PT model did not influence the ℓ_u values significantly. Therefore, the influence of concentration and pressure on the transport parameters must be more complex. Identifying possible concentration and pressure dependence has not been attempted for two reasons. First, there is little theoretical background to predict the form of such a relationship. Second, it would be difficult to extrapolate the resulting equations to other solutes and membranes. In any case, it may be stated that the nature of the solute and solvent transport is a strong function of the operating conditions. Yet IT type models have been found previously to do an excellent job of representing the solute transport in the absence of strong solute-membrane affinity (28). It can be hypothesized that the unsatisfactory behavior of the phenomenological models for the aromatic hydrocarbon data is related to the inability of the models to account for the strong solute-membrane attraction.

More recently, two papers by Thiel et al. (91, 92) have addressed the above problem. The phenomenological transport equations of irreversible thermodynamics were modified to account for possible interaction between solute and membrane. This interaction enters as an external force acting on the binary solvent/solute solution in the membrane phase. The resulting transport equations are similar in form to the four parameter finely-porous model.

Good agreement has been found between the single-solute aromatic hydrocarbon data and the model.

Since these models are phenomenological, the transport parameters are not linked to physicochemical concepts such as solute diffusivity in the membrane or surface pore size. For example, it was noted that σ for the IT-PT models varied as a function of solute and membrane annealing temperature. However, it would be incorrect to try to explain the behavior in terms of differences in the solute and membrane character. In order to do this, it is necessary to turn to models which are dependent on a transport mechanism. These models are considered in the next sections.

3.7 Nonporous Membrane Transport Models

When the membrane is considered to be nonporous, a solution-diffusion type of mechanism is usually used to describe the reverse osmosis transport. In this section the results of applying the solution-diffusion model and two modifications of the solution-diffusion model are discussed.

3.7.1 Solution-Diffusion Relationship

The solution-diffusion model assumes that the membrane surface is homogeneous and nonporous. Therefore, a given polymer should have a fixed (or intrinsic) separation and flux per unit thickness for a fixed solute-solvent system. These values are a function of the solubility and diffusivity of the solute and solvent in the polymer and the membrane thickness. If any imperfections (pinholes, pores, or void spaces) exist, the solute can "leak" with the solvent through these passageways and less than ideal separation (with a corresponding increase in flux) will be observed. It has been found that annealing asymmetric cellulose acetate membranes acts to increase salt-water separation and decrease

the flux, as discussed in Section 1.2.1. According to the solution-diffusion mechanism, the annealing step is thought to decrease the size and/or number of imperfections, possibly by increasing crystallinity or by closing pinholes. The six cellulose acetate membranes used in the current work may be considered to have various number and size of imperfections. Membrane 1 is closest to a true SD type membrane while membrane 6 has the most and/or largest imperfections. In spite of imperfections, it is not unusual to apply a solution-diffusion type mechanism to all reverse osmosis membranes; this approach is examined in this section.

For the SD type nonporous membrane transport models, the parameter ($D_{BM}\ C_{BM}\ V_B/RT\ \Delta x$) was determined from the pure water permeation data. Since no independent method of measuring D_{BM}, C_{BM}, and Δx was employed, the values are treated as a single grouped parameter. Noting the similarity between Equation (10) and Equation (26), the grouped parameter ($D_{BM}\ C_{BM}\ V_B/RT\ \Delta x$) can be identified as being numerically the same as ℓ_p. Therefore, the ℓ_p values listed in Table 5 are also the ($D_{BM}\ C_{BM}\ V_B/RT\ \Delta x$) parameters for the SD type models.

Equation (28) predicts the relationship between volume flux and separation for the SD model:

$$\frac{1}{f'} = 1 + \left(\frac{D_{AM}K}{\Delta x}\right)\frac{1}{J_v} \tag{29}$$

The SD relationship is a two parameter model of Form a) (Equation (68)). The unknown parameters are $\ell_p = (D_{BM}\ C_{BM}\ V_B/RT\ \Delta x)$ and $(D_{AM}\ K/\Delta x)$. The parameters estimated for the SD model are listed in Table 10, and the curves of an f' versus J_v plot are illustrated in Figures 17-19 for the solutes benzene, toluene, and cumene, respectively. As the dashed lines in Figures 17-19 illustrate, the form of the SD model is not consistent with the data. In fact, the data follow the opposite trend predicted by the SD model; that is, f' actually decreases, rather than increases as predicted, as a function of increasing J_v. The $D_{AM}\ K/\Delta x$ values

Table 10

Parameters for the Solution-Diffusion[a] (SD) and Kimura-Sourirajan Analysis[b] (KSA) Relationships

Film	Solute	$E_1 \times 10^5$ m/s	s
1	Benzene	1.993	0.311
1	Toluene	0.6388	0.370
1	Cumene	0.07917	0.424
2	Benzene	2.786	0.279
2	Toluene	1.155	0.342
2	Cumene	0.5992	0.429
3	Benzene	9.678	0.225
3	Toluene	3.886	0.279
3	Cumene	3.276	0.385
4	Benzene	14.47	0.147
4	Toluene	8.070	0.226
4	Cumene	6.734	0.290
5	Benzene	65.86	0.167
5	Toluene	16.01	0.170
5	Cumene	6.207	0.233
6	Benzene	10.41	0.166
6	Toluene	4.588	0.244
6	Cumene	2.156	0.240

[a] For the SD model, $E_1 = D_{AM}\, K/\Delta x$ and by definition $E_0 = 1.0$.

[b] For the KSA relationship $E_1 = D_{AM}\, K/\iota$ and by definition $E_0 = 1.0$.

decrease in the order benzene > toluene > cumene and decrease with increasing annealing temperature (except for membrane 6). The s values are larger than for any other model. These results indicate that the SD model is not appropriate for the hydrocarbon solute data.

Similar results concerning the inapplicability of the SD model for phenol-water separation have been reported previously (7,12). The conclusion is that either the parameters are not independent of operating conditions or that at least one of the assumptions of the SD model is incorrect. As discussed for the IT models, the possible dependence of the adjustable parameters on operating conditions is difficult to identify and the resulting model is usually less general. Therefore, only the validity of the assumptions in the model was investigated. At least four different possibilities have been suggested to explain why the SD model is inappropriate. One assumption questioned by previous authors (7,12) is the validity of assuming that water and solute flows were independent. The existence of so-called "flow coupling" between solvent and solute could qualitatively explain the observed decrease in separation with increasing volume flux. Two methods of accounting for flow coupling have been proposed. The first (7) of these is identical to the IT-KS approach, which has already been discussed. The second method (45) leads to the finely porous model, which is a porous membrane transport model and is discussed later. The second possible explanation for the inapplicability of the SD model is that the membrane surface is not homogeneous. This potential explanation would suggest either a solution-diffusion imperfection model, which is described elsewhere in this dissertation, or again a porous membrane model. The third possibility is the validity of excluding the $V_A \Delta P$ term in the chemical potential equation. The modification of the SD model to account for the $V_A \Delta P$ term is discussed later as the ESD model.

A fourth possibility is that the presence of the solute may cause the polymer to swell, thereby changing the transport properties of the membrane (80). Since the

performance of the membranes is reproducible, it must be concluded that any swelling that does take place is reversible. This means that the membrane returns to its original state after the solute is washed out with pure water. Since it has been implicitly assumed in the SD model that the membrane structure is unchanged by the presence of the solute, then swelling would lead to parameters that are dependent on operating conditions. In fact, reversible swelling may be the reason that the SD model as represented by Equations (26) and (29) does not work. The possibility of identifying and quantifying swelling has not been pursued in this work. Therefore, modification of the assumptions in the SD model lead to either the IT-KS, SDI, ESD, or to a porous membrane model. The SDI and ESD models are discussed next.

In a qualitative sense the following consideration may be made concerning solvent flux. The SD model assumes that the solute and solvent are transported independently through the membrane. Therefore, changes in the feed concentration should not affect the solvent flux as long as the solute concentration is small so that $\Delta P >> \Delta\pi$. For the present case, as has already been discussed, the solvent flux is influenced strongly by the presence of the solute. A possible explanation for this observed behavior is that the presence of the solute in the membrane material alters the structure of the polymer to reduce the water flux. The nature of the alteration may be a change in the swelling of the polymeric material due to an interference of the specific interactions between solvent and membrane caused by the solute-membrane attraction (80). Data for the swelling of the polymeric membrane by water as a function of phenol concentration (16,17) are approximately consistent with the observed reduction in flux due to phenol in the feed solution of reverse osmosis experiments (13,16). However, it is not clear from these results if the change in water content is due to a change in the membrane structure, a change in the water-solute-membrane interactions, or both.

3.7.2 Solution-Diffusion Imperfection Relationship

As presented in the Section 1.2.3, the solution-diffusion imperfection (SDI) model was developed to include the influence of transport through small imperfections which may exist in the surface of the membrane. Equation (32) may be applied to the data directly. However, when the concentrations used are sufficiently low that $\Delta P >> \Delta\pi$ then Equation (32) may be rearranged as:

$$\frac{1}{f'} = 1 + \frac{\kappa'''}{\kappa'} + \left(\frac{\kappa''}{\kappa'}\right)\left(\frac{RT}{J_v}\right) \tag{33}$$

The SDI relationship is a 3 parameter model of Form c) (Equation (70)). The three parameters are κ', κ'', and κ'''.

The aromatic hydrocarbon data were analyzed with Equation (33) and the results are summarized in Table 11. That the data can be correlated by a f'versus ΔP plot is illustrated in Figures 23-25. The E_0 and E_1 values as well as the ratios κ''/κ' and κ'''/κ' are given in Table 11. Noting the similarity between Equation (10) and (30) for the case of pure water ($\Delta\pi = 0$) leads to:

$$\ell_p = \kappa' + \kappa''' \tag{78}$$

With the ℓ_p values from Table 5 and Equation (78), the individual κ', κ'', and κ''' values may be calculated and are listed in Table 11. The E_0 values for the IT-PT-A and SDI models are similar. E_1 values for the two models follow similar trends although the magnitudes are different. Therefore, the dependence of E_0 and E_1 on membrane annealing temperature and solute is similar to that described for the IT-PT-A model. The s values are almost identical for the IT-PT-A and SDI models. The SDI model is actually quite similar in form to the IT-PT-A model. When $\Delta P >> \Delta\pi$, then ΔP is related to J_v, as illustrated earlier for the IT-PT model:

$$J_v = \ell_p \Delta P \tag{75}$$

indicating that J_v and ΔP are related to each other by a linear equation. Therefore, Form a) and Form c) in Table 3 are equivalent and it is not surprising that the IT-PT-A and SDI

Table 11

Parameters for the Solution-Diffusion Imperfection (SDI) Model

Film	Solute	E_0	$E_1 = \kappa''/\kappa'$	s	κ'''/κ'	$\kappa' \times 10^{10}$	$\kappa'' \times 10^{10}$	$\kappa''' \times 10^{10}$
		$kmol/m^3$				m/s kPa	$\frac{kmol}{m^2 s kPa}$	m/s kPa
1	Benzene	5.902	-1.130	0.113	4.902	2.164	-2.445	10.61
1	Toluene	3.685	-0.6284	0.116	2.685	3.465	-2.178	9.305
1	Cumene	2.127	-0.2716	0.215	1.127	6.004	-1.631	6.766
2	Benzene	6.405	-1.221	0.088	5.405	2.436	-2.974	13.16
2	Toluene	4.220	-0.7312	0.116	3.220	3.697	-2.703	11.90
2	Cumene	3.084	-0.4777	0.181	2.084	5.059	-2.416	10.54
3	Benzene	11.32	-2.426	0.089	10.32	1.937	-4.700	19.99
3	Toluene	6.642	-1.296	0.097	5.642	3.032	-4.279	18.63
3	Cumene	4.935	-0.8903	0.199	3.935	4.444	-3.956	17.49
4	Benzene	12.31	-2.266	0.072	11.31	2.669	-6.047	30.18
4	Toluene	8.458	-1.659	0.095	7.458	3.884	-6.443	28.97
4	Cumene	6.354	-1.171	0.132	5.354	5.170	-6.054	27.68
5	Benzene	35.13	-8.725	0.095	34.13	1.143	-9.969	39.00
5	Toluene	12.70	-2.622	0.076	11.70	3.161	-8.287	36.98
5	Cumene	5.570	-0.8522	0.097	4.570	7.206	-6.141	32.93
6	Benzene	7.527	-0.9531	0.116	6.527	5.874	-5.598	38.34
6	Toluene	4.357	-0.5217	0.120	3.357	10.15	-5.294	34.06
6	Cumene	2.789	-0.1839	0.109	1.789	15.85	-2.915	28.36

Figure 23. The effect of operating pressure on separation for the benzene-water-cellulose acetate system at 25°C. (□) experimental points; (—) solution-diffusion imperfection model (SDI).

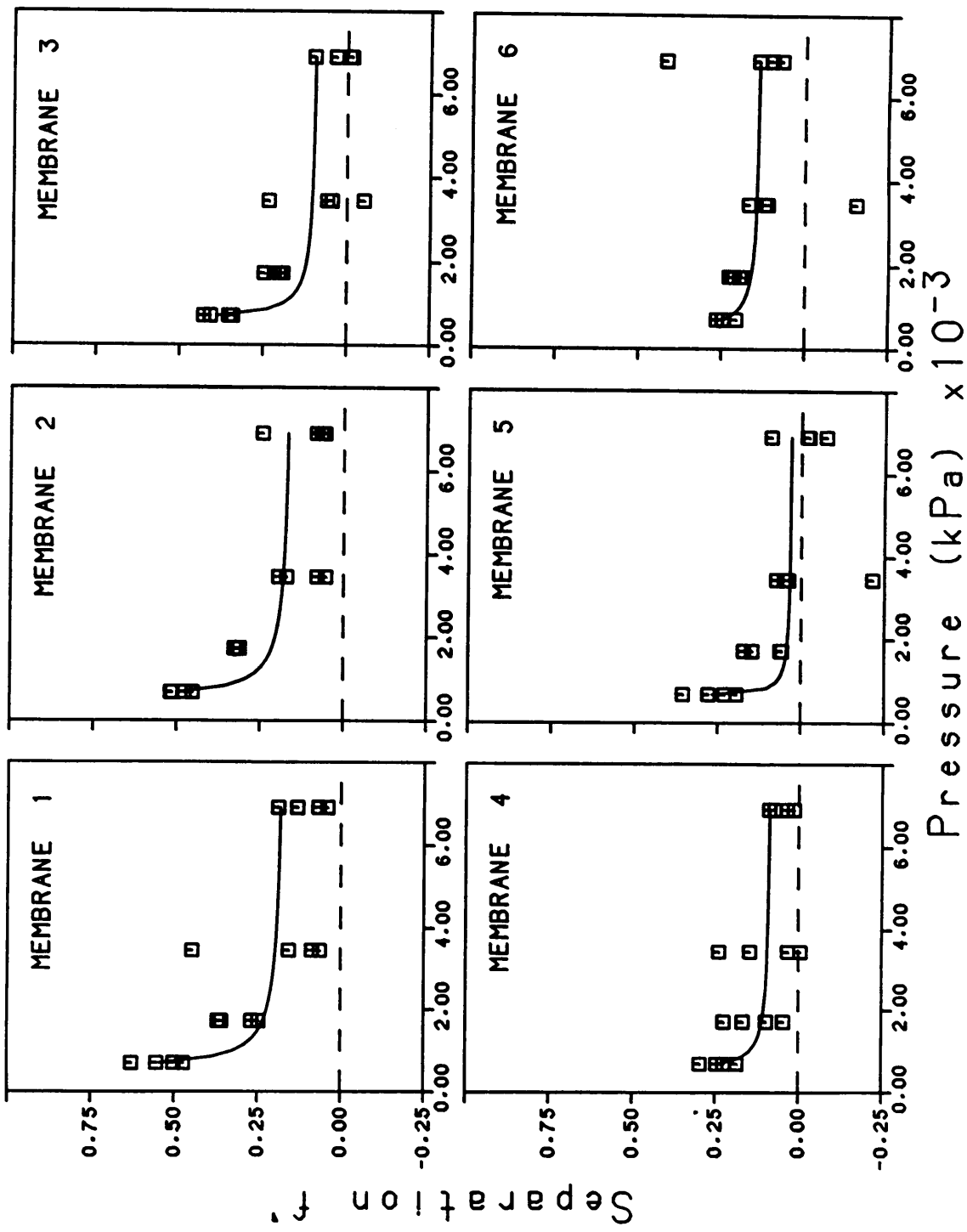
MEMBRANE 1
MEMBRANE 2
MEMBRANE 3
MEMBRANE 4
MEMBRANE 5
MEMBRANE 6
Separation f'
Pressure (kPa) x10-3
0.75
0.50
0.25
0.00
-0.25
0.00
2.00
4.00
6.00

Figure 24. The effect of operating pressure on separation for the toluene-water-cellulose acetate system at 25°C. (□) experimental points; (—) solution-diffusion imperfection model (SDI).

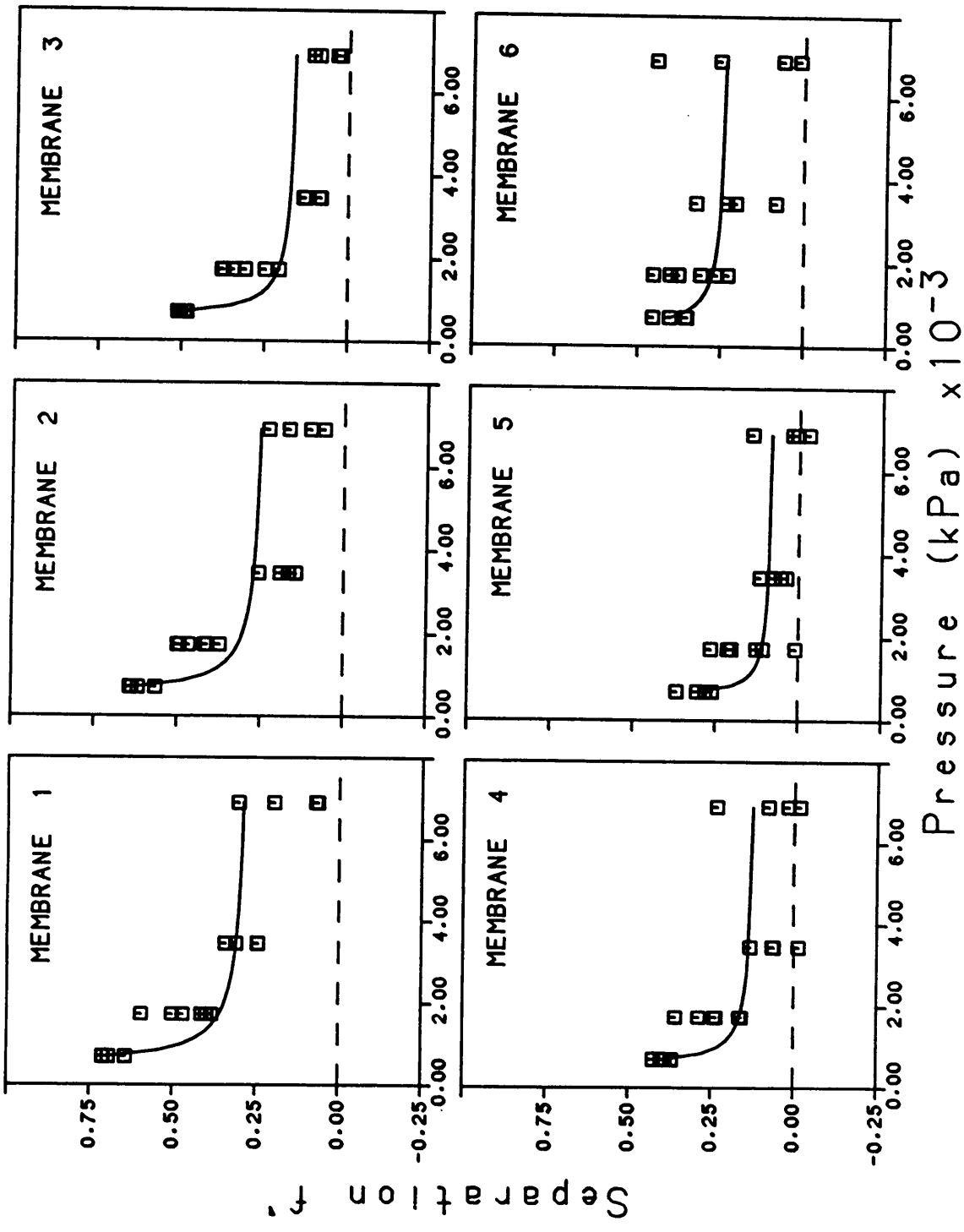
MEMBRANE 1
MEMBRANE 2
MEMBRANE 3
MEMBRANE 4
MEMBRANE 5
MEMBRANE 6
Separation f'
Pressure (kPa) x10-3
0.75
0.50
0.25
0.00
-0.25
0.00
2.00
4.00
6.00

Figure 25. The effect of operating pressure on separation for the cumene-water-cellulose acetate system at 25°C. (□) experimental points; (—) solution-diffusion imperfection model (SDI).

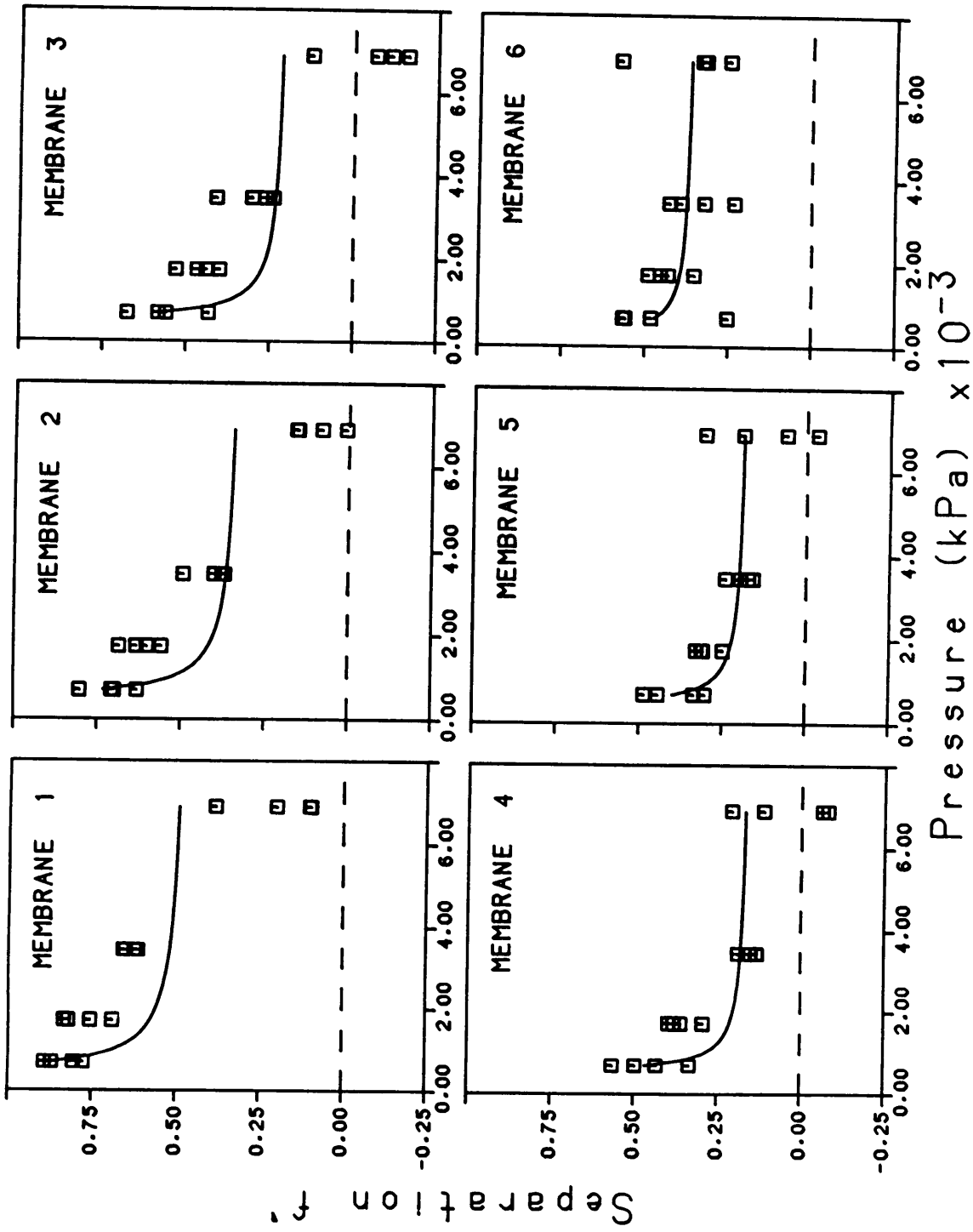
MEMBRANE 1
MEMBRANE 2
MEMBRANE 3
MEMBRANE 4
MEMBRANE 5
MEMBRANE 6
Separation f'
Pressure (kPa) x10-3
0.75
0.50
0.25
0.00
-0.25
0.00
2.00
4.00
6.00

models give similar results.

The ratio of κ''' to κ' represents the relative contribution of flow through imperfections to diffusive flow. This ratio (from Table 11) varies from 1.13 (for cumene and membrane 1) to 34.1 (for benzene and membrane 5) which indicates that a large portion, between 53% and 97%, of the water flux is occurring through imperfections. Since annealing at higher temperatures decreases the number and/or size of imperfections, it would be expected that κ'''/κ' should increase with decreasing annealing temperature. This result is confirmed by experimental κ'''/κ' values. The κ'''/κ' ratio for a given membrane decreases in the solute order benzene > toluene > cumene. Thus the pore flow contribution decreases with both increasing solute size and increasing solute-membrane affinity. Perhaps the solute molecules are partially blocking the imperfections and the extent of the blocking increases both with solute size and with solute-membrane affinity. This explanation is consistent with the qualitative discussion in Section 3.3. This result indicates that the importance of the pore flow decreases in the order benzene > toluene > cumene. It would be expected from the basic premise of the SDI model that κ', κ'', and κ''' should all be positive. Yet, the κ'' values are negative in all cases. For κ'' to be negative, either the solute diffusivity in the membrane or the solute partition coefficient should be negative. Since it is impossible for either of these physicochemical parameters to be negative, it may be concluded that negative values of κ'' are inconsistent with the SDI model. Therefore, although the κ' and κ''' parameters seem reasonable, the negative κ'' values cast doubt on the applicability of the SDI model.

3.7.3 Extended Solution-Diffusion Relationship

The extended solution-diffusion model (ESD) allows the influence of pressure induced solute transport to be included in the model. The possibility of pressure induced solute transport occurring is dictated by the presence of the $V_A \Delta P$ term in the solute chemical

potential equation (see Equation (34)). Usually it is safe to ignore the $V_A \Delta P$ term since it is much less than the concentration term. This simplification breaks down at high pressure, low separation, and high V_A. Before examining the results of the ESD model, it is appropriate to determine if the $V_A \Delta P$ term is important for the aromatic hydrocarbon-water-cellulose acetate data.

The criterion for ignoring the pressure induced solute transport is:

$$|\ln (C_{A2}/C_{A3})| >> V_A \Delta P/RT \tag{79}$$

Substituting in the definition of f' gives:

$$|\ln (1/(1 - f'))| >> V_A \Delta P/RT \tag{80}$$

In order to check this inequality, it is necessary to have values for V_A and experimental data for f' as a function of ΔP. Partial molar volumes, V_A, have been estimated from the density and molecular weight of the solutes (7) and are listed in Table 1. The dependence of f' on ΔP is illustrated in Figures 23-25. The results of evaluating Equation (80) are shown in Table 12. At one extreme, with large f' and small ΔP values, Equation (80) is valid and the $V_A \Delta P/RT$ term may be ignored. At the other extreme, with small f' and large ΔP values, Equation (80) is not valid and $V_A \Delta P/RT$ may not be ignored. The remaining results are between these extremes. It appears that the influence of pressure induced solute transport may be ignored only for the highest separation data. In fact, the pressure induced solute term may dominate over the concentration term. Therefore, the $V_A \Delta P/RT$ term should be included in the analysis for the aromatic hydrocarbon data.

Having established the importance of including the $V_A \Delta P/RT$ term in the model, the results of fitting the data to ESD model can be considered.

The form of the ESD model is identical to the IT-PT-A model, so the E_0 and E_1 values in Table 7 and the curves in Figures 17-19 apply to both models. The definitions of E_0

Table 12

Evaluation of the Significance of Pressure Induced Solute Transport

	Benzene	Toluene	Cumene
Case 1: Large f' and small ΔP = 690 kPa			
f'	0.65	0.73	0.90
$\ln(1/1 - f')$	1.050	1.309	2.303
$V_A \Delta P/RT$	0.02475	0.02952	0.03898
Is $\ln(1/1 - f') >> V_A \Delta P/RT$?	Yes	Yes	Yes
Case 2: Small f' and large ΔP = 6900 kPa			
f'	0.01	0.01	0.03
$\ln(1/1 - f')$	0.0100	0.0100	0.0305
$V_A \Delta P/RT$	0.2475	0.2952	0.3898
Is $\ln(1/1 - f') >> V_A \Delta P/RT$?	No	No	No

and E_1 in Table 3 are used to calculate the ℓ_{AP} and D_{AM} $K/\Delta x$ values listed in Table 7. Similar to the case for the IT-PT-A model, C_{A2} is not constant, so an average C_{A2} for all experiments for each solute was used to calculate an approximate value of ℓ_{AP}. The ℓ_{AP} values were found to decrease both with increasing annealing temperature and with solute nonpolar character: benzene < toluene < cumene. Therefore, the pressure-induced solute transport decreases as the membrane permeability decreases, which is consistent with the premises of the ESD model. Since ℓ_{AP} should be directly proportional to V_A (listed in Table 1), it would be expected that ℓ_{AP} should increase with the solute order benzene < toluene < cumene. In fact, the opposite trend is observed. The D_{AM} $K/\Delta x$ values calculated are negative. This result is impossible since D_{AM}, K, and Δx all must be positive. Therefore, the actual data are inconsistent with the ESD model.

3.8 Porous Membrane Transport Models

Once the membrane is considered to be porous, describing the transport through a reverse osmosis membrane becomes more complicated. Three of these models, the Kimura-Sourirajan analysis of the preferential sorption-capillary flow mechanism, the finely-porous model, and surface force-pore flow model are discussed in this section with respect to the aromatic hydrocarbon-water-cellulose acetate membrane system.

3.8.1 Kimura-Sourirajan Analysis

Kimura and Sourirajan assumed that the membrane is microporous and that all transport takes place through membrane pores. The application of the KSA relationship to the present data has been given in Sections 3.2 and 3.3 of the RESULTS AND DISCUSSIONS. The KSA model in the original form is not capable of explaining the observed data. However, the empirical Equation (40) can be used to represent the so-called

pore blocking effect. Both the KSA and SD models are similar in mathematical form, even through the underlying concepts are different. Therefore, the parameters in Table 10 and the curves in Figures 17-19 also apply to the KSA model. The trends in (D_{AM} K/τ) as a function of annealing temperature and solute are the same as for the SD model. The KSA model is not able to describe the decrease in separation observed with increasing pressure. According to the KSA model, the discrepancy between theory and experimental result is due to the strong solute-membrane affinity. When the solute is strongly sorbed to the membrane material, the transport in the pore is too complicated to be described by this simple one-dimensional model. Two other attempts at describing the data with a porous model are discussed below.

3.8.2 Finely-Porous Model

As discussed in Section 1.2.4, the finely-porous model (FPM) is a one-dimensional transport model based on a combined viscous flow and frictional model. The model can be used as either a three parameter model, FPM-3, or as a four parameter model, FPM-4. These two approaches are presented separately below.

Three Parameter Finely-Porous Model. In the three parameter model it is assumed that the partition coefficient is the same on the high and low pressure sides of a membrane for an experiment. Mathematically, this assumption can be expressed as $K_2 = K_3 = K$. The relationship between f' and J_v is given as:

$$\frac{1}{f'} = \frac{1-(1-K/b)\exp[-(\tau/\varepsilon D_{AB})J_v]}{(1-K/b)\{1-\exp[-(\tau/\varepsilon D_{AB})J_v]\}} \qquad (46)$$

The FPM-3 relationship is a three parameter model of Form b) (see Equation (69)). The three parameters are A, b/K, and τ/ε.

The aromatic hydrocarbon data were analyzed by the FPM-3 model and results are summarized in Table 9 and in Figures 17-19. Noting that FPM-3 model is of the same general form as the IT-KS model, it is not surprising that the same E_i values and the same lines in Figures 17-19 are generated. However, as illustrated in Table 9, the parameters are interpreted differently for the two models. In all cases the value of τ/ε was estimated as a value sufficiently large that the exponential terms in the model approached zero. As a result, the (1 – K/b) term is simply an average of the experimental f' values. The b/K values increase in the order benzene < toluene < cumene and decrease with increasing annealing temperature (except for membrane 6). The b/K values seem reasonable, but the result that τ/ε equals infinity is impossible. In order for τ/ε to be infinite, either τ should be infinite, corresponding to an infinitely thick membrane, or the ε should be zero, corresponding to no pores in the membrane. Both of the above possibilities are unreasonable physically for the FPM model.

The conclusion is that the FPM-3 model is not capable of quantitatively describing the observed decrease in separation with increasing volume flux. Therefore, the FPM-3 model must be rejected as a possible model for describing the aromatic hydrocarbon-water-cellulose acetate data. The exact reasons why this model failed are difficult to determine. However, it was found that relaxing the assumption that the partition coefficient K was constant greatly improved the model. The results of this analysis are discussed in the next section.

Four Parameter Finely-Porous Model. When the assumption that the partition coefficient remains constant is relaxed, the FPM-4 model results. As discussed in Section 1.2.4, the relationship between f' and J_v for the FPM-4 model is:

$$\frac{1}{f'} = \frac{1-(1-K_3/b)\exp[-(\tau/\varepsilon D_{AB})J_v]}{(1-K_2/b)-(1-K_3/b)\exp[-(\tau/\varepsilon D_{AB})J_v]} \tag{43}$$

This model is a four parameter model of Form d) (see Equation (71)). The four parameters are A, b/K_2, K_3/K_2, and τ/ε.

The aromatic hydrocarbon data were analyzed by the FPM-4 model and the results are summarized in Table 13 and in Figures 26-28. The agreement between the model and experimental data is good. The standard deviation values, s, are small. The model is capable of predicting several different shapes for the f' versus J_v relationship. These include a concave upward curve which is the most usual case, a concave downward curve (see the case of membrane 1 for the solute cumene) or a curve with an inflection point (see the case of membranes 2 and 3 for the solute cumene). Also, the model predicts that separation may become negative at higher volume fluxes (see the case of membrane 5 for the solute benzene and of membrane 3 for the solute cumene). None of the other models examined have been able to predict a concave downward curve or a continuous change from positive to negative separation. It is interesting to note that previously this model has been applied primarily to cases where separation increases with increasing flux (for example, NaCl-water-cellulose acetate system). However, the model does an excellent job of following the trend of the data when the separation decreases with increasing pressure.

The estimated parameters are listed in Table 13. The results for benzene and toluene are similar to each other in that the b/K_2 parameters appear to be independent of pore size and solute. The average b/K_2 value for benzene and toluene is 1.091 ± 0.046 (95% confidence limit). Based on the Faxen Equation (63), it would be expected that b should be a function of both pore size and solute. Also, since K_3/K_2 varies as a function of both pore size and solute, it is expected that K_2 could vary with both pore size and solute. Since we expect both b and K_2 to vary with pore size and solute, it is surprising to find that b/K_2 is approximately independent of pore size and solute, at least for benzene and toluene. It is possible that the variations in b and K_2 are cancelling each other such that b/K_2 is

Table 13

Parameters for the Four Parameter Finely-Porous (FPM-4) Model

Film	Solute	E_0 $(1-K_3/b)$	E_1 $(1-K_2/b)$ x 10^2	E_2 $(\tau/\varepsilon\ D_{AB})$ x 10^{-5}	s	b/K_2	K_3/K_2	τ/ε x 10^4 m
	Benzene	-1.617	10.10	6.820	0.097	1.112	2.911	7.475
1	Toluene	-2.902	14.55	7.160	0.068	1.170	4.567	6.931
	Cumene	39.39	657.0	1.967	0.061	-0.1797	6.893	1.572
	Benzene	-1.510	9.297	5.813	0.058	1.102	2.767	6.371
2	Toluene	-2.564	11.86	6.014	0.061	1.134	4.043	5.822
	Cumene	-3.985	-11.26	2.763	0.061	0.8988	4.481	2.208
	Benzene	-1.022	1.760	3.577	0.064	1.018	2.058	3.920
3	Toluene	-1.738	4.829	4.070	0.053	1.051	2.877	3.940
	Cumene	-3.161	-55.94	1.320	0.097	0.6410	2.669	1.055
	Benzene	-0.3839	5.362	1.985	0.071	1.057	1.462	2.176
4	Toluene	-1.151	5.294	2.689	0.079	1.056	2.271	2.603
	Cumene	-1.330	0.2086	1.617	0.090	1.002	2.334	1.292
	Benzene	-0.8303	-1.827	2.304	0.087	0.9821	1.798	2.525
5	Toluene	-0.7857	3.679	2.148	0.070	1.038	1.854	2.079
	Cumene	-0.7144	10.50	1.227	0.087	1.117	1.916	0.980
	Benzene	-0.3377	13.16	2.286	0.119	1.151	1.540	2.505
6	Toluene	-0.5746	17.96	1.340	0.114	1.219	1.919	1.297
	Cumene	-0.3870	35.53	1.687	0.112	1.551	2.151	1.348

Figure 26. The effect of volume flux on separation for the benzene-water-cellulose acetate system at 25°C. (□) experimental points; (—) the four parameter finely-porous model (FPM-4); (– – –) the four parameter finely-porous model with the pore size parameter, τ/ε, forced to be constant for all three solutes.

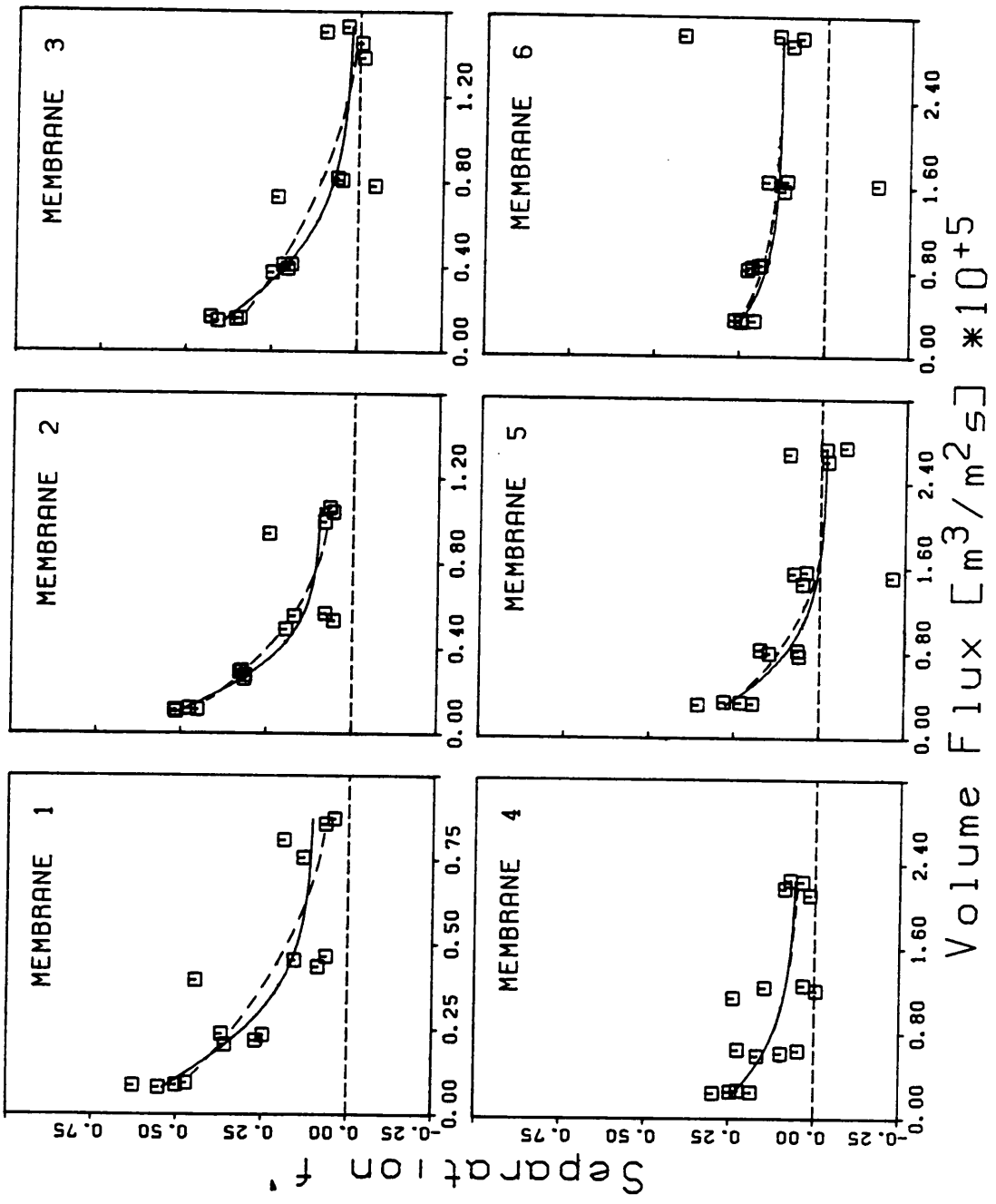
MEMBRANE 1
MEMBRANE 2
MEMBRANE 3
MEMBRANE 4
MEMBRANE 5
MEMBRANE 6
Separation f'
Volume Flux [m3/m2s] *10+5
-0.25
0.00
0.25
0.50
0.75
0.40
0.80
1.20
1.60
2.40

Figure 27. The effect of volume flux on separation for the toluene-water-cellulose acetate system at 25°C. (□) experimental points; (—) the four parameter finely-porous model (FPM-4); (– – –) the four parameter finely-porous model with the pore size parameter, τ/ε, forced to be constant for all three solutes.

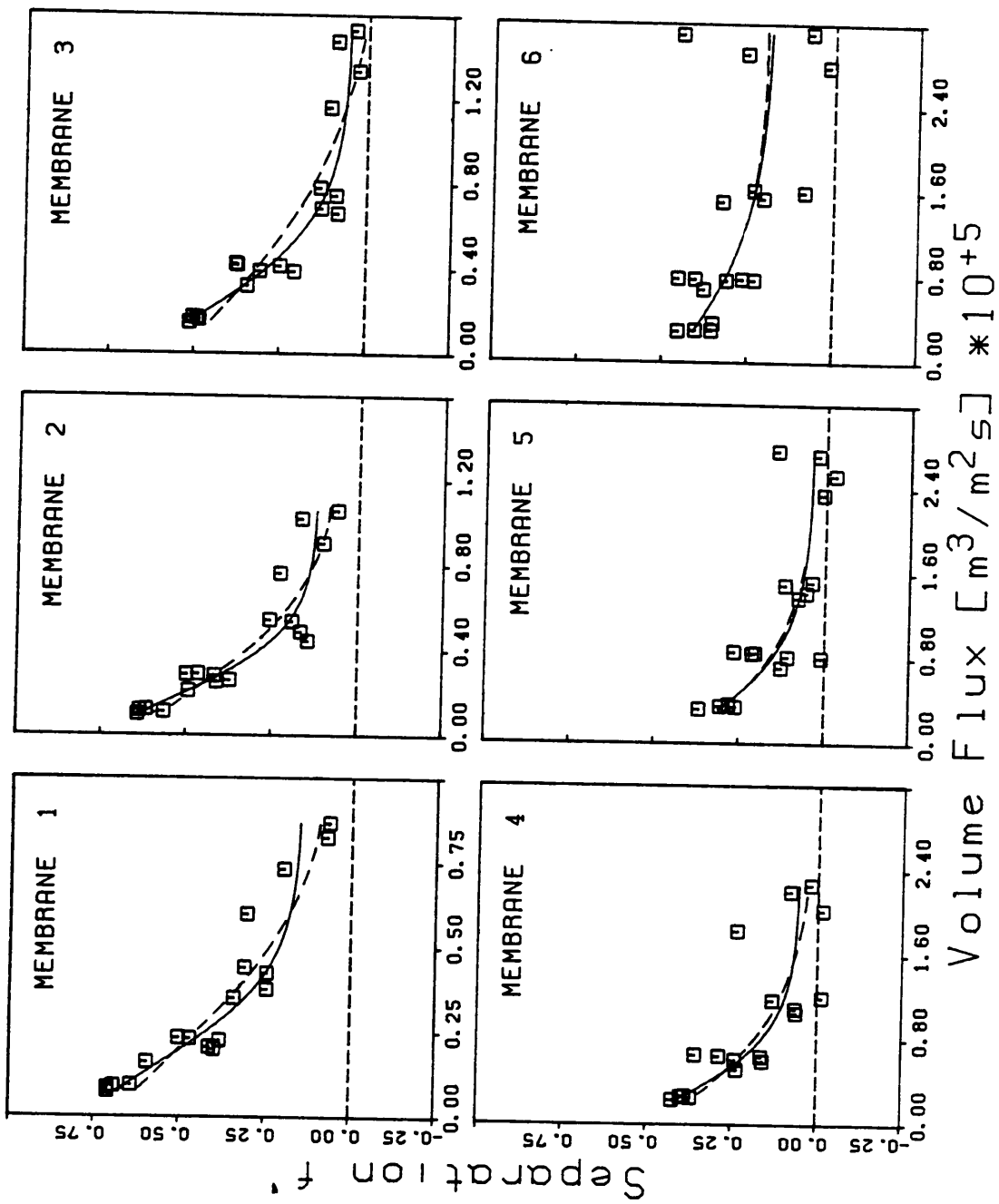
MEMBRANE 1
MEMBRANE 2
MEMBRANE 3
MEMBRANE 4
MEMBRANE 5
MEMBRANE 6
Separation f
Volume Flux [m3/m2s] *10+5
0.00
0.40
0.80
1.20
1.60
2.40
0.25
0.50
0.75

Figure 28. The effect of volume flux on separation for the cumene-water-cellulose acetate system at 25°C. (□) experimental points; (—) the four parameter finely-porous model (FPM-4); (– – –) the four parameter finely-porous model with the pore size parameter, τ/ε, forced to be constant for all three solutes.

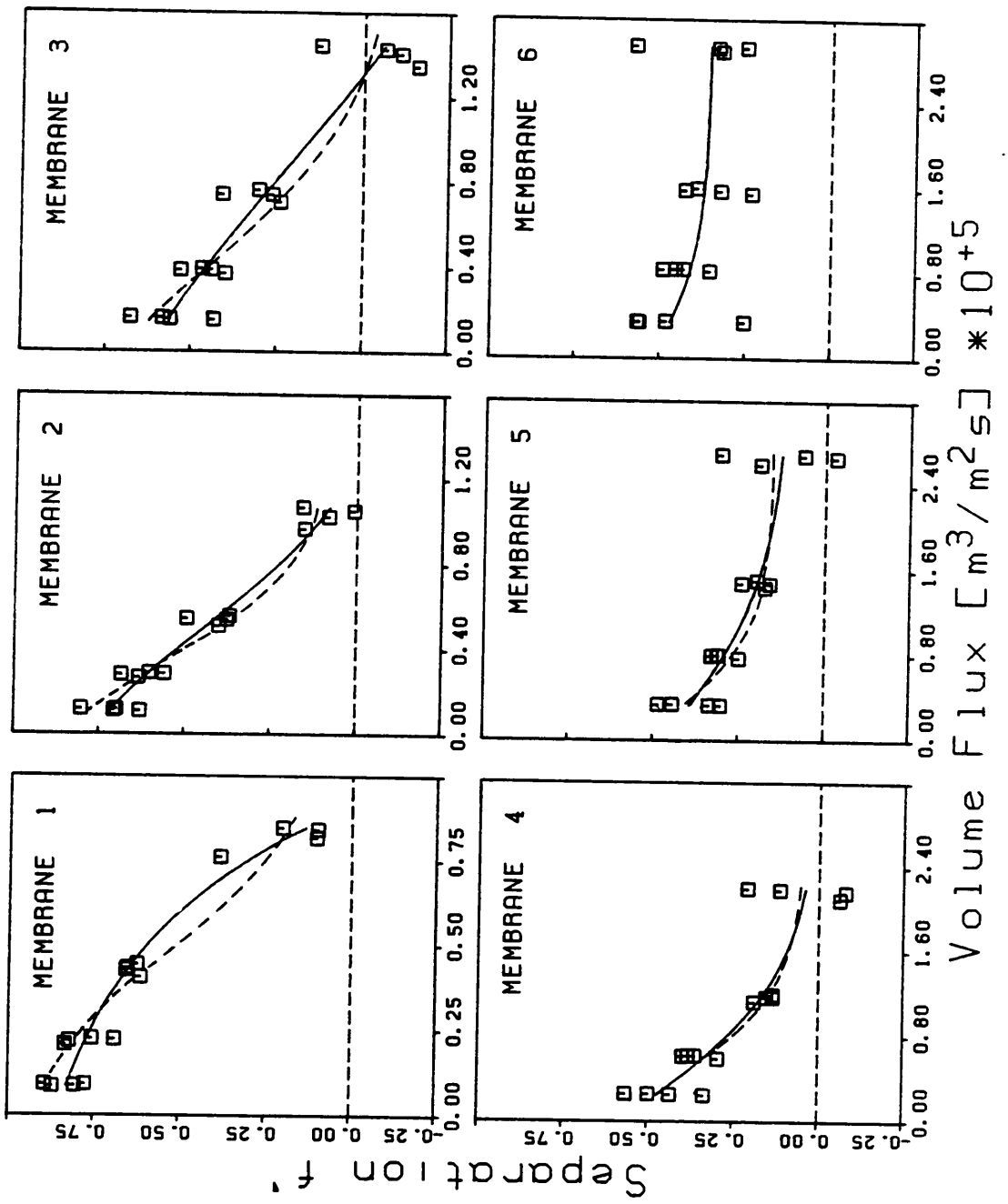
MEMBRANE 1
MEMBRANE 2
MEMBRANE 3
MEMBRANE 4
MEMBRANE 5
MEMBRANE 6
Separation f'
Volume Flux [m3/m2s] *10+5

approximately constant. From the estimated values for b/K_2 and $(1 - K_3/b)$, the ratio of the partition coefficient on the low and high pressure side of the membrane, K_3/K_2, listed in Table 13, can be calculated. These ratios are clearly greater than one and are a function of pore size and solute. The overall trend indicates that K_3/K_2 increases in the solute order benzene < toluene < cumene and increases with increasing annealing temperature, although there is some scatter. This result is unusual in that K is often considered to be constant for a given solute and membrane material. Here, the partition coefficient appears to be different on the high and low pressure sides of the membrane, and the difference is a function of pore size. These differences may reflect that K is a function of membrane structure, concentration, and/or pressure. Pressure should have a insignificant effect on K for the case of a liquid solution, since liquids are almost incompressible. Therefore, the observed variation in K is probably caused by the asymmetric structure of the membrane and/or a concentration dependence. The parameter ι/ε is approximately the same for benzene and toluene for each membrane, but does increase with increasing annealing temperature, with some scatter. This result is encouraging since it was expected that ι/ε should increase with increasing annealing temperature. Increasing annealing temperature causes a reduction in pore diameter, which decreases the fractional pore area, ε, and hence increases ι/ε.

Comparing the results for cumene with those for benzene and toluene, similar values for the various parameters are observed. However, there is more scatter in the numerical values and the trends are not as clear.

As discussed above and earlier in this dissertation, assuming that the membrane is not temporarily altered by the solute in the concentrated boundary layer, it is expected that the pore size parameter, ι/ε, should be independent of the solute used. Therefore, the data were reanalyzed, assuming that ι/ε was constant for each membrane. In this case 7 parameters were estimated for each membrane (b/K_2 and K_3/K_2 for each of the 3 solutes plus

Table 14

Parameters for the Four Parameter Finely-Porous (FPM-4) Model with the Pore Size Parameter (τ/ε) Forced to be Constant for All Solutes

Film	Solute	E_0 $(1-K_3/b)$	E_1 $(1-K_2/b)$ x 10^2	E_2 τ/ε x 10^4 m	s	b/K_2	K_3/K_2
1	Benzene	-1.237	2.235	4.110	0.085	1.023	2.289
	Toluene	-2.179	4.531			1.047	3.330
	Cumene	-11.99	5.539			1.059	13.76
2	Benzene	-1.113	3.452	3.664	0.071	1.036	2.188
	Toluene	-1.867	5.066			1.053	3.020
	Cumene	-4.944	8.540			1.093	6.500
3	Benzene	-0.8110	-5.848	2.017	0.084	0.9447	1.711
	Toluene	-1.215	-4.491			0.9570	2.120
	Cumene	-2.728	-9.631			0.9122	3.400
4	Benzene	-0.3572	4.040	1.697	0.081	1.042	1.414
	Toluene	-0.8916	1.345			1.014	1.917
	Cumene	-1.492	4.331			1.045	2.605
5	Benzene	-0.6723	-3.903	1.807	0.081	0.9624	1.609
	Toluene	-0.7158	2.751			1.028	1.764
	Cumene	-0.9216	15.51			1.184	2.274
6	Benzene	-0.2456	12.26	1.555	0.113	1.140	1.420
	Toluene	-0.6180	19.05			1.235	1.999
	Cumene	-0.4183	35.89			1.560	2.212

τ/ε for the membrane) based on 50 experimental data. The parameters can be estimated with more confidence than previously with 3 parameters based on 16-18 data points. The recalculated values are given in Table 14 and the f' versus J_v relationships are illustrated in Figures 26-28. The solid lines represent the calculated correlation based on separate parameters for each solute and membrane combination. The dashed line is the model recalculated with τ/ε forced to be constant for a given membrane. It is clear from Figures 26-28 that the data are as equally well represented by the recalculated line as by the initial model. That a better estimate of the parameters was obtained is confirmed by the smaller s (standard deviation) values obtained (listed in Table 14). From this table, b/K_2 is observed to be approximately constant at 1.074 $\pm$ 0.075 (95% confidence) for all membranes and solutes. Even for cumene an average value seems to be appropriate. Again, it must be emphasized that b/K_2 would not be expected to be a constant, however the experimental results indicate that this is true. The ratio of partition coefficients K_3/K_2 decreases with increasing pore size and increases for the three solutes (benzene < toluene < cumene). As before, the K_3/K_2 terms are neither constant nor equal to 1.0. With the recalculated parameters, the trend in K_3/K_2 may be clearly seen for all three solutes. Finally, the pore size parameter τ/ε is found to decrease with increasing pore size, as expected. The net result of the above analysis is that a better estimate of the unknown parameters is obtained. As a result, the trends in the parameters, which were pointed out above, are clearer.

Previously in this work, $\ln C^*_{NaCl}$ was used as a pore size parameter. For the FPM-4 relationship, the pore size parameter, τ/ε, has been calculated. Figure 29 illustrates the relationship between the two pore size parameters $\ln C^*_{NaCl}$ and τ/ε. As would be expected, an inverse and unique relationship is found between τ/ε and $\ln C^*_{NaCl}$ for the six membranes. The curve is a hand-drawn line through the data points and is not a least squares fit. In order to support the shape of this curve, data collected independently (70) for similar cellulose

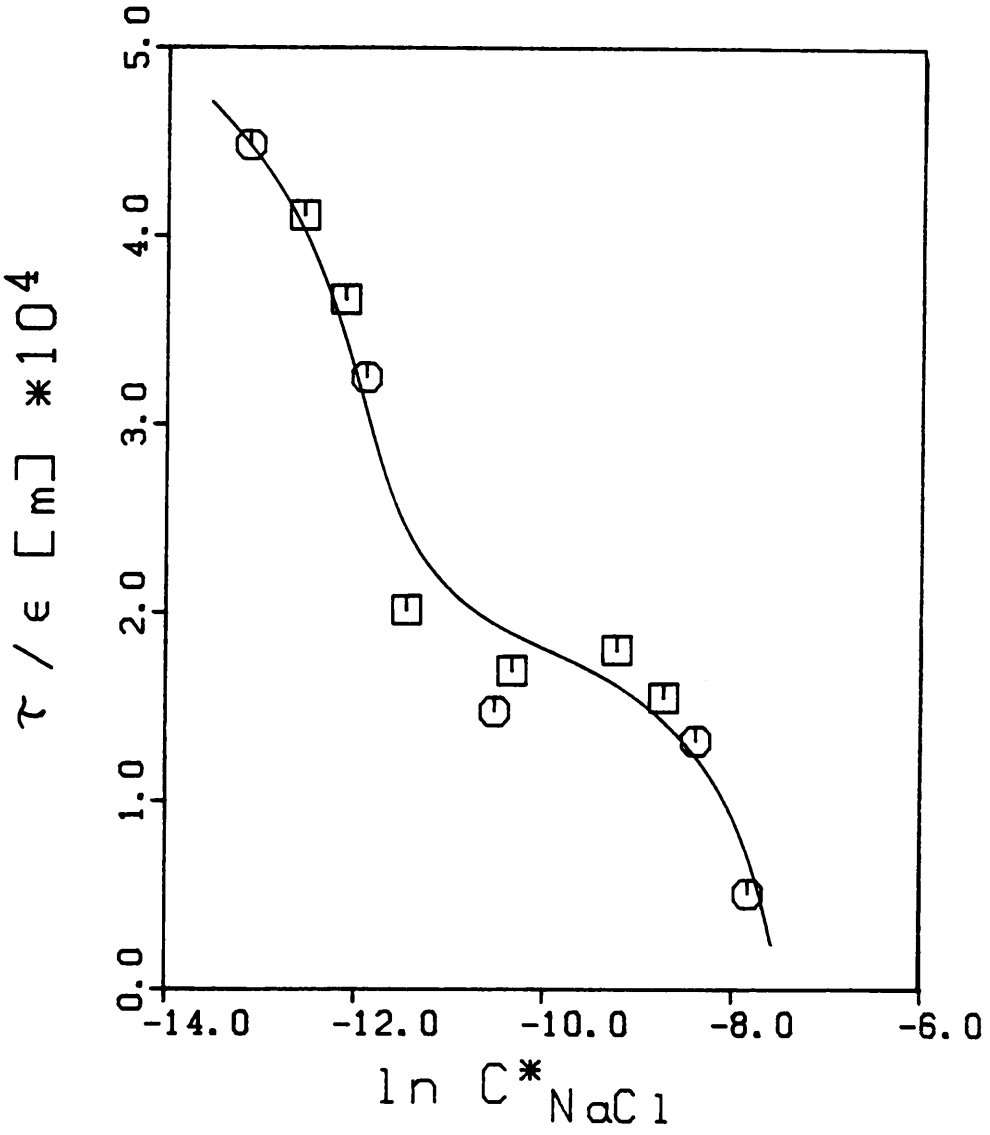

Figure 29. The relationship between the pore size parameters, τ/ε and $\ln C^*_{NaCl}$. (□) values determined for membranes 1-6; (O) values determined independently for five different cellulose acetate membranes with the solutes cyclohexane, cyclohexene, and 1,3-cyclohexadiene.

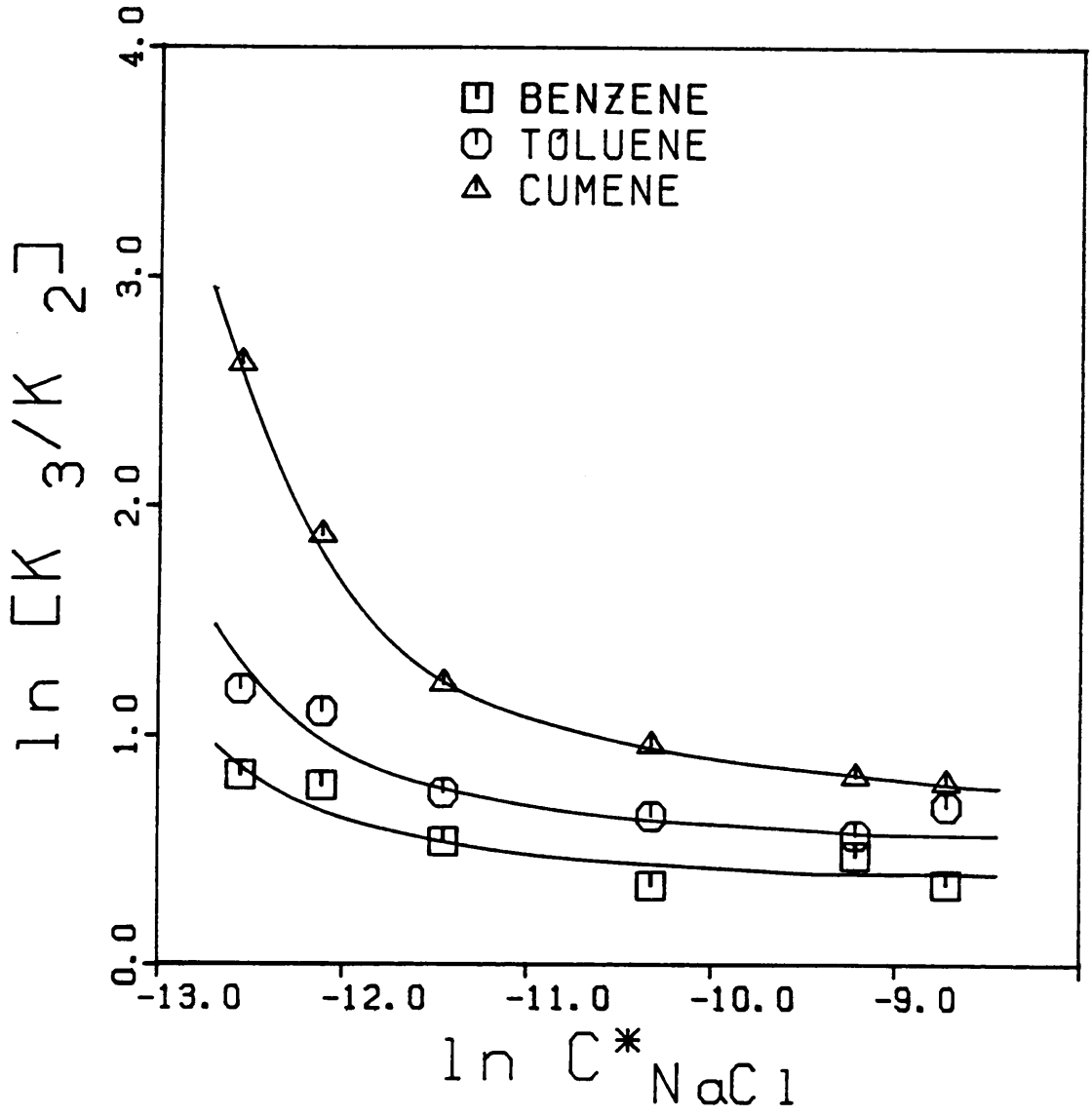

Figure 30. The relationship between the ratio of the partition coefficients on the low and high pressure side of the membrane, K_3/K_2, and the pore size parameter, $\ln C^*_{NaCl}$

acetate membranes and similar solutes (cyclic hydrocarbons) are also included in the figure. These additional data help confirm the shape of the curve although it is desirable to have more data in the middle pore size range.

Figure 30 illustrates the relationship between $\ln [K_3/K_2]$ and the pore size parameter $\ln C^*_{NaCl}$. This figure emphasizes the trends in K_3/K_2 as a function of solute and pore size as discussed above. Also, Figure 30 can be used to estimate the K_3/K_2 parameter for other cellulose acetate membranes for the solutes shown.

It can be concluded that the four parameter finely-porous model is successful at describing the separation of aromatic hydrocarbons from water by reverse osmosis. Since the pore size parameter τ/ε for each membrane is independent of solute, this lends credibility to the physical interpretation of the model. That b/K_2 is constant (independent of pore size and solute) is an unexpected result. Although this result simplifies the application of the model, care should be exercised in extrapolating this to other solutes without checking the correlation first. Also, the partition coefficient was found to be different on the high and low pressure side of the membrane. Future work should include a theoretical and an experimental examination of the behavior of the partition coefficient as a function of concentration, membrane structure, and possibly pressure. The possibility of independently estimating the partition coefficient using high pressure liquid chromatography (50, 81) or equilibrium sorption studies (7, 16) is being investigated.

To apply the model in a predictive sense for similar hydrocarbon solutes, concentrations, and pressures, it is necessary to have a relationship between the volume flux and the operating pressure. As was discussed in Section 3.3, the flux of solution through the membrane is usually less than the pure water flux. One possible method for describing the pore blocking effect is to use the empirical correlation represented by Equation (40) and Figure 15. The method will have limitations, due to the empirical nature of Equation (40).

Therefore, it would be difficult and dangerous to extrapolate these correlations beyond the limits of the present study. Further work needs to be done with more solutes to aid in generalizing the correlations. A more fundamental description of how pore blocking takes place needs to be incorporated into the model to describe the reduction in flux due to pore blocking. With additional information on the partition coefficients and a general description of the pore blocking phenomenon, the FPM-4 relationship promises to be useful in representing and explaining the separation of hydrocarbon type solutes by reverse osmosis.

3.8.3 Surface Force - Pore Flow Model

The surface force-pore flow model (SF-PF) has been discussed in Section 1.2.4. This model is more complex in several respects than any of the other models presented. The mathematical equations are more complex, the solution of the equations is more difficult, and more adjustable parameters appear in the model. To add to the complexity, the model can be used in various forms. In their original paper, Matsuura and Sourirajan (49) used the model in a different form than in their later papers (50, 60). The major difference concerns the form in which the friction function is expressed. The friction function has been discussed in Section 1.2.5 and is discussed again later.

Because of the mathematical complexity of the model, numerical solutions rather than analytical solutions are required. The numerical techniques used are discussed later in this section. Suffice it to say at this point that the solutions on the computer were time consuming and expensive.

The net result of the above considerations is that only preliminary results can be presented at this time. More work is required before results for all the membranes and solutes can be presented with confidence.

The remainder of this section addresses the following points. Two modifications that have been made to the original SF-PF model are presented. The numerical programs used in the analysis are discussed. The model is applied to NaCl-water data presented by Matsuura and Sourirajan (49) and to the NaCl-water data reported in this dissertation. The experimental results for the toluene-water system for two membranes are examined. Finally, suggestions are made concerning the use of the SF-PF model.

Pressure Dependence of the Solute Chemical Potential. As discussed for the ESD model, the pressure term in the solute chemical potential Equation (34) is significant compared to the concentration term. These results are summarized in Table 12. In the original development of the SF-PF model (49) the pressure induced solute transport was ignored. How the pressure term can be included in the model is presented in this section. The following mathematical development parallels the approach presented by Matsuura and Sourirajan (49) in their derivation of Equation (57).

The solute in the membrane pore has three forces acting on it: a diffusion driving force, $F_A(r,z)$, the frictional force between the solute and solvent, $F_{AB}(r,z)$, and the frictional force between the solute and membrane, $F_{AM}(r,z)$. At steady state, these forces balance so that:

$$F_A(r,z) + F_{AB}(r,z) + F_{AM}(r,z) = 0 \tag{81}$$

The expressions describing the latter two of the three forces are unaffected by the change in the chemical potential equation. From reference (49), the expressions are given as:

$$F_{AB}(r,z) = -X_{AB}[u_A(r,z) - u_B(r)] \tag{82}$$

$$F_{AM}(r,z) = -X_{AM}(r)\, N_A(r)/C_{AM}(r,z) \tag{83}$$

However, the diffusional driving force now includes the pressure term:

$$F_A(r,z) = -\frac{\partial \mu_A(r,z)}{\partial z} \tag{84}$$

$$F_A(r,z) = -\left| \frac{RT}{C_{AM}(r,z)} \frac{\partial C_{AM}(r,z)}{\partial z} + V_A \frac{\partial P(r,z)}{\partial z} \right| \tag{85}$$

Equations (82), (83), (85), and the definition of b given in Equation (44) written as a function of r, can be combined and rearranged to give:

$$N_A(r) = \left| -\frac{RT}{X_{AB}} \frac{\partial C_{AM}(r,z)}{\partial z} - \frac{V_A C_{AM}(r,z)}{X_{AB}} \left(\frac{\partial P(r,z)}{\partial z} \right) + C_{AM}(r,z)\, u_B(r) \right| / b(r) \tag{86}$$

Note that, from reference (49):

$$\frac{\partial P(r,z)}{\partial z} = \frac{P(r,\iota) - P(r,0)}{\iota} \tag{87}$$

$$\frac{\partial P(r,z)}{\partial z} = -\frac{\Delta P}{\iota} + \frac{RT}{\iota} \left(C_{A2} - C_{A3}(r) \right) \left| 1 - e^{-\phi(r)} \right| \tag{88}$$

Defining $\Delta P(r)$ as:

$$\Delta P(r) = -(P(r,\iota) - P(r,0)) \tag{89}$$

then:

$$\Delta P(r) = \Delta P - RT\,(C_{A2} - C_{A3}(r))\,[1 - e^{-\phi(r)}] \tag{90}$$

and Equation (86) may be rewritten as:

$$N_A(r) = \left| -\frac{RT}{X_{AB}} \frac{\partial C_{AM}(r,z)}{\partial z} + \frac{V_A C_{AM}(r,z)\, \Delta P(r)}{X_{AB}\, \iota} + C_{AM}(r,z)\, u_B(r) \right| / b(r) \tag{91}$$

Using the boundary conditions (49):

$$C_{AM}(r,0) = C_{A2}\, e^{-\phi(r)} \tag{92}$$

and

$$C_{AM}(r,\iota) = C_{A3}(r)\, e^{-\phi(r)} \tag{93}$$

and noting that:

$$C_{A3}(r) = N_A(r)/u_B(r) \tag{94}$$

then Equation (91) can be integrated with respect to z to give:

$$\frac{C_{A3}(r)}{C_{A2}} = \frac{\exp\left[\frac{X_{AB}{}^{\iota}}{RT}\left(u_B(r)+\frac{V_A\Delta P}{X_{AB}{}^{\iota}}\right)\right]}{1+\frac{b(r)}{\exp(-\phi(r))}\left(\frac{u_B(r)}{u_B(r)+\frac{V_A\Delta P}{X_{AB}{}^{\iota}}}\right)\left(\exp\left[\frac{X_{AB}{}^{\iota}}{RT}\left(u_B(r)+\frac{V_A\Delta P}{X_{AB}{}^{\iota}}\right)\right]-1\right)} \tag{95}$$

The integration of Equation (91) to give Equation (95) is presented in Appendix D.

Defining:

$$\beta_3(\rho) = \frac{V_A\Delta P(\rho)}{RT} \tag{96}$$

and using the other previously defined dimensionless groups (Equations (47) to (51)) and Equation (96), then Equation (95) can be rewritten as:

$$C_A(\rho) = \frac{\exp(\alpha(\rho)+\beta_3(\rho))}{1+\frac{b(\rho)}{\exp(-\phi(\rho))}\left(\frac{\alpha(\rho)}{\alpha(\rho)+\beta_3(\rho)}\right)\left(\exp(\alpha(\rho)+\beta_3(\rho))-1\right)} \tag{97}$$

This result can be compared with Equation (57) as derived by Matsuura and Sourirajan (49):

$$C_A(\rho) = \frac{\exp(\alpha(\rho))}{1+\frac{b(\rho)}{\exp(-\phi(\rho))}\left(\exp(\alpha(\rho))-1\right)} \tag{57}$$

When $\alpha(\rho) >> \beta_3(\rho)$, Equation (97) correctly reduces to Equation (57).

For dilute solutions the pressure term will dominate over the concentration term in Equation (90). In this case then $\Delta P = \Delta P$ and:

$$\beta_3 = \frac{V_A\Delta P}{RT} \tag{98}$$

Therefore, Equation (97) is further simplified by using a constant β_3 value. This dilute solution assumption must be used with caution. When the solute is attracted strongly to the membrane material, then $C_{A3}(\rho)$ may be large near the membrane surface. The best approach is to use Equation (97) where no dilute assumption has been made.

Friction Function. In the INTRODUCTION, several approaches to describe the friction function, b(ρ), were discussed. Since the SF-PF model is a two-dimensional representation of flow in a pore, it is possible to allow the friction function to vary both as a function of radial position in the pore and as a function of relative solute size, λ. Equations (65) and (66) are the two forms used by Matsuura and coworkers (49, 50, 60). For convenience these equations are repeated here:

$$b(\rho) = \begin{cases} \exp(10) & \text{when } d(\rho) \le \mathbf{D} \\ \exp(\mathbf{E}/d(\rho)) & \text{when } d(\rho) > \mathbf{D} \end{cases} \tag{65}$$

and

$$1/b = \begin{cases} 1 - 2.104\lambda + 2.09\lambda^3 - 0.95\lambda^5 & \text{when } \lambda \le 0.2275 \\ 1/(44.57 - 416.2\lambda + 934.9\lambda^2 + 302.4\lambda^3) & \text{when } \lambda > 0.2275 \end{cases} \tag{66}$$

The former is a function of both solute (**D** and **E** are different for each solute) and radial position (given here as distance from the wall, d(ρ)). The latter relationship is a function of only relative solute size, λ. In this work, a further modification of the form of the friction function is suggested.

It seems logical that as the solute moves away from the pore wall towards the pore center, the value of b should approach the Faxen Equation solution (given by Equation (63), or equivalently, the first half of Equation (66)). For Equation (65), b approaches 1.0 as d is increased instead of yielding the Faxen solution. On the other hand, Equation (66) has not included a radial dependence for b.

Based on the above observations, an approach which combines the feature of both Equations (63) and (65) is suggested. Let:

$$b(\rho) = b_{Faxen} \exp(\mathbf{E}/d(\rho)) \tag{99}$$

where b_{Faxen} is given by Faxen in Equation (63). As the solute moves away from the pore wall, b decreases exponentially, similar to Equation (65). However, b now approaches the Faxen solution near the pore center. Equation (99) appears to be more appropriate than

either equation used by Matsuura and Sourirajan. It must be recognized that Equation (99) is a semi-empirical representation of the friction forces acting on the solute in the pore and that **E** must be determined experimentally. It is expected that **E** is a function of the solute only for a given membrane material.

Steric Exclusion. The influence of steric exclusion was presented in Section 1.2.5. Several authors have used the Ferry-Faxen Equation (67) to include the effect of the size of the solute molecule on transport through membrane pores. Steric exclusion of the solute is included in the model through an additional contribution to the friction function, b.

In the SF-PF model a different approach is used. The finite size of the solute molecule is taken into account by the potential function given in Equation (61):

$$\phi(\rho) = \begin{cases} 10 & \text{when } d(\rho) \leq \mathbf{D} \\ \dfrac{\mathbf{B}}{d(\rho)^3} & \text{when } d(\rho) > \mathbf{D} \end{cases} \tag{61}$$

The solute molecule is strongly repelled by the membrane when the solute is less than a critical distance **D** from the surface of the membrane, where **D** is an effective radius for the solute. Therefore, the steric exclusion of solute is taken into account by the potential function rather than by the friction function.

Flux versus Pore Size for Different Membranes. The SF-PF model predicts that the flux of pure water should vary as a function of pore radius to the fourth power (49):

$$n_p \alpha R_e^4 \tag{100}$$

However, experimentally it is difficult to test this relationship. A series of membranes that have been annealed at different temperatures have different pore sizes and different water fluxes. However, there is no guarantee that the annealing process has altered only the average pore radius. In addition, the effective pore length, τ, the shape of the pore size

distribution, and the number of pores must remain unchanged. Previously, Glueckauf (82) found that the pure water flux varied as:

$$n_p \alpha R_e^{1.5} \tag{101}$$

The lower dependency on R_e is probably caused by the above mentioned factors. Matsuura and Sourirajan (49) used Equation (101) as an integral part of their application of the SF-PF model. The data for six membranes annealed at different temperatures were forced to follow Equation (101) in their parameter estimation scheme. In subsequent work by Sourirajan and coworkers (50), it was found that:

$$n_p \alpha R_e^{3.2} \tag{102}$$

was more appropriate. This dependency is closer to the predicted fourth power.

The conclusion which can be drawn from the previous work summarized here is that the relationship between n_p and R_e is dependent on the mechanism of the annealing process. If the annealing process is ideal in the sense that only the average pore size is changed, then Equation (100) should be valid. For the membranes used in this work, the dependency between n_p and R_e is unknown. Therefore, in the current project no relationship between n_p and R_e is assumed. The R_e values for each membrane are determined independently.

Numerical Analysis. Before continuing to the results of applying the SF-PF model, it is appropriate to summarize the numerical methods. The equations of interest from a numerical methods point of view are the differential Equation (56) and the integrals in Equations (54) and (55).

Equation (56) is an ordinary nonlinear nonhomogeneous second order differential equation:

$$\frac{d^2\alpha(\rho)}{d\rho^2} + \frac{1}{\rho}\frac{d\,\alpha(\rho)}{d\rho} + \frac{\beta_2}{\beta_1} + \frac{1}{\beta_1}(1 - \exp(-\phi(\rho))(C_A(\rho) - 1)$$

$$- \frac{1}{\beta_1}(b(\rho) - 1)\,\alpha(\rho)\,C_A(\rho) = 0 \qquad (56)$$

where $C_A(\rho)$ is given by Equation (97). The manner in which the dimensionless velocity, $\alpha(\rho)$, varies as a function of dimensionless radial position, ρ, is described by this differential equation. The two boundary conditions are given by:

$$\frac{d\,\alpha(\rho)}{d\,\rho} = 0 \qquad \text{when } \rho = 0 \qquad (58)$$

and

$$\alpha(\rho) = 0 \qquad \text{when } \rho = 1 \qquad (59)$$

which indicate that the $\alpha(\rho)$ is finite at the pore center and that there is no slip at the wall, respectively.

For pure water permeation, the fourth and fifth terms in Equation (56) are zero and the analytical solution is:

$$\alpha(\rho) = \frac{\beta_2}{4\beta_1}(1 - \rho^2) \qquad (103)$$

Equation (103) can be integrated to average the flux in the radial direction which gives the following relationship for the flow rate of pure water through a single pore:

$$Q_p = g\,\pi\,R_e^4\,\Delta P/8\,\eta\,\iota \qquad (104)$$

which is the well known Poiseuille equation (see for instance reference (29)). In other words the velocity distribution is parabolic. The fourth and fifth terms in Equation (56) distort the velocity distribution from the usual parabolic shape, reflecting the influence of friction forces and surface-solute interactions. No analytical solution is known for Equation (56), except as above, and therefore a numerical solution is necessary.

Equation (56) can be rewritten as two simultaneous first order equations, and a fourth order Runge-Kutta method (see for instance reference (83)) may be used. However, to

apply the Runge-Kutta method, it is necessary that both boundary conditions be known at one end of the interval. For the given problem, one boundary condition is known at each end of the interval producing a two point boundary value problem. Therefore, the procedure is as follows:

1) Estimate $\alpha(\rho)$ at $(\rho) = 0$, noting that $d\alpha(\rho)/d\rho = 0$.

2) Integrate with Runge-Kutta from $\rho = 0$ to $\rho = 1$.

3) At $\rho = 1$, check if $\alpha(1) = 0$.

4) If $\alpha(1) \neq 0$, then update the estimate of $\alpha(0)$ and repeat 2)-4).

5) If $\alpha(1) = 0$, then the solution is complete.

Several unidimensional search algorithms are possible to update $\alpha^n(0)$, for the n^{th} iteration, based on $\alpha^{n-1}(1)$, for the previous iteration. The simplest method seems to work as well as any, that is:

$$\alpha^n(0) = \alpha^{n-1}(0) - \alpha^{n-1}(1) \tag{105}$$

A good initial estimate (step 1) above) for this algorithm is suggested by the approximate solution given earlier as Equation (103) at $\rho = 0$:

$$\alpha^0(0) = \beta_2/4\,\beta_1 \tag{106}$$

The end result of the above application of the Runge-Kutta technique is that $\alpha(\rho)$ is known at various values of ρ over the interval $0 \leq \rho \leq 1$. Fifty equal size steps were used over the interval.

The evaluation of the integrals in Equation (54) and hence in Equation (55) is relatively simple:

$$f' = 1 - \frac{\int_0^1 C_A(\rho)\,\alpha(\rho)\,\rho\,d\,\rho}{\int_0^1 \alpha(\rho)\,\rho\,d\,\rho} \tag{55}$$

A trapezoidal method (84) can be used to integrate the above integrals from the $\alpha(\rho)$ values determined above by solving the differential Equation (56).

The above information summarizes the numerical techniques required to apply the SF-PF model. However, if the model parameters (A, **A** or **B**, **D**, **E**, and R_W) are unknown then they need to be determined based on experimental data. The method of searching for parameters was discussed in Section 3.5. It was often found that ZXSSQ (75) was unsatisfactory as a search routine. The ZXSSQ algorithm would generate relatively large changes in some of the parameters resulting in the overall calculation algorithm becoming unstable. The GRG2 code (79), which is a constrained nonlinear parameter estimation algorithm, provided a useful alternative. By constraining the parameters to reasonable limits, it was possible to find optimum parameters. Since the SF-PF model simultaneously predicts the separation, f', and the extent of pore blocking, the sum of the squares error (SSQ) in both of the performance variables was used to evaluate the model. The optimization routine tries to minimize SSQ, calculated as:

$$SSQ = SSQ_{f'} + SSQ_{(1-n_T/n_P)} \tag{107}$$

where

$$SSQ_{f'} = \sum_{i=1}^{n} \left| f'_i - f'_{cal} \right|^2 \tag{108}$$

$$SSQ_{(1-n_T/n_P)} = \sum_{i=1}^{n} \left| (1-n_T/n_P)_i - (1-n_T/n_P)_{cal} \right|^2 \tag{109}$$

The f'_{cal} and $(1 - n_T/n_P)_{cal}$ represent the model-calculated values corresponding to the experimental value of f_i' and $(1 - n_T/n_P)_i$, respectively. It is possible to weigh one SSQ_i over the other, but an equal weighting was used in this work. The absolute values of f' and $(1 - n_T/n_P)$ are of the same order of magnitude and so an even weighting seems reasonable.

From the above discussion it can be seen that the calculations involved in estimating parameters for the SF-PF model are lengthy. This situation is caused by having iterations within iterations within iterations. For example, it was not unusual to have the EXP Fortran subroutine, which is required in Equations (56), (57), and (99), to be called more than a million times. The computing time and cost were quite large. Unfortunately, this put real limits on how much evaluation could be done with this model.

NaCl-Water Data. The computer programs developed to describe the SF-PF model were tested by reanalyzing the NaCl-water data reported by Matsuura and Sourirajan (49). In order to simulate the model used by Matsuura and Sourirajan, it was necessary to make the following adjustments to the computer program. R_B was set to zero, since Matsuura and Sourirajan did not take into account the size of the water molecule. The function $b(\rho)$ was set to 1.0, which is equivalent to stating that the diffusivity of the solute in the pore is the same as the bulk solution diffusivity. Equation (101) was used to force the 1.5 power dependence of R_e on n_p. For an inorganic solute, Equation (60) was used to describe the potential function. An iterative search was applied to find the best **A** value to fit the data for all six membranes. **A** was found to be approximately 50×10^{-10} m compared to the value of 21×10^{-10} m reported by Matsuura and Sourirajan (49). However, when the calculation was redone based on the data for their membranes 3 and 6 only (85), good agreement was found between their data and the computer program developed. The R_W values agreed within 5% and the **A** value was 18×10^{-10} m. The minimum in the sum of the squares error, SSQ, as a function of **A** was broad, which implies a relatively large uncertainty in **A**. The analysis as described in this paragraph has several questionable assumptions built into it and was only used to check the computer subroutines against the results reported previously. These problems are discussed later.

In order to use the SF-PF model on the NaCl-water data, it is useful to have an estimate of the size of the NaCl molecule. The size of the solute molecule is required to use the modified Faxen Equation (99). Since NaCl exists in solution as hydrated Na^+ and Cl^- ions, which differ in size, it is difficult to determine the correct solute size to use in the modified Faxen Equation.

The application of the SF-PF model suggested by Sourirajan and coworkers (49, 50, 60) depends on defining the membrane pore size from NaCl-water data alone. In order to be successful with this approach, they had to carefully exclude some of the NaCl-water data on an arbitrary basis. Also, one of Equations (100), (101), or (102) had to be chosen to describe the dependence of water flux as a function of pore size. When the above approach was applied to the NaCl-water data reported in this work, no minimum in SSQ could be found as a function of **A**.

In the current work, a different approach which avoids the above difficulties was employed. The method allowed the pore size to be determined simultaneously along with the other unknowns for the organic solute data only. This approach avoids the problem of defining the pore size based on NaCl-water data and the problems of specifying a relationship between pore size and water flux for different membranes. The actual method used is discussed in the next section.

Toluene-Water Data. As a preliminary evaluation of the SF-PF model, the toluene-water data for two of the membranes was evaluated. A summary of the equations used is given as follows. The basic equations of the SF-PF model given by Equations (47)-(56), (58), (59), (62), (97), and (98) were used. The surface potential for an organic solute was described by Equation (61). For the friction function, the modified Faxen Equation (99) was applied. The adjustable parameters for a given membrane are A, R_W, **B**, **D**, and **E**. The pure water

permeability coefficient, A, has been calculated and is given for each membrane in Table 5. The distance of closest approach of the solute to the pore wall, **D**, can be approximated by the solute radius, R_A. There are several methods possible to calculate the solute radius (62). In this work the Stokes-Einstein equation was used:

$$R_A = \frac{RT}{6\pi\eta D_{AB} N_o} \tag{110}$$

Therefore the values for solute radius, listed in Table 1, were calculated based on the solute diffusivity and Equation (110). Preliminary studies indicate that the adjustable parameter in the friction function, **E**, can be set to zero. Setting **E** = 0.0 is equivalent to using only the Faxen equation to represent the friction function, b.

The above approximations simplify the model to two adjustable parameters, R_W and **B**. The data for separation and pore blocking are used to estimate the unknown parameters, using the numerical techniques outlined earlier in this section. Unfortunately, even with only two adjustable parameters, numerical optimization is time consuming and expensive.

The results obtained for membranes 1 and 3 are summarized in Figures 31-34. Figures 31 and 33 illustrate the agreement between calculated and experimental separation for membranes 1 and 3, respectively. Similarly, Figures 32 and 34 illustrate the agreement between the calculated and the experimental extent of pore blocking. The calculated separation corresponds well with the experimental separation in the low separation region. However, in the high separation region, the model systematically underestimates the separation. The agreement between calculated and experimental extent of pore blocking is excellent. The model well represents the extent of pore blocking. This result is significant. Of all the models examined, only the SF-PF model is able to predict the extent of pore blocking from first principles. The KSA model uses Equation (40) to describe the extent of pore blocking but the equation is empirical and is not derived from the model.

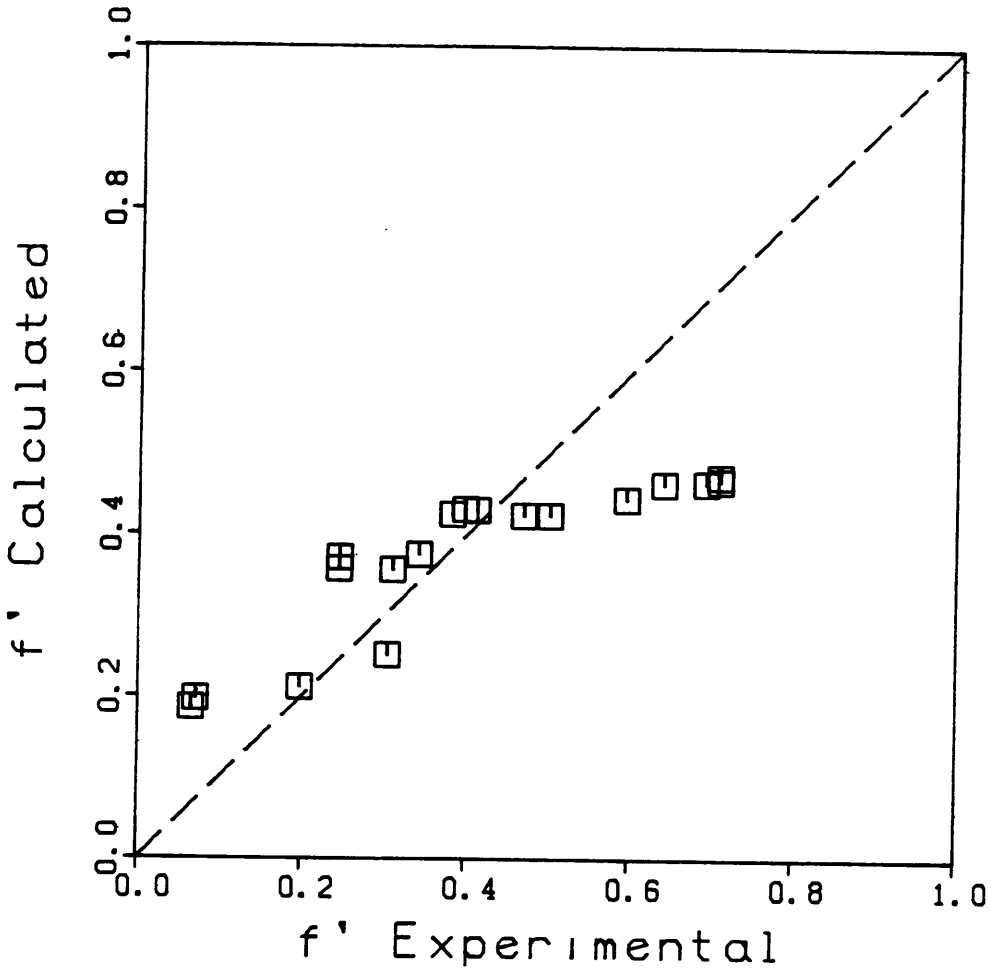

Figure 31. Comparison of the separation measured and the separation calculated by the surface force-pore flow model for the solute toluene and membrane 1.

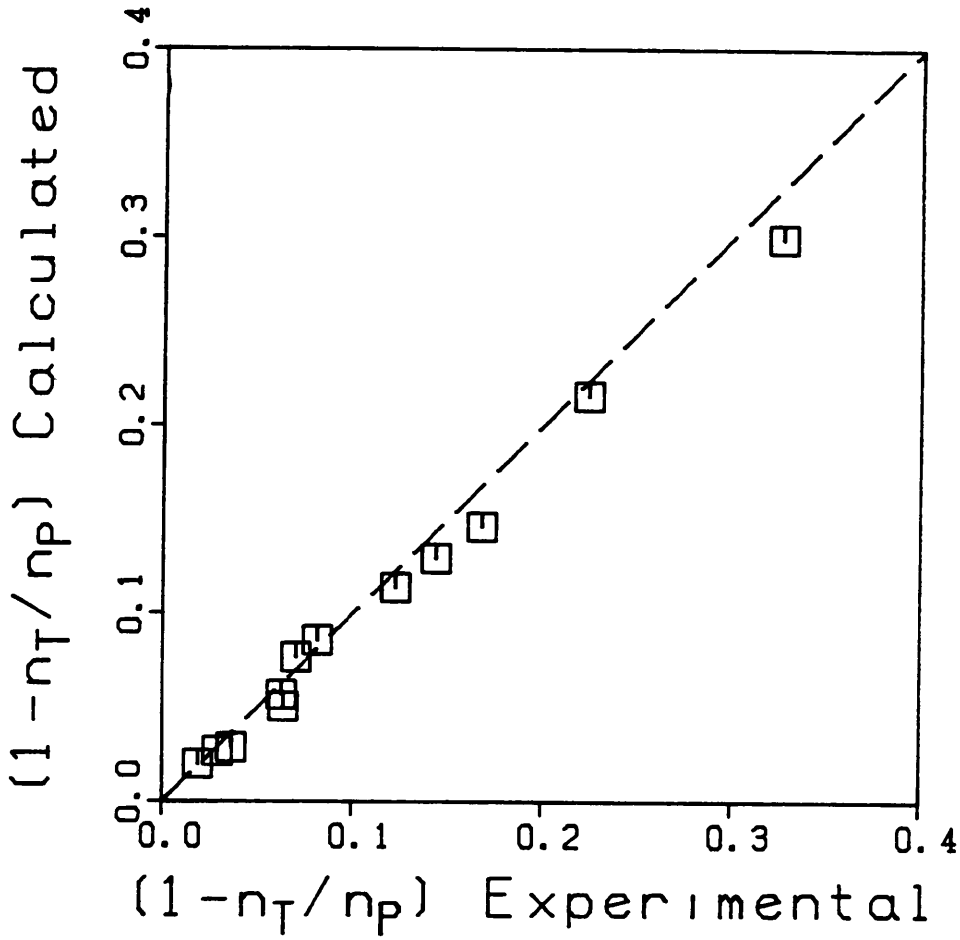

Figure 32. Comparison of the extent of pore blocking ($1 - n_T/n_P$), measured and calculated by the surface force-pore flow model for the solute toluene and membrane 1.

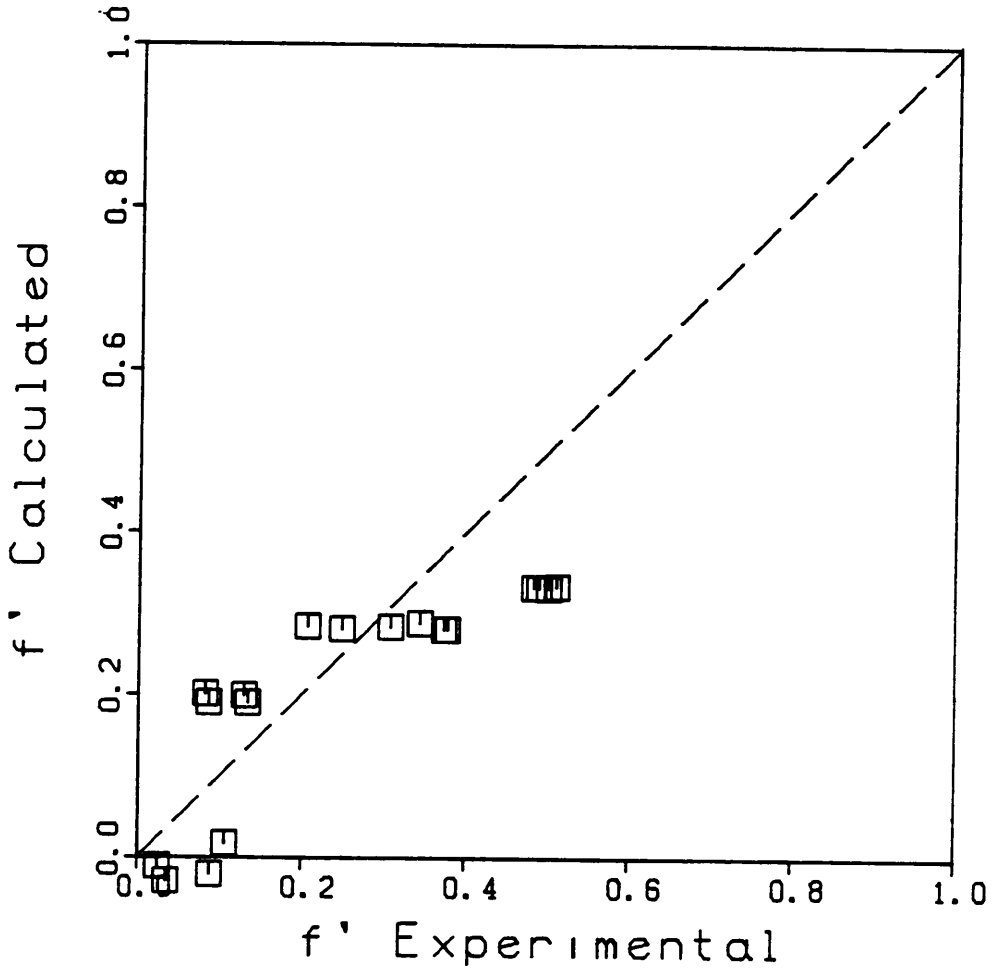

Figure 33. Comparison of the separation measured and the separation calculated by the surface force-pore flow model for the solute toluene and membrane 3.

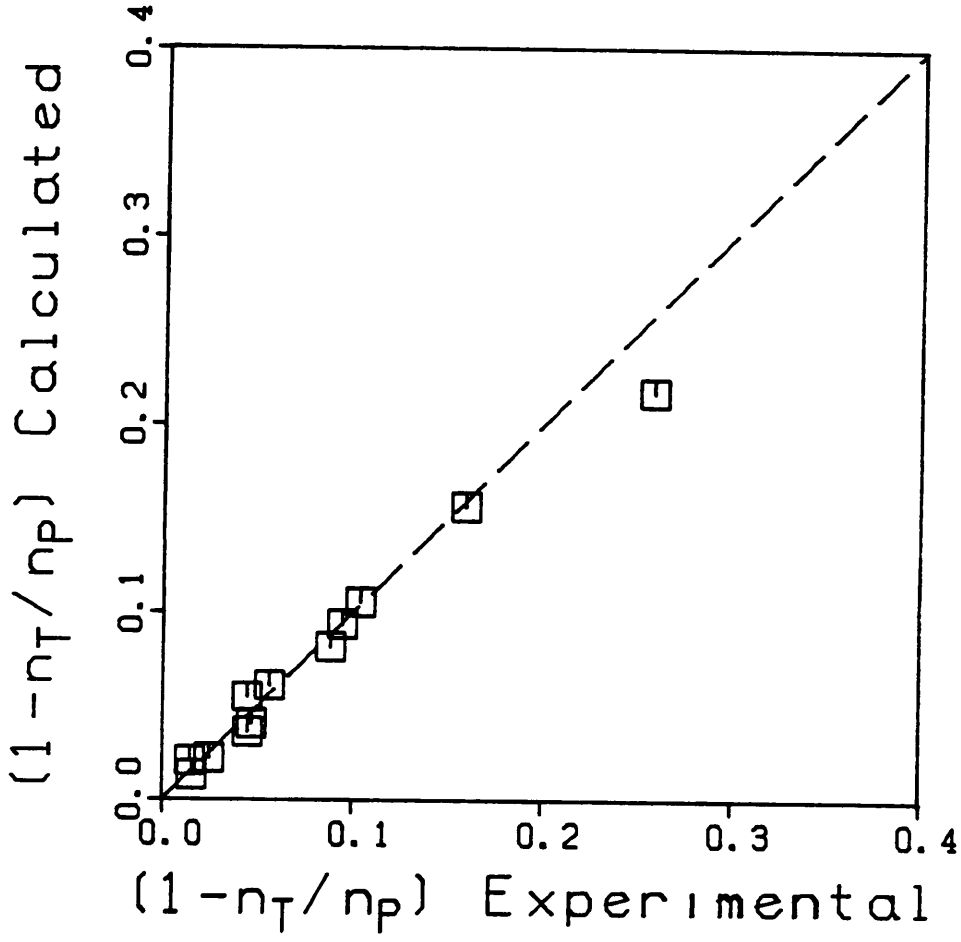

Figure 34. Comparison of the extent of pore blocking ($1 - n_T/n_p$), measured and calculated by the surface force-pore flow model for the solute toluene and membrane 3.

Table 15

Parameters for the Surface Force-Pore Flow (SF-PF) Model for the Solute Toluene

	Membrane 1	Membrane 3
Parameters		
R_W, x 10^{10}, m	4.511	5.217
B, x 10^{30}, m^3	157.7	152.3
D^a, x 10^{10}, m	2.52	2.52
E^a, m	0.0	0.0
Sum of Square Errors		
SSQ_f,	0.302	0.196
$SSQ_{(1 - n_f/n_p)}$	0.005	0.004

[a] These parameters were fixed at the values shown.

The values of R_W and **B** generated for the two membranes are compiled in Table 15. Since membrane 3 is the more open of the two membranes, it is expected that R_W for membrane 3 would be larger than R_W for membrane 1. The results in Table 15 confirm that R_W is about 16% larger for membrane 3 than for membrane 1. These values of R_W are consistent in magnitude with those calculated with the SF-PF model by Sourirajan and coworkers for similar cellulose acetate membranes (49, 50). Similar magnitude values are also predicted by the theories proposed by Glueckauf (82) and Bean (56). On the other hand, since the polymer and solute are fixed, **B** should be the same for both membranes. The values of **B** determined agree within $\pm 2\%$, which supports the above expectation. The larger SSQ value for separation compared to the extent of pore blocking reflects the relative deviation between the model and the experimental results.

Again it must be emphasized that the numerical difficulties in determining the values of R_W and **B** were large. It was necessary to adjust the initial estimate of the parameters manually until the minimum in SSQ was almost reached. At this point the automated search routine (either ZXSSQ or GRG2) would converge to the solution. If the initial estimate was too far from the solution, ZXSSQ would generate a relatively large step in one of the parameters and the search would diverge from the solution. For GRG2, an initial guess too far from the solution would generate a search that adjusted the parameters by small increments such that little or no change in SSQ resulted. The routine would then terminate prematurely before the minimum was reached. Apparently neither ZXSSQ nor GRG2 are doing a good job in this case. Future work should include trying other search routines.

Rather than apply the SF-PF model to all the solutes and all of the membranes, this part of the project was halted. It is now necessary to reevaluate each of the numerical routines for accuracy and efficiency and try to improve the practical application of the SF-PF model.

In summary, the results for the SF-PF model are both encouraging and discouraging. On the positive side, the model is able to predict both the trends in separation and the trends in flux which no other one model could do. The accuracy of the prediction of separation was satisfactory in the low separation region, but deviated in the higher separation region. For the extent of pore blocking, the prediction was excellent. On the negative side, the application of the model is at the moment impractical. The numerical analysis is expensive in terms of real time and computer time. Future work should center around the reevaluation of the numerical program. In addition, the exact form of the friction function and the potential functions may be modified to improve the accuracy of the prediction.

CONCLUSIONS

This dissertation has examined both the qualitative and quantitative aspects of describing reverse osmosis transport phenomena in the presence of strong solute-membrane affinity. The major findings and conclusions of this research are summarized here.

Experimental data for the flux and separation of aqueous solutions has been reported for various solutes, membranes, and operating conditions. The three organic solutes were benzene, toluene, and cumene. Results have been reported at four pressures ranging from 670 to 6900 kPa and at several concentrations ranging from 5 to 260 ppm, for all three organic solutes and for all six cellulose acetate membranes. The six membranes were annealed at different temperatures in order to provide a series of membranes with gradated properties. Additional experiments to characterize and monitor the membrane performance with the solute sodium chloride were also performed.

The performance for the organic solutes was found to be markedly different than that for the solute sodium chloride. The difference in behavior is the result of the strong attraction between the solute and the membrane. These results have been explained, in a qualitative sense, by the preferential sorption-capillary flow mechanism. Performance varied systematically with the nonpolar character of the solute. An empirical equation, which describes the decrease in flux as a function of concentration, has been proposed. The results obtained are consistent with similar experiments performed by others.

Several transport models have been examined with respect to their ability to describe the observed data for the aromatic hydrocarbon-water-cellulose acetate systems. Included in this study are four phenomenological transport models (three forms of the irreversible thermodynamics-phenomenological transport model, IT-PT-A, IT-PT-B, and IT-PT-C, and the irreversible thermodynamics - Kedem Spiegler model, IT-KS), three nonporous

models (the solution-diffusion, SD, solution-diffusion imperfection, SDI, and extended solution-diffusion models, ESD), and four porous models (the Kimura-Sourirajan Analysis, KSA, two forms of the finely porous model, FPM-3 and FPM-4, and the surface force-pore flow model, SF-PF). Of the models examined, the experimental data were best represented by the FPM-4 and SF-PF models.

The four parameter version of the finely porous model, FPM-4, was able to quantitatively describe the observed data. The parameters generated for the FPM-4 model indicated that the pore size parameter, ι/ε, could be considered constant for a given membrane for all solutes. The partition coefficient on the high and the low pressure sides of the membrane differ. The partition coefficient is apparently changing as a function of membrane structure and/or concentration.

Considerable difficulty and expense (computer time) was encountered with applying the SF-PF model. Preliminary results for the solute toluene and two of the membranes were promising. The separation was well represented in the lower separation region and the model did an excellent job of predicting the flux characteristics. The average pore radii for the two membranes calculated by the SF-PF model were 4.51×10^{-10} m and 5.22×10^{-10} m, which are reasonable compared to estimates made by other researchers. The parameter **B** in the potential function equation was found to be constant for the two membranes analyzed by the SF-PF model.

The remaining models examined performed in less than a satisfactory manner. The IT-PT-A, ESD, and SDI relationships were able to curve fit the experimental data. However, the parameters generated were not consistent with basic premises of any of these models. The forms of the SD, KSA, IT-KS, and FPM-3 models were inconsistent with the observed data, and the IT-PT-B and IT-PT-C models were less satisfactory than the IT-PT-A model.

The conclusion is that none of the phenomenological or nonporous transport models examined are completely satisfactory at describing the reverse osmosis data for the aromatic hydrocarbon-water-cellulose acetate systems. The simple picture of solute and water dissolving in and diffusing through a homogeneous membrane is not sufficient in this case. In addition, modification of the solution-diffusion model to account for surface imperfections and to correct the chemical potential driving force for pressure induced solute transport are not sufficient to explain the observed data. The coefficients of the SDI model suggest that a major portion of the transport is occurring through imperfections, which implies that a porous model may be more correct. The mechanism-independent phenomenological transport models should always be applicable. That the phenomenological models are not applicable has been demonstrated. The failure of the phenomenological models is probably related to the nature of the solute-membrane attraction. The porous models were the most promising of all the models examined. However, this result does not necessarily mean that a porous transport mechanism is correct. More work is required to further resolve the problem of modelling reverse osmosis transport in the presence of strong solute-membrane affinity.

RECOMMENDATIONS

A great deal of work still needs to be done before a full understanding of transport in reverse osmosis membranes is reached. This statement is particularly true for systems such as those addressed in this dissertation in which a strong attraction between the solute and membrane exists. The ultimate goal of this research is to develop a transport model which will describe the performance of a membrane under a variety of operating conditions for any solute (or solutes). In addition, it should be possible to predict the performance of a membrane for a new solute by relating the parameters in the transport model to the physicochemical nature of the solute. To realize these objectives both experimental and theoretical work remains to be done. The following is a list of recommendations for further work:

1) More data on the phenomena of strong solute-membrane attraction need to be collected. Although several authors have reported results, the breadth of systems examined has been limited. The approach here has been to measure many data for a few systems in order that the experimental behavior could be well established. It is now necessary to expand to other solutes. The purpose of this work would be to examine the influence of different interactive forces between the solute and the membrane on transport behavior as represented by the coefficients in the transport model. The solutes studied in this dissertation are aromatic hydrocarbons which are attracted to the membrane by nonpolar forces. Other solutes, such as aliphatic and alicyclic hydrocarbons, could be used to test the extension of the model to other cases where nonpolar forces dominate. Phenol and substituted phenols could be used to extend the model to include attraction to the membrane by polar forces. Higher alcohols, such as hexanol, could be used to include the effect of both polar and nonpolar forces. From this broad base of data it should be possible to develop

a model that can predict the behavior of cellulose acetate membranes for any strongly attracting solute.

2) Along the same idea as 1), new data needs to be collected for other membrane materials and compared with the results reported here. Other cellulosic membranes and commercially available polyamide and polyamide derivative membranes should be included in this study. The purpose of this research is twofold. First, the general form of the relationships developed in 1) could be tested for other membranes. Second, the model could be extended to include the effect of the physicochemical nature of the membrane. The second objective would require the independent development of a theory that can relate membrane structure to membrane performance.

3) It would be interesting to perform some mixed solute experiments. This work could include systems with one solute attracted and one repelled by the membrane (for example, toluene and NaCl) and with two solutes that both are attracted to the membrane (for example, benzene and toluene). The purpose of examining mixed solute systems is as follows. Industrial separation problems are almost always multicomponent systems. Therefore it is practically important to expand the theoretical treatment to include more than one solute. From a theoretical point of view, addition of another component increases the number of interaction forces present. For some systems, particularly with dilute solutions, the solutes may behave independently. With NaCl as one solute the influence of osmotic pressure on the model can be examined. This effect is difficult to study otherwise because most of the organic solutes have limited solubilities and hence limited osmotic pressures.

4) Almost all the data reported are at room temperature. It can be expected that the solute-solvent-membrane interation forces will each vary as a function of temperature. An Arrhenius type relationship can be used to describe the temperature dependence of the interactions and apparent activation energies can be calculated. The magnitude of the activation energy is an indication of the nature of the interaction force. This study could lead to a better understanding of the solute-solvent-membrane interactions.

5) The results reported here for the FPM-4 model suggest that the partition coefficient is not the same on the high and low pressure sides of the membrane. The dependence of the partition coefficient can be determined as a function of membrane structure by measuring equilibrium sorption of a solute on cellulose acetate powder, and on membrane samples annealed at different temperatures. The concentration dependence can be determined by measuring equilibrium sorption at different concentrations. These data can then be compared with the ratio of partition coefficients determined from the transport model. It is also possible to incorporate an expected dependence into a reformulation of the finely-porous model.

6) Along with the experimental study in recommendation 5) it would be possible to measure the water content of membranes annealed at different temperatures and treated at different solute concentrations. Measurements may be difficult as small changes in water content are expected. If no change is found then it is reasonable to assume that for a given membrane the pore size (in the finely-porous and the surface force-pore flow model) is independent of solute and solute concentration. If the water content does change then it may be possible to relate the water content to the observed change in flux with solute concentration.

7) Further work must be extended to improve the numerical methods used in the SF-PF model. At the moment the SF-PF model is impractical to apply on a routine basis to reverse osmosis systems. A more efficient and reliable search routine is required to estimate the unknown parameters in the model. It is necessary to examine the relative importance of each of the terms in the differential equation which describes the solution velocity in a pore (Equation (56)). Elimination of some terms would reduce computation time. It is possible to apply orthogonal collocation methods to the solution of the differential equation. Once the computational problems are reduced it is possible to modify the model by changing the form of the friction function and the solute-membrane interaction potential to improve the performance of the model. The influence of pore size distribution, noncylindrical pore geometry, and nonspherical solute geometry can also be included in the model.

8) The fact that the phenomenological models would not explain the experimental data is disturbing. Reasonable arguements why this happens have been presented. Yet it should be possible with further work to extend these models in a logical manner so that they would be successful. A theorectical study should be undertaken to examine the inclusion of attractive forces between the solute and membrane, along with the usual relationship between fluxes and forces, to produce a new transport model.

It is hoped that the above recommendations will provide a useful guide to further research efforts.

NOMENCLATURE

A	pure water permeability coefficient, kmol/m^2 s kPa.
A	force constant defined by Equation (60), m.
A_0	pure water permeability coefficient extrapolated to zero operating pressure as defined by Equation (15), kmol/m^2 s kPa.
B_1	constant defined by Equation (D-7) in Appendix D, m^{-1}.
B_2	constant defined by Equation (D-8) in Appendix D, kmol/m^4.
B	solute-membrane attraction constant defined by Equation (61), m^3.
b	friction parameter defined by Equation (44).
b_{Faxen}	friction parameter calculated by Equation (63).
C	molar density, kmol/m^3.
C_i	molar density at location i, kmol/m^3.
C_{ij}	molar concentration of component i in phase j, kmol/m^3.
C^*_{NaCl}	membrane pore size parameter with reference to the solute NaCl as defined by Equation (13).
C_A	dimensionless concentration defined by Equation (49).
D	closest distance of approach between solute and membrane, m.
D_{ij}	diffusivity of component i in component j, m^2/s.
d	distance from the center of the solute molecule to the membrane, m.
d.f.	degrees of freedom.
E	constant defined by Equation (65), m.
E_0, E_1, E_2	generalized transport parameters in Equations (68)-(71) and Table 3.
F_A	driving force for diffusion of the solute in a pore, kJ/m kmol.
F_{AB}	friction force between the solute and solvent, kJ/m kmol.
F_{AM}	friction force between the solute and pore wall, kJ/m kmol.

F_i	generalized thermodynamic force defined by Equation (16).
f	separation.
f'	separation calculated based on the boundary layer concentration.
$(-\Delta\Delta G/RT)_i$	free energy parameter for ion i.
g	density, kg/m^3.
J_i	generalized thermodynamic flux defined by Equation (16).
J_v	solvent volume flux, m^3/m^2 s.
K	solute partition coefficient.
K_i	solute partition coefficient at location i.
k	mass transfer coefficient, m/s.
L_{ij}	generalized thermodynamic phenomenological coefficients defined by Equation (16).
ℓ_{AP}	pressure-induced solute transport parameter, $kmol/m^2$ s kPa.
ℓ_p	hydraulic permeability coefficient, m/s kPa.
ℓ_π	osmotic permeability coefficient, m/s kPa.
N_i	molar flux of component i, $kmol/m^2$ s.
N_o	Avogadro's number, $kmol^{-1}$.
n	refractive index.
n_P	pure solvent mass flux, kg/m^2 s.
n_T	total solution mass flux, kg/m^2 s.
M_i	molecular mass of component i, kg/kmol.
m_{Ai}	molal concentration at location i, $kmol/m^3$.
ΔP	pressure difference across the membrane, kPa.
$\Delta \mathbf{P}$	effective pressure driving force defined by Equation (89), kPa.
P	polarizability, m^3.
p_A	solute permeability coefficient, m^2/s.

p_B	water permeability coefficient, $m^2/s\ kPa$.
Q_P	mass rate of pure water through a single pore, kg/s.
R	gas constant, kJ/kmol K.
R_W	radius of a pore, m.
R_e	effective radius of a pore as defined by Equation (52), m.
R_i	radius of component i, m.
r	radial position in a pore, m.
SSQ_i	residual sum of squares in response i.
s	standard deviation.
T	temperature, K.
u_B	velocity of solvent in a pore, m/s.
V_i	partial molar volume of component i, m^3/kmol.
X_{Ai}	mole fraction at location i.
x	coordinate direction perpendicular to the membrane, m.
Δx	membrane thickness, m.
Y	term defined by Equation (D-5) in Appendix D, $kmol/m^3$.
Y'	term defined by Equation (D-6) in Appendix D, $kmol/m^4$.
z	axial position in a pore, m.

Greek Symbols

α	dimensionless solvent velocity in a pore as defined by Equation (48).
β_1	dimensionless ratio defined by Equation (50).
β_2	dimensionless ratio of the applied pressure to the osmotic pressure at the pore entrance as defined by Equation (51).
β_3	dimensionless ratio defined by Equation (96).
γ	constant defined by Equation (15).

ε	fractional pore area.
Z, ζ	constants defined by Equation (40).
Z', ζ'	constants defined by Equation (41).
η	solution viscosity, kPa s.
$\kappa', \kappa'', \kappa'''$	transport parameters in the solution-diffusion imperfection model as defined by Equations (30) and (31).
λ	ratio of solute radius to pore radius.
μ_i	chemical potential of component i, kJ/kmol.
$\Delta\mu_i$	chemical potential difference across the membrane for component i, kJ/kmol.
π_i	osmotic pressure of solution i, kPa.
$\Delta\pi$	osmotic pressure difference across the membrane, kPa.
ρ	dimensionless radial position in a pore as defined by Equation (47).
σ	reflection coefficient.
ι	effective thickness of a membrane, m.
Φ	dimensionless potential function of force exerted on a solute molecule by a pore wall.
X_{ij}	friction coefficient between components i and j, kJ s/kmol m^2.
ω	transport parameter defined by Equation (21), kmol/m^2 s kPa.

Subscripts

A	solute
B	solvent
cal	calculated
e	effective
f'	with respect to f'
ln	logarithmic average
M	membrane

P	pure water
ref	reference
T	total solution
W	wall
$(1-n_T/n_P)$	with respect to $(1-n_T/n_P)$
1	feed solution
2	boundary layer solution
3	permeate solution

APPENDIX A

Derivation of the Solution-Diffusion Imperfection Model for Low Osmotic Pressure and Dilute Solutions

The purpose of this appendix is to illustrate the simplification of the SDI relationship for the case of low osmotic pressures ($\Delta P >> \Delta\pi$) and low concentrations. This analysis uses the SDI model as presented by Equation (32) and van't Hoff's law given by Equation (12) to derive Equation (33). The derivation of Equation (33) is not available in the literature and is therefore presented here explicitly.

The SDI model as presented by Jonsson and Boesen (34) is represented by:

$$\frac{1}{1-f'} = \frac{(\Delta P - \Delta\pi) + (\kappa'''/\kappa')\Delta P}{(\kappa''/\kappa')(\Delta\pi/C_{A2}) + (\kappa'''/\kappa')\Delta P} \tag{32}$$

When $\Delta P >> \Delta\pi$ then the above equation becomes:

$$\frac{1}{1-f'} = \frac{1 + \kappa'''/\kappa'}{(\kappa''/\kappa')(\Delta\pi/\Delta P\, C_{A2}) + (\kappa'''/\kappa')} \tag{A-1}$$

Substituting the van't Hoff Equation (12) into the definition of $\Delta\pi$ gives:

$$\Delta\pi = \pi_2 - \pi_3 \tag{A-2}$$

$$\Delta\pi = C_{A2}\,RT - C_{A3}\,RT \tag{A-3}$$

$$\Delta\pi = (C_{A2} - C_{A3})\,RT \tag{A-4}$$

Substituting Equation (A-4) into Equation (A-1) gives:

$$\frac{1}{1-f'} = \frac{1 + \kappa'''/\kappa'}{(\kappa''/\kappa')\left(\frac{C_{A2}-C_{A3}}{C_{A2}}\right)\left(\frac{RT}{\Delta P}\right) + \kappa'''/\kappa'} \tag{A-5}$$

Recognizing that $f' = (C_{A2} - C_{A3})/(C_{A2}$ (from Equation (7)) and inverting Equation (A-5) leads to:

$$1-f' = \frac{(\kappa''/\kappa')\,f'\,(RT/\Delta P)}{1 + \kappa'''/\kappa'} + \frac{\kappa'''/\kappa'}{1 + \kappa'''/\kappa'} \tag{A-6}$$

Collecting terms and rearranging Equation (A-6) gives:

$$f'\left(1 + \frac{(\kappa''/\kappa')(RT/\Delta P)}{1 + \kappa'''/\kappa'}\right) = 1 - \frac{\kappa'''/\kappa'}{1 + \kappa'''/\kappa'} \tag{A-7}$$

$$\frac{1}{f'} = \frac{1 + \kappa'''/\kappa' + \kappa''/\kappa'(RT/\Delta P)}{1 + \kappa'''/\kappa' - \kappa'''/\kappa'} \tag{A-8}$$

$$\frac{1}{f'} = 1 + \kappa'''/\kappa' + \kappa''/\kappa'(RT/\Delta P) \tag{33}$$

which is the form of the SDI model used in this project.

APPENDIX B

Raw Data for the NaCl-Water-Cellulose Acetate System

In this appendix the data obtained for the solute NaCl with the six cellulose acetate membranes are presented. The water flux reported, in kg/m^2s, is the average of measurements made with a pure water feed before and after the solution experiment. The solution flux, in kg/m^2s, was measured with NaCl present in the feed. The feed concentration is the average of samples collected at the start and end of the permeate sampling period. The separation is calculated based on the feed concentration by Equation (1). The other symbols and the units are defined in the NOMENCLATURE section.

Table B- 1

Data for Experiment Number 93

Solute: NaCl
Pressure: 6900. kPa
Feed Concentration: 10496.7 ppm
Feed Flow Rate: 400.0 mL/min

Membrane	1	2	3	4	5	6
Water Flux	.8631E-02	.1047E-01	.1520E-01	.2246E-01	.2787E-01	.2533E-01
Solution Flux	.7520E-02	.9124E-02	.1307E-01	.1919E-01	.2383E-01	.2175E-01
XA1	.3271E-02	.3271E-02	.3271E-02	.3271E-02	.3271E-02	.3271E-02
XA2	.3543E-02	.3560E-02	.3905E-02	.4223E-02	.4614E-02	.5380E-02
XA3	.6343E-04	.8277E-04	.1233E-03	.2738E-03	.6533E-03	.1452E-02
Separation	0.9807	0.9748	0.9624	0.9165	0.8008	0.5569
A	.6946E-07	.8425E-07	.1223E-06	.1807E-06	.2243E-06	.2039E-06
k	.9255E-04	.1053E-03	.7140E-04	.6969E-04	.5763E-04	.2824E-04
DAMK/TAU	.1374E-06	.2177E-06	.4274E-06	.1333E-05	.3936E-05	.8036E-05
lnC* NaCl	-12.5651	-12.1051	-11.4305	-10.2930	-9.2101	-8.4964

Table B- 2

Data for Experiment Number 97

Solute: NaCl
Pressure: 6900. kPa
Feed Concentration: 10570.3 ppm
Feed Flow Rate: 400.0 mL/min

Membrane	1	2	3	4	5	6
Water Flux	.8656E-02	.1054E-01	.1517E-01	.2245E-01	.2769E-01	.2442E-01
Solution Flux	.7556E-02	.9195E-02	.1307E-01	.1924E-01	.2395E-01	.2136E-01
XA1	.3294E-02	.3294E-02	.3294E-02	.3294E-02	.3294E-02	.3294E-02
XA2	.3499E-02	.3554E-02	.3864E-02	.4159E-02	.4368E-02	.4957E-02
XA3	.6343E-04	.9190E-04	.1256E-03	.2802E-03	.6702E-03	.1458E-02
Separation	0.9808	0.9722	0.9620	0.9152	0.7971	0.5581
A	.6966E-07	.8485E-07	.1221E-06	.1807E-06	.2229E-06	.1965E-06
k	.1234E-03	.1183E-03	.7927E-04	.7643E-04	.6986E-04	.3310E-04
DAMK/TAU	.1399E-06	.2447E-06	.4404E-06	.1393E-05	.4345E-05	.8900E-05
lnC* NaCl	-12.5474	-11.9881	-11.4004	-10.2488	-9.1113	-8.3943

Table B- 3

Data for Experiment Number 98

Solute: NaCl
Pressure: 6900. kPa
Feed Concentration: 9911.8 ppm
Feed Flow Rate: 400.0 mL/min

Membrane	1	2	3	4	5	6
Water Flux	.8614E-02	.1051E-01	.1511E-01	.2241E-01	.2750E-01	.2425E-01
Solution Flux	.7545E-02	.9165E-02	.1303E-01	.1912E-01	.2364E-01	.2126E-01
XA1	.3087E-02	.3087E-02	.3087E-02	.3087E-02	.3087E-02	.3087E-02
XA2	.3415E-02	.3537E-02	.3851E-02	.4248E-02	.4474E-02	.4787E-02
XA3	.5982E-04	.8586E-04	.1205E-03	.2678E-03	.6364E-03	.1347E-02
Separation	0.9807	0.9723	0.9611	0.9135	0.7944	0.5643
A	.6932E-07	.8454E-07	.1216E-06	.1803E-06	.2213E-06	.1952E-06
k	.7356E-04	.6589E-04	.5700E-04	.5555E-04	.5280E-04	.3118E-04
DAMK/TAU	.1348E-06	.2286E-06	.4218E-06	.1288E-05	.3926E-05	.8324E-05
lnC* NaCl	-12.5841	-12.0561	-11.4434	-10.3269	-9.2128	-8.4612

Table B- 4

Data for Experiment Number 101

Solute: NaCl
Pressure: 6900. kPa
Feed Concentration: 9453.1 ppm
Feed Flow Rate: 405.0 mL/min

Membrane	1	2	3	4	5	6
Water Flux	.8639E-02	.1046E-01	.1510E-01	.2241E-01	.2756E-01	.3201E-01
Solution Flux	.7541E-02	.9146E-02	.1303E-01	.1916E-01	.2371E-01	.2623E-01
XA1	.2944E-02	.2944E-02	.2944E-02	.2944E-02	.2944E-02	.2944E-02
XA2	.3493E-02	.3471E-02	.3813E-02	.4176E-02	.4431E-02	.6316E-02
XA3	.5569E-04	.7581E-04	.1112E-03	.2492E-03	.6145E-03	.1325E-02
Separation	0.9811	0.9743	0.9623	0.9156	0.7917	0.5507
A	.6952E-07	.8417E-07	.1215E-06	.1803E-06	.2218E-06	.2576E-06
k	.4338E-04	.5433E-04	.4880E-04	.5099E-04	.4808E-04	.2329E-04
DAMK/TAU	.1225E-06	.2047E-06	.3926E-06	.1219E-05	.3823E-05	.6960E-05
lnC* NaCl	-12.6803	-12.1665	-11.5152	-10.3827	-9.2394	-8.6401

Table B- 5

Data for Experiment Number 103

Solute: NaCl
Pressure: 6900. kPa
Feed Concentration: 10478.3 ppm
Feed Flow Rate: 400.0 mL/min

Membrane	1	2	3	4	5	6
Water Flux	.8641E-02	.1053E-01	.1518E-01	.2254E-01	.2781E-01	.3211E-01
Solution Flux	.7536E-02	.9131E-02	.1300E-01	.1911E-01	.2386E-01	.2612E-01
XA1	.3265E-02	.3265E-02	.3265E-02	.3265E-02	.3265E-02	.3265E-02
XA2	.3517E-02	.3668E-02	.4009E-02	.4400E-02	.4584E-02	.6581E-02
XA3	.5952E-04	.8401E-04	.1242E-03	.2819E-03	.7022E-03	.1412E-02
Separation	0.9818	0.9744	0.9621	0.9139	0.7855	0.5683
A	.6954E-07	.8470E-07	.1222E-06	.1814E-06	.2238E-06	.2584E-06
k	.9994E-04	.7683E-04	.6129E-04	.5942E-04	.5754E-04	.2544E-04
DAMK/TAU	.1301E-06	.2146E-06	.4168E-06	.1311E-05	.4321E-05	.7134E-05
lnC* NaCl	-12.6201	-12.1195	-11.4556	-10.3097	-9.1169	-8.6155

Table B- 6

Data for Experiment Number 109

Solute: NaCl
Pressure: 6900. kPa
Feed Concentration: 10257.5 ppm
Feed Flow Rate: 415.0 mL/min

Membrane	1	2	3	4	5	6
Water Flux	.9080E-02	.1086E-01	.1561E-01	.2316E-01	.2819E-01	.3122E-01
Solution Flux	.7756E-02	.9355E-02	.1334E-01	.1951E-01	.2401E-01	.2537E-01
XA1	.3196E-02	.3196E-02	.3196E-02	.3196E-02	.3196E-02	.3196E-02
XA2	.3998E-02	.3828E-02	.4053E-02	.4541E-02	.4703E-02	.6471E-02
XA3	.6011E-04	.7967E-04	.1230E-03	.2747E-03	.6533E-03	.1292E-02
Separation	0.9812	0.9751	0.9616	0.9143	0.7961	0.5966
A	.7307E-07	.8740E-07	.1256E-06	.1864E-06	.2269E-06	.2513E-06
k	.3414E-04	.5076E-04	.5436E-04	.5163E-04	.5164E-04	.2535E-04
DAMK/TAU	.1187E-06	.1993E-06	.4187E-06	.1259E-05	.3878E-05	.6326E-05
lnC* NaCl	-12.7116	-12.1932	-11.4509	-10.3500	-9.2251	-8.7357

Table B- 7

Data for Experiment Number 114

Solute: NaCl
Pressure: 6900. kPa
Feed Concentration: 10331.1 ppm
Feed Flow Rate: 415.0 mL/min

Membrane	1	2	3	4	5	6
Water Flux	.8987E-02	.1076E-01	.1549E-01	.2276E-01	.2913E-01	.3035E-01
Solution Flux	.7736E-02	.9318E-02	.1324E-01	.1931E-01	.2347E-01	.2459E-01
XA1	.3219E-02	.3219E-02	.3219E-02	.3219E-02	.3219E-02	.3219E-02
XA2	.3824E-02	.3710E-02	.4046E-02	.4393E-02	.5962E-02	.6529E-02
XA3	.6296E-04	.8199E-04	.1261E-03	.2819E-03	.6617E-03	.1288E-02
Separation	0.9805	0.9746	0.9609	0.9127	0.7950	0.6006
A	.7232E-07	.8660E-07	.1246E-06	.1831E-06	.2344E-06	.2442E-06
k	.4424E-04	.6425E-04	.5600E-04	.5751E-04	.3224E-04	.2462E-04
DAMK/TAU	.1298E-06	.2111E-06	.4270E-06	.1326E-05	.2934E-05	.6043E-05
lnC* NaCl	-12.6218	-12.1358	-11.4314	-10.2981	-9.5041	-8.7815

Table B- 8

Data for Experiment Number 119

Solute: NaCl
Pressure: 6900. kPa
Feed Concentration: 10441.5 ppm
Feed Flow Rate: 415.0 mL/min

Membrane	1	2	3	4	5	6
Water Flux	.9129E-02	.1090E-01	.1539E-01	.2289E-01	.2772E-01	.3038E-01
Solution Flux	.7748E-02	.9329E-02	.1299E-01	.1921E-01	.2337E-01	.2457E-01
XA1	.3254E-02	.3254E-02	.3254E-02	.3254E-02	.3254E-02	.3254E-02
XA2	.4154E-02	.3995E-02	.4342E-02	.4654E-02	.4967E-02	.6600E-02
XA3	.6869E-04	.9004E-04	.1377E-03	.2965E-03	.6904E-03	.1318E-02
Separation	0.9790	0.9724	0.9578	0.9091	0.7884	0.5958
A	.7346E-07	.8775E-07	.1238E-06	.1842E-06	.2230E-06	.2445E-06
k	.3120E-04	.4444E-04	.4348E-04	.4963E-04	.4570E-04	.2447E-04
DAMK/TAU	.1306E-06	.2156E-06	.4266E-06	.1310E-05	.3777E-05	.6130E-05
lnC* NaCl	-12.6160	-12.1144	-11.4323	-10.3107	-9.2514	-8.7672

Table B- 9

Data for Experiment Number 122

Solute: NaCl
Pressure: 6900. kPa
Feed Concentration: 10294.3 ppm
Feed Flow Rate: 420.0 mL/min

Membrane	1	2	3	4	5	6
Water Flux	.8825E-02	.1086E-01	.1505E-01	.2254E-01	.2760E-01	.3022E-01
Solution Flux	.7565E-02	.9300E-02	.1276E-01	.1893E-01	.2322E-01	.2441E-01
XA1	.3207E-02	.3207E-02	.3207E-02	.3207E-02	.3207E-02	.3207E-02
XA2	.3931E-02	.3972E-02	.4249E-02	.4628E-02	.4994E-02	.6595E-02
XA3	.7426E-04	.8586E-04	.1338E-03	.2859E-03	.6651E-03	.1283E-02
Separation	0.9769	0.9733	0.9584	0.9111	0.7932	0.6008
A	.7102E-07	.8741E-07	.1211E-06	.1814E-06	.2221E-06	.2432E-06
k	.3648E-04	.4256E-04	.4382E-04	.4785E-04	.4367E-04	.2404E-04
DAMK/TAU	.1460E-06	.2060E-06	.4159E-06	.1249E-05	.3571E-05	.5894E-05
lnC* NaCl	-12.5045	-12.1603	-11.4576	-10.3582	-9.3074	-8.8064

Table B-10

Data for Experiment Number 127

Solute: NaCl
Pressure: 6900. kPa
Feed Concentration: 9781.3 ppm
Feed Flow Rate: 405.0 mL/min

Membrane	1	2	3	4	5	6
Water Flux	.8807E-02	.1093E-01	.1504E-01	.2280E-01	.2797E-01	.3023E-01
Solution Flux	.7592E-02	.9378E-02	.1272E-01	.1911E-01	.2361E-01	.2473E-01
XA1	.3046E-02	.3046E-02	.3046E-02	.3046E-02	.3046E-02	.3046E-02
XA2	.3797E-02	.3927E-02	.4300E-02	.4669E-02	.4896E-02	.6254E-02
XA3	.6807E-04	.8199E-04	.1323E-03	.2755E-03	.6449E-03	.1230E-02
Separation	0.9777	0.9732	0.9567	0.9098	0.7888	0.5968
A	.7087E-07	.8798E-07	.1210E-06	.1835E-06	.2250E-06	.2433E-06
k	.3385E-04	.3613E-04	.3564E-04	.4154E-04	.4139E-04	.2430E-04
DAMK/TAU	.1389E-06	.2004E-06	.4047E-06	.1200E-05	.3585E-05	.6057E-05
lnC* NaCl	-12.5543	-12.1875	-11.4849	-10.3976	-9.3036	-8.7791

Table B-11

Data for Experiment Number 132

Solute: NaCl
Pressure: 6900. kPa
Feed Concentration: 10551.9 ppm
Feed Flow Rate: 420.0 mL/min

Membrane	1	2	3	4	5	6
Water Flux	.8805E-02	.1092E-01	.1488E-01	.2260E-01	.2758E-01	.3012E-01
Solution Flux	.7614E-02	.9353E-02	.1264E-01	.1901E-01	.2346E-01	.2462E-01
XA1	.3288E-02	.3288E-02	.3288E-02	.3288E-02	.3288E-02	.3288E-02
XA2	.3732E-02	.3959E-02	.4211E-02	.4597E-02	.4773E-02	.6368E-02
XA3	.7426E-04	.8989E-04	.1406E-03	.2965E-03	.6853E-03	.1318E-02
Separation	0.9775	0.9728	0.9574	0.9101	0.7921	0.6000
A	.7086E-07	.8784E-07	.1197E-06	.1818E-06	.2220E-06	.2424E-06
k	.5907E-04	.4922E-04	.4928E-04	.5251E-04	.5203E-04	.2615E-04
DAMK/TAU	.1550E-06	.2178E-06	.4376E-06	.1314E-05	.3937E-05	.6423E-05
lnC* NaCl	-12.4449	-12.1046	-11.4069	-10.3076	-9.2099	-8.7205

Table B-12

Data for Experiment Number 137

Solute: NaCl
Pressure: 6900. kPa
Feed Concentration: 10184.0 ppm
Feed Flow Rate: 400.0 mL/min

Membrane	1	2	3	4	5	6
Water Flux	.8715E-02	.1082E-01	.1468E-01	.2244E-01	.2716E-01	.2976E-01
Solution Flux	.7516E-02	.9291E-02	.1253E-01	.1896E-01	.2322E-01	.2433E-01
XA1	.3173E-02	.3173E-02	.3173E-02	.3173E-02	.3173E-02	.3173E-02
XA2	.3795E-02	.3912E-02	.4120E-02	.4506E-02	.4653E-02	.6330E-02
XA3	.7658E-04	.9205E-04	.1440E-03	.3063E-03	.6870E-03	.1292E-02
Separation	0.9759	0.9711	0.9548	0.9037	0.7840	0.5937
A	.7013E-07	.8707E-07	.1182E-06	.1806E-06	.2185E-06	.2395E-06
k	.4115E-04	.4331E-04	.4615E-04	.4976E-04	.4975E-04	.2469E-04
DAMK/TAU	.1552E-06	.2244E-06	.4546E-06	.1386E-05	.4026E-05	.6236E-05
lnC* NaCl	-12.4436	-12.0745	-11.3687	-10.2540	-9.1875	-8.7501

Table B-13

Data for Experiment Number 141

Solute: NaCl
Pressure: 6900. kPa
Feed Concentration: 8463.7 ppm
Feed Flow Rate: 415.0 mL/min

Membrane	1	2	3	4	5	6
Water Flux	.8711E-02	.1083E-01	.1471E-01	.2241E-01	.2733E-01	.2976E-01
Solution Flux	.7687E-02	.9534E-02	.1288E-01	.1738E-01	.2115E-01	.2236E-01
XA1	.2634E-02	.2634E-02	.2634E-02	.2634E-02	.2634E-02	.2634E-02
XA2	.3235E-02	.3314E-02	.3484E-02	.6330E-02	.6716E-02	.7873E-02
XA3	.5893E-04	.7116E-04	.1124E-03	.2383E-03	.5521E-03	.1063E-02
Separation	0.9777	0.9730	0.9574	0.9097	0.7908	0.5970
A	.7010E-07	.8719E-07	.1184E-06	.1803E-06	.2200E-06	.2395E-06
k	.3670E-04	.4061E-04	.4442E-04	.1866E-04	.1951E-04	.1524E-04
DAMK/TAU	.1430E-06	.2098E-06	.4304E-06	.6814E-06	.1898E-05	.3491E-05
lnC* NaCl	-12.5254	-12.1421	-11.4233	-10.9640	-9.9396	-9.3302

Table B-14

Data for Experiment Number 145

Solute: NaCl
Pressure: 6900. kPa
Feed Concentration: 10331.1 ppm
Feed Flow Rate: 400.0 mL/min

Membrane	1	2	3	4	5	6
Water Flux	.8774E-02	.1084E-01	.1466E-01	.2239E-01	.2726E-01	.2954E-01
Solution Flux	.7524E-02	.9301E-02	.1250E-01	.1882E-01	.2303E-01	.2424E-01
XA1	.3219E-02	.3219E-02	.3219E-02	.3219E-02	.3219E-02	.3219E-02
XA2	.3930E-02	.3931E-02	.4145E-02	.4630E-02	.4932E-02	.6269E-02
XA3	.7782E-04	.9364E-04	.1460E-03	.3079E-03	.6954E-03	.1309E-02
Separation	0.9759	0.9710	0.9548	0.9046	0.7845	0.5941
A	.7061E-07	.8723E-07	.1180E-06	.1802E-06	.2194E-06	.2377E-06
k	.3698E-04	.4541E-04	.4756E-04	.4771E-04	.4449E-04	.2539E-04
DAMK/TAU	.1524E-06	.2275E-06	.4572E-06	.1343E-05	.3784E-05	.6396E-05
lnC* NaCl	-12.4618	-12.0610	-11.3629	-10.2852	-9.2495	-8.7246

Table B-15

Data for Experiment Number 149

Solute: NaCl
Pressure: 6900. kPa
Feed Concentration: 10312.7 ppm
Feed Flow Rate: 400.0 mL/min

Membrane	1	2	3	4	5	6
Water Flux	.8680E-02	.1083E-01	.1464E-01	.2231E-01	.2706E-01	.2941E-01
Solution Flux	.7519E-02	.9253E-02	.1245E-01	.1874E-01	.2303E-01	.2406E-01
XA1	.3213E-02	.3213E-02	.3213E-02	.3213E-02	.3213E-02	.3213E-02
XA2	.3698E-02	.4038E-02	.4188E-02	.4646E-02	.4751E-02	.6319E-02
XA3	.8230E-04	.9853E-04	.1442E-03	.3063E-03	.6853E-03	.1293E-02
Separation	0.9745	0.9694	0.9552	0.9049	0.7873	0.5983
A	.6985E-07	.8716E-07	.1178E-06	.1796E-06	.2177E-06	.2367E-06
k	.5233E-04	.3947E-04	.4522E-04	.4687E-04	.4851E-04	.2500E-04
DAMK/TAU	.1716E-06	.2320E-06	.4449E-06	.1325E-05	.3886E-05	.6190E-05
lnC* NaCl	-12.3431	-12.0416	-11.3901	-10.2986	-9.2230	-8.7574

Table B-16

Data for Experiment Number 155

Solute: NaCl
Pressure: 6900. kPa
Feed Concentration: 10220.8 ppm
Feed Flow Rate: 400.0 mL/min

Membrane	1	2	3	4	5	6
Water Flux	.8710E-02	.1085E-01	.1470E-01	.2238E-01	.2723E-01	.2955E-01
Solution Flux	.7489E-02	.9277E-02	.1250E-01	.1887E-01	.2314E-01	.2420E-01
XA1	.3184E-02	.3184E-02	.3184E-02	.3184E-02	.3184E-02	.3184E-02
XA2	.3863E-02	.4013E-02	.4193E-02	.4562E-02	.4805E-02	.6331E-02
XA3	.7503E-04	.8865E-04	.1437E-03	.3063E-03	.6954E-03	.1327E-02
Separation	0.9765	0.9722	0.9550	0.9041	0.7821	0.5842
A	.7009E-07	.8734E-07	.1183E-06	.1801E-06	.2191E-06	.2378E-06
k	.3804E-04	.3920E-04	.4373E-04	.4833E-04	.4619E-04	.2441E-04
DAMK/TAU	.1487E-06	.2101E-06	.4446E-06	.1361E-05	.3919E-05	.6413E-05
lnC* NaCl	-12.4861	-12.1407	-11.3910	-10.2724	-9.2144	-8.7221

Table B-17

Data for Experiment Number 160

Solute: NaCl
Pressure: 6900. kPa
Feed Concentration: 10551.9 ppm
Feed Flow Rate: 420.0 mL/min

Membrane	1	2	3	4	5	6
Water Flux	.8653E-02	.1079E-01	.1463E-01	.2227E-01	.2719E-01	.2936E-01
Solution Flux	.7440E-02	.9252E-02	.1240E-01	.1869E-01	.2303E-01	.2415E-01
XA1	.3288E-02	.3288E-02	.3288E-02	.3288E-02	.3288E-02	.3288E-02
XA2	.3871E-02	.3958E-02	.4268E-02	.4682E-02	.4901E-02	.6291E-02
XA3	.7967E-04	.9527E-04	.1491E-03	.3241E-03	.7207E-03	.1377E-02
Separation	0.9758	0.9711	0.9548	0.9017	0.7814	0.5820
A	.6964E-07	.8686E-07	.1177E-06	.1792E-06	.2188E-06	.2363E-06
k	.4470E-04	.4872E-04	.4574E-04	.4860E-04	.4730E-04	.2556E-04
DAMK/TAU	.1567E-06	.2287E-06	.4497E-06	.1393E-05	.3975E-05	.6766E-05
lnC* NaCl	-12.4336	-12.0555	-11.3794	-10.2490	-9.2004	-8.6684

APPENDIX C

Raw Data for the Aromatic Hydrocarbon-Water-Cellulose Acetate System

In this appendix the data obtained for the three aromatic hydrocarbon solutes benzene, toluene, and cumene are presented. The data are tabulated in order by experiment number which corresponds to the order in which the data were obtained. Tables C-1 to C-3 summarize the information by solute, pressure, and concentration. The water flux, in kg/m^2s, is the average of measurements made with a pure water feed before and after the solution experiment. The solution flux, in kg/m^2s, was measured with the organic solute present in the feed. The feed concentration is the average of samples collected at the start and the end of the permeate sampling period. The separation is calculated based on the feed concentration by Equation (6). "Pore-blocking" is the extent of pore blocking as defined on page 21. Other symbols are defined in the NOMENCLATURE section.

Table C-1

Summary of the Data Collected for the Solute Benzene

Solute	Pressure kPa	Feed Concentration ppm	Experiment Number	Table Number
Benzene	690	53.4	129	C-32
		116.7	133	C-33
		138.2	128	C-31
		259.2	136	C-35
	1725	24.2	134	C-34
		40.4	125	C-30
		124.8	124	C-29
		227.0	123	C-28
	3450	38.4	118	C-25
		63.2	117	C-24
		90.7	116	C-23
		252.8	115	C-22
	6900	46.2	113	C-21
		77.9	112	C-20
		149.4	111	C-19
		243.9	110	C-18

Table C-2

Summary of the Data Collected for the Solute Toluene

Solute	Pressure kPa	Feed Concentration ppm	Experiment Number	Table Number
Toluene	690	11.2	102	C-13
		32.4	99	C-12
		76.7	96	C-11
		153.9	95	C-10
	1725	17.2	91A	C-7
		18.5	91B	C-8
		35.4	90	C-6
		85.1	89	C-5
		97.5	88	C-4
		214.1	94	C-9
	3450	45.4	121	C-27
		51.6	139	C-37
		136.7	138	C-36
		161.2	120	C-26
	6900	26.1	108	C-17
		55.8	106	C-16
		93.3	105	C-15
		211.4	104	C-14

Table C-3

Summary of the Data Collected for the Solute Cumene

Solute	Pressure kPa	Feed Concentration ppm	Experiment Number	Table Number
Cumene	690	6.8	154	C-49
		8.1	153	C-48
		15.9	152	C-47
		17.3	151	C-46
	1725	9.9	159	C-53
		12.2	158	C-52
		16.1	157	C-51
		25.9	156	C-50
	3450	7.7	150	C-45
		10.2	148	C-44
		16.0	147	C-43
		26.5	146	C-42
	6900	4.5	144	C-41
		8.1	143	C-40
		12.7	142	C-39
		24.6	140	C-38

Table C- 4

Data for Experiment Number 88

Solute: TOLUENE
Pressure: 1725. kPa
Feed Concentration: 97.5 ppm
Feed Flow Rate: 400.0 mL/min

Membrane	1	2	3	4	5	6
Water Flux	.2399E-02	.2932E-02	.4310E-02	.6660E-02	.8659E-02	.7883E-02
Solution Flux	.1996E-02	.2504E-02	.3862E-02	.6014E-02	.8044E-02	.7749E-02
XA1	.1906E-04	.1906E-04	.1906E-04	.1906E-04	.1906E-04	.1906E-04
XA2	.1949E-04	.1962E-04	.1948E-04	.1955E-04	.1910E-04	.2073E-04
XA3	.1174E-04	.1159E-04	.1546E-04	.1645E-04	.1893E-04	.1599E-04
Separation	0.3840	0.3920	0.1890	0.1370	0.0070	0.1610
Pore Blocking	0.1680	0.1460	0.1040	0.0970	0.0710	0.0170

Table C- 5

Data for Experiment Number 89

Solute: TOLUENE
Pressure: 1725. kPa
Feed Concentration: 85.1 ppm
Feed Flow Rate: 400.0 mL/min

Membrane	1	2	3	4	5	6
Water Flux	.2416E-02	.2928E-02	.4275E-02	.6686E-02	.8680E-02	.8039E-02
Solution Flux	.2069E-02	.2583E-02	.3871E-02	.6115E-02	.8110E-02	.7692E-02
XA1	.1664E-04	.1664E-04	.1664E-04	.1664E-04	.1664E-04	.1664E-04
XA2	.1705E-04	.1709E-04	.1720E-04	.1731E-04	.1702E-04	.1867E-04
XA3	.1002E-04	.1075E-04	.1190E-04	.1315E-04	.1519E-04	.1288E-04
Separation	0.3980	0.3540	0.2850	0.2100	0.0870	0.2260
Pore Blocking	0.1437	0.1179	0.0945	0.0854	0.0656	0.0431

Table C- 6

Data for Experiment Number 90

Solute: TOLUENE
Pressure: 1725. kPa
Feed Concentration: 35.4 ppm
Feed Flow Rate: 400.0 mL/min

Membrane	1	2	3	4	5	6
Water Flux	.2414E-02	.2940E-02	.4324E-02	.6718E-02	.8718E-02	.8027E-02
Solution Flux	.2263E-02	.2788E-02	.4120E-02	.6436E-02	.8428E-02	.7847E-02
XA1	.6927E-05	.6927E-05	.6927E-05	.6927E-05	.6927E-05	.6927E-05
XA2	.7097E-05	.7156E-05	.7124E-05	.7123E-05	.7258E-05	.7643E-05
XA3	.4385E-05	.4177E-05	.5355E-05	.5958E-05	.5715E-05	.5632E-05
Separation	0.3670	0.3970	0.2270	0.1400	0.1750	0.1870
Pore Blocking	0.0625	0.0517	0.0470	0.0420	0.0333	0.0225

Table C- 7

Data for Experiment Number 91

Solute: TOLUENE
Pressure: 1725. kPa
Feed Concentration: 17.2 ppm
Feed Flow Rate: 400.0 mL/min

Membrane	1	2	3	4	5	6
Water Flux	.2408E-02	.2945E-02	.4287E-02	.6668E-02	.8676E-02	.7923E-02
Solution Flux	.2338E-02	.2883E-02	.4225E-02	.6587E-02	.8575E-02	.7910E-02
XA1	.3364E-05	.3364E-05	.3364E-05	.3364E-05	.3364E-05	.3364E-05
XA2	.3477E-05	.3492E-05	.3515E-05	.3584E-05	.3570E-05	.4016E-05
XA3	.1732E-05	.1870E-05	.2187E-05	.2301E-05	.2624E-05	.2197E-05
Separation	0.4850	0.4440	0.3500	0.3160	0.2200	0.3470
Pore Blocking	0.0291	0.0211	0.0144	0.0122	0.0116	0.0017

Table C- 8

Data for Experiment Number 91

Solute: TOLUENE
Pressure: 1725. kPa
Feed Concentration: 18.5 ppm
Feed Flow Rate: 400.0 mL/min

Membrane	1	2	3	4	5	6
Water Flux	.2408E-02	.2945E-02	.4287E-02	.6668E-02	.8676E-02	.7923E-02
Solution Flux	.2321E-02	.2853E-02	.4181E-02	.6498E-02	.8498E-02	.7839E-02
XA1	.3626E-05	.3626E-05	.3626E-05	.3626E-05	.3626E-05	.3626E-05
XA2	.3739E-05	.3773E-05	.3785E-05	.3812E-05	.3792E-05	.4230E-05
XA3	.1983E-05	.1893E-05	.2371E-05	.2716E-05	.3024E-05	.2531E-05
Separation	0.4530	0.4780	0.3460	0.2510	0.1660	0.3020
Pore Blocking	0.0363	0.0315	0.0248	0.0255	0.0205	0.0107

Table C- 9

Data for Experiment Number 94

Solute: TOLUENE
Pressure: 1725. kPa
Feed Concentration: 214.1 ppm
Feed Flow Rate: 400.0 mL/min

Membrane	1	2	3	4	5	6
Water Flux	.2399E-02	.2936E-02	.4287E-02	.6653E-02	.8607E-02	.7739E-02
Solution Flux	.1615E-02	.2069E-02	.3179E-02	.5193E-02	.7111E-02	.6857E-02
XA1	.4188E-04	.4188E-04	.4188E-04	.4188E-04	.4188E-04	.4188E-04
XA2	.4304E-04	.4310E-04	.4317E-04	.4329E-04	.4288E-04	.4761E-04
XA3	.1742E-04	.2186E-04	.2831E-04	.3308E-04	.3744E-04	.2965E-04
Separation	0.5840	0.4780	0.3240	0.2100	0.1060	0.2920
Pore Blocking	0.3266	0.2951	0.2585	0.2195	0.1738	0.1139

Table C-10

Data for Experiment Number 95

Solute: TOLUENE
Pressure: 690. kPa
Feed Concentration: 153.9 ppm
Feed Flow Rate: 400.0 mL/min

Membrane	1	2	3	4	5	6
Water Flux	.9614E-03	.1208E-02	.1721E-02	.2730E-02	.3573E-02	.3109E-02
Solution Flux	.7458E-03	.9759E-03	.1447E-02	.2353E-02	.3208E-02	.2930E-02
XA1	.3010E-04	.3010E-04	.3010E-04	.3010E-04	.3010E-04	.3010E-04
XA2	.3056E-04	.3064E-04	.3074E-04	.3096E-04	.3110E-04	.3232E-04
XA3	.8880E-05	.1102E-04	.1502E-04	.1782E-04	.1969E-04	.1767E-04
Separation	0.7050	0.6340	0.5010	0.4080	0.3460	0.4130
Pore Blocking	0.2242	0.1919	0.1594	0.1380	0.1022	0.0576

Table C-11

Data for Experiment Number 96

Solute: TOLUENE
Pressure: 690. kPa
Feed Concentration: 76.7 ppm
Feed Flow Rate: 400.0 mL/min

Membrane	1	2	3	4	5	6
Water Flux	.9748E-03	.1222E-02	.1756E-02	.2760E-02	.3567E-02	.3120E-02
Solution Flux	.8555E-03	.1100E-02	.1601E-02	.2554E-02	.3401E-02	.3016E-02
XA1	.1500E-04	.1500E-04	.1500E-04	.1500E-04	.1500E-04	.1500E-04
XA2	.1526E-04	.1527E-04	.1533E-04	.1540E-04	.1537E-04	.1600E-04
XA3	.4425E-05	.6660E-05	.7921E-05	.9706E-05	.1139E-04	.9571E-05
Separation	0.7050	0.5560	0.4720	0.3530	0.2410	0.3620
Pore Blocking	0.1224	0.1001	0.0884	0.0748	0.0464	0.0335

Table C-12

Data for Experiment Number 99

Solute: TOLUENE
Pressure: 690. kPa
Feed Concentration: 32.4 ppm
Feed Flow Rate: 400.0 mL/min

Membrane	1	2	3	4	5	6
Water Flux	.9762E-03	.1221E-02	.1756E-02	.2760E-02	.3588E-02	.3057E-02
Solution Flux	.9143E-03	.1156E-02	.1677E-02	.2659E-02	.3485E-02	.2980E-02
XA1	.6344E-05	.6344E-05	.6344E-05	.6344E-05	.6344E-05	.6344E-05
XA2	.6460E-05	.6478E-05	.6493E-05	.6536E-05	.6533E-05	.6710E-05
XA3	.1986E-05	.2360E-05	.3312E-05	.3927E-05	.4543E-05	.4333E-05
Separation	0.6870	0.6280	0.4780	0.3810	0.2840	0.3170
Pore Blocking	0.0634	0.0536	0.0450	0.0366	0.0289	0.0253

Table C-13

Data for Experiment Number 102

Solute: TOLUENE
Pressure: 690. kPa
Feed Concentration: 11.2 ppm
Feed Flow Rate: 400.0 mL/min

Membrane	1	2	3	4	5	6
Water Flux	.9606E-03	.1215E-02	.1738E-02	.2737E-02	.3673E-02	.3665E-02
Solution Flux	.9425E-03	.1193E-02	.1711E-02	.2701E-02	.3654E-02	.3648E-02
XA1	.2183E-05	.2183E-05	.2183E-05	.2183E-05	.2183E-05	.2183E-05
XA2	.2221E-05	.2229E-05	.2236E-05	.2247E-05	.2245E-05	.2334E-05
XA3	.7967E-06	.8556E-06	.1113E-05	.1375E-05	.1617E-05	.1517E-05
Separation	0.6350	0.6080	0.4900	0.3700	0.2590	0.3050
Pore Blocking	0.0188	0.0187	0.0156	0.0134	0.0052	0.0047

Table C-14

Data for Experiment Number 104

Solute: TOLUENE
Pressure: 6900. kPa
Feed Concentration: 211.4 ppm
Feed Flow Rate: 400.0 mL/min

Membrane	1	2	3	4	5	6
Water Flux	.8595E-02	.1036E-01	.1491E-01	.2210E-01	.2714E-01	.3106E-01
Solution Flux	.5999E-02	.7611E-02	.1160E-01	.1827E-01	.2347E-01	.2795E-01
XA1	.4135E-04	.4135E-04	.4135E-04	.4135E-04	.4135E-04	.4135E-04
XA2	.4343E-04	.4328E-04	.4264E-04	.4575E-04	.4147E-04	.4182E-04
XA3	.3023E-04	.3341E-04	.3808E-04	.3494E-04	.4123E-04	.4123E-04
Separation	0.2690	0.1920	0.0790	0.1550	0.0030	0.0030
Pore Blocking	0.3020	0.2655	0.2220	0.1731	0.1353	0.1002

Table C-15

Data for Experiment Number 105

Solute: TOLUENE
Pressure: 6900. kPa
Feed Concentration: 93.3 ppm
Feed Flow Rate: 400.0 mL/min

Membrane	1	2	3	4	5	6
Water Flux	.8647E-02	.1042E-01	.1499E-01	.2219E-01	.2730E-01	.3089E-01
Solution Flux	.7325E-02	.9031E-02	.1336E-01	.2021E-01	.2530E-01	.2915E-01
XA1	.1825E-04	.1825E-04	.1825E-04	.1825E-04	.1825E-04	.1825E-04
XA2	.1896E-04	.1868E-04	.1840E-04	.1813E-04	.1798E-04	.2300E-04
XA3	.1522E-04	.1679E-04	.1794E-04	.1842E-04	.1851E-04	.1710E-04
Separation	0.1660	0.0800	0.0170	-.0090	-.0140	0.0630
Pore Blocking	0.1529	0.1335	0.1087	0.0892	0.0735	0.0565

Table C-16

Data for Experiment Number 106

Solute: TOLUENE
Pressure: 6900. kPa
Feed Concentration: 55.8 ppm
Feed Flow Rate: 400.0 mL/min

Membrane	1	2	3	4	5	6
Water Flux	.9071E-02	.1085E-01	.1562E-01	.2313E-01	.2828E-01	.3185E-01
Solution Flux	.8253E-02	.1018E-01	.1476E-01	.2199E-01	.2717E-01	.3095E-01
XA1	.1091E-04	.1091E-04	.1091E-04	.1091E-04	.1091E-04	.1091E-04
XA2	.1107E-04	.1139E-04	.1125E-04	.1133E-04	.1103E-04	.1728E-04
XA3	.1030E-04	.9488E-05	.1025E-04	.1043E-04	.1080E-04	.9543E-05
Separation	0.0560	0.1300	0.0600	0.0440	0.0100	0.1250
Pore Blocking	0.0901	0.0617	0.0550	0.0492	0.0392	0.0281

Table C-17

Data for Experiment Number 108

Solute: TOLUENE
Pressure: 6900. kPa
Feed Concentration: 26.1 ppm
Feed Flow Rate: 400.0 mL/min

Membrane	1	2	3	4	5	6
Water Flux	.9001E-02	.1088E-01	.1560E-01	.2323E-01	.2835E-01	.3152E-01
Solution Flux	.8678E-02	.1056E-01	.1527E-01	.2265E-01	.2761E-01	.3109E-01
XA1	.5099E-05	.5099E-05	.5099E-05	.5099E-05	.5099E-05	.5099E-05
XA2	.5172E-05	.5180E-05	.5163E-05	.5145E-05	.5528E-05	.5387E-05
XA3	.4839E-05	.4869E-05	.4981E-05	.5048E-05	.4742E-05	.5038E-05
Separation	0.0510	0.0450	0.0230	0.0100	0.0700	0.0120
Pore Blocking	0.0359	0.0296	0.0212	0.0249	0.0261	0.0136

Table C-18

Data for Experiment Number 110

Solute: BENZENE
Pressure: 6900. kPa
Feed Concentration: 243.9 ppm
Feed Flow Rate: 400.0 mL/min

Membrane	1	2	3	4	5	6
Water Flux	.9001E-02	.1082E-01	.1557E-01	.2292E-01	.2788E-01	.3090E-01
Solution Flux	.7563E-02	.9383E-02	.1381E-01	.2105E-01	.2603E-01	.2925E-01
XA1	.5628E-04	.5628E-04	.5628E-04	.5628E-04	.5628E-04	.5628E-04
XA2	.5764E-04	.5946E-04	.5603E-04	.5661E-04	.5567E-04	.6104E-04
XA3	.5009E-04	.4491E-04	.5684E-04	.5583E-04	.5690E-04	.5493E-04
Separation	0.1100	0.2020	-.0100	0.0080	-.0110	0.0240
Pore Blocking	0.1598	0.1328	0.1130	0.0814	0.0665	0.0536

Table C-19

Data for Experiment Number 111

Solute: BENZENE
Pressure: 6900. kPa
Feed Concentration: 149.4 ppm
Feed Flow Rate: 400.0 mL/min

Membrane	1	2	3	4	5	6
Water Flux	.9055E-02	.1086E-01	.1561E-01	.2298E-01	.2801E-01	.3095E-01
Solution Flux	.8089E-02	.9939E-02	.1449E-01	.2167E-01	.2671E-01	.2999E-01
XA1	.3447E-04	.3447E-04	.3447E-04	.3447E-04	.3447E-04	.3447E-04
XA2	.3576E-04	.3513E-04	.3439E-04	.3585E-04	.3616E-04	.3651E-04
XA3	.2902E-04	.3226E-04	.3464E-04	.3268E-04	.3282E-04	.3392E-04
Separation	0.1580	0.0640	-.0050	0.0520	0.0480	0.0160
Pore Blocking	0.1067	0.0847	0.0714	0.0568	0.0463	0.0312

Table C-20

Data for Experiment Number 112

Solute: BENZENE
Pressure: 6900. kPa
Feed Concentration: 77.9 ppm
Feed Flow Rate: 400.0 mL/min

Membrane	1	2	3	4	5	6
Water Flux	.9034E-02	.1087E-01	.1567E-01	.2297E-01	.2789E-01	.3084E-01
Solution Flux	.8557E-02	.1039E-01	.1501E-01	.2230E-01	.2721E-01	.3018E-01
XA1	.1797E-04	.1797E-04	.1797E-04	.1797E-04	.1797E-04	.1797E-04
XA2	.1822E-04	.1822E-04	.1856E-04	.1826E-04	.1782E-04	.2686E-04
XA3	.1700E-04	.1718E-04	.1675E-04	.1761E-04	.1811E-04	.1560E-04
Separation	0.0540	0.0440	0.0680	0.0200	-.0080	0.1320
Pore Blocking	0.0528	0.0446	0.0423	0.0289	0.0244	0.0214

Table C-21

Data for Experiment Number 113

Solute: BENZENE
Pressure: 6900. kPa
Feed Concentration: 46.2 ppm
Feed Flow Rate: 400.0 mL/min

Membrane	1	2	3	4	5	6
Water Flux	.9028E-02	.1086E-01	.1558E-01	.2300E-01	.2795E-01	.3077E-01
Solution Flux	.8713E-02	.1059E-01	.1527E-01	.2247E-01	.2734E-01	.3020E-01
XA1	.1067E-04	.1067E-04	.1067E-04	.1067E-04	.1067E-04	.1067E-04
XA2	.1076E-04	.1085E-04	.1079E-04	.1102E-04	.1027E-04	.1199E-04
XA3	.1033E-04	.1011E-04	.1042E-04	.1023E-04	.1104E-04	.1032E-04
Separation	0.0320	0.0520	0.0230	0.0410	-.0350	0.0330
Pore Blocking	0.0349	0.0243	0.0202	0.0233	0.0217	0.0185

Table C-22

Data for Experiment Number 115

Solute: BENZENE
Pressure: 3450. kPa
Feed Concentration: 252.8 ppm
Feed Flow Rate: 400.0 mL/min

Membrane	1	2	3	4	5	6
Water Flux	.4712E-02	.5711E-02	.8266E-02	.1253E-01	.1559E-01	.1653E-01
Solution Flux	.3942E-02	.4899E-02	.7255E-02	.1132E-01	.1449E-01	.1564E-01
XA1	.5833E-04	.5833E-04	.5833E-04	.5833E-04	.5833E-04	.5833E-04
XA2	.6102E-04	.5974E-04	.6081E-04	.6216E-04	.5928E-04	.6253E-04
XA3	.3378E-04	.4812E-04	.4655E-04	.4731E-04	.5629E-04	.5495E-04
Separation	0.4210	0.1750	0.2020	0.1890	0.0350	0.0580
Pore Blocking	0.1634	0.1422	0.1223	0.0963	0.0709	0.0535

Table C-23

Data for Experiment Number 116

Solute: BENZENE
Pressure: 3450. kPa
Feed Concentration: 90.7 ppm
Feed Flow Rate: 400.0 mL/min

Membrane	1	2	3	4	5	6
Water Flux	.4737E-02	.5727E-02	.8297E-02	.1261E-01	.1577E-01	.1668E-01
Solution Flux	.4338E-02	.5311E-02	.7801E-02	.1199E-01	.1512E-01	.1617E-01
XA1	.2092E-04	.2092E-04	.2092E-04	.2092E-04	.2092E-04	.2092E-04
XA2	.2112E-04	.2107E-04	.2073E-04	.2089E-04	.1954E-04	.1923E-04
XA3	.1929E-04	.1994E-04	.2178E-04	.2100E-04	.2375E-04	.2222E-04
Separation	0.0780	0.0470	-.0410	-.0040	-.1350	-.0620
Pore Blocking	0.0843	0.0727	0.0598	0.0495	0.0413	0.0306

Table C-24

Data for Experiment Number 117

Solute: BENZENE
Pressure: 3450. kPa
Feed Concentration: 63.2 ppm
Feed Flow Rate: 400.0 mL/min

Membrane	1	2	3	4	5	6
Water Flux	.4753E-02	.5771E-02	.8339E-02	.1267E-01	.1580E-01	.1671E-01
Solution Flux	.4532E-02	.5523E-02	.8054E-02	.1232E-01	.1543E-01	.1650E-01
XA1	.1458E-04	.1458E-04	.1458E-04	.1458E-04	.1458E-04	.1458E-04
XA2	.1484E-04	.1493E-04	.1471E-04	.1519E-04	.1495E-04	.1615E-04
XA3	.1253E-04	.1238E-04	.1404E-04	.1298E-04	.1384E-04	.1341E-04
Separation	0.1410	0.1510	0.0370	0.1100	0.0510	0.0800
Pore Blocking	0.0464	0.0430	0.0342	0.0277	0.0233	0.0127

Table C-25

Data for Experiment Number 118

Solute: BENZENE
Pressure: 3450. kPa
Feed Concentration: 38.4 ppm
Feed Flow Rate: 400.0 mL/min

Membrane	1	2	3	4	5	6
Water Flux	.4766E-02	.5773E-02	.8299E-02	.1268E-01	.1583E-01	.1667E-01
Solution Flux	.4648E-02	.5649E-02	.8166E-02	.1248E-01	.1561E-01	.1655E-01
XA1	.8859E-05	.8859E-05	.8859E-05	.8859E-05	.8859E-05	.8859E-05
XA2	.8924E-05	.8957E-05	.8961E-05	.8939E-05	.8976E-05	.9469E-05
XA3	.8363E-05	.8248E-05	.8434E-05	.8655E-05	.8629E-05	.8407E-05
Separation	0.0560	0.0690	0.0480	0.0230	0.0260	0.0510
Pore Blocking	0.0248	0.0215	0.0160	0.0154	0.0140	0.0072

Table C-26

Data for Experiment Number 120

Solute: TOLUENE
Pressure: 3450. kPa
Feed Concentration: 161.2 ppm
Feed Flow Rate: 400.0 mL/min

Membrane	1	2	3	4	5	6
Water Flux	.4749E-02	.5704E-02	.8172E-02	.1247E-01	.1555E-01	.1654E-01
Solution Flux	.3520E-02	.4434E-02	.6608E-02	.1055E-01	.1369E-01	.1512E-01
XA1	.3153E-04	.3153E-04	.3153E-04	.3153E-04	.3153E-04	.3153E-04
XA2	.3260E-04	.3208E-04	.3198E-04	.3204E-04	.3233E-04	.3873E-04
XA3	.2147E-04	.2746E-04	.2935E-04	.3008E-04	.2986E-04	.2614E-04
Separation	0.3190	0.1290	0.0690	0.0460	0.0530	0.1710
Pore Blocking	0.2588	0.2226	0.1914	0.1539	0.1196	0.0858

Table C-27

Data for Experiment Number 121

Solute: TOLUENE
Pressure: 3450. kPa
Feed Concentration: 45.4 ppm
Feed Flow Rate: 400.0 mL/min

Membrane	1	2	3	4	5	6
Water Flux	.4757E-02	.5758E-02	.8174E-02	.1255E-01	.1566E-01	.1662E-01
Solution Flux	.4424E-02	.5430E-02	.7811E-02	.1204E-01	.1518E-01	.1619E-01
XA1	.8873E-05	.8873E-05	.8873E-05	.8873E-05	.8873E-05	.8873E-05
XA2	.9212E-05	.9212E-05	.9118E-05	.8837E-05	.8989E-05	.1030E-04
XA3	.6362E-05	.6859E-05	.7897E-05	.8962E-05	.8660E-05	.7906E-05
Separation	0.2830	0.2270	0.1100	-.0100	0.0240	0.1090
Pore Blocking	0.0699	0.0570	0.0444	0.0407	0.0310	0.0262

Table C-28

Data for Experiment Number 123

Solute: BENZENE
Pressure: 1725. kPa
Feed Concentration: 227.0 ppm
Feed Flow Rate: 400.0 mL/min

Membrane	1	2	3	4	5	6
Water Flux	.2410E-02	.2966E-02	.4173E-02	.6495E-02	.8335E-02	.8682E-02
Solution Flux	.2044E-02	.2571E-02	.3709E-02	.5887E-02	.7733E-02	.8226E-02
XA1	.5238E-04	.5238E-04	.5238E-04	.5238E-04	.5238E-04	.5238E-04
XA2	.5338E-04	.5347E-04	.5361E-04	.5367E-04	.5295E-04	.5684E-04
XA3	.3426E-04	.3672E-04	.4038E-04	.4468E-04	.4986E-04	.4395E-04
Separation	0.3460	0.2990	0.2290	0.1470	0.0480	0.1610
Pore Blocking	0.1521	0.1332	0.1112	0.0936	0.0722	0.0525

Table C-29

Data for Experiment Number 124

Solute: BENZENE
Pressure: 1725. kPa
Feed Concentration: 124.8 ppm
Feed Flow Rate: 400.0 mL/min

Membrane	1	2	3	4	5	6
Water Flux	.2416E-02	.2978E-02	.4177E-02	.6491E-02	.8326E-02	.8687E-02
Solution Flux	.2176E-02	.2740E-02	.3898E-02	.6135E-02	.7983E-02	.8427E-02
XA1	.2879E-04	.2879E-04	.2879E-04	.2879E-04	.2879E-04	.2879E-04
XA2	.2923E-04	.2943E-04	.2937E-04	.2922E-04	.2962E-04	.3115E-04
XA3	.2139E-04	.2027E-04	.2344E-04	.2638E-04	.2525E-04	.2448E-04
Separation	0.2570	0.2960	0.1860	0.0840	0.1230	0.1500
Pore Blocking	0.0991	0.0798	0.0669	0.0548	0.0412	0.0300

Table C-30

Data for Experiment Number 125

Solute: BENZENE
Pressure: 1725. kPa
Feed Concentration: 40.4 ppm
Feed Flow Rate: 400.0 mL/min

Membrane	1	2	3	4	5	6
Water Flux	.2404E-02	.2957E-02	.4156E-02	.6489E-02	.8333E-02	.8674E-02
Solution Flux	.2332E-02	.2894E-02	.4095E-02	.6373E-02	.8227E-02	.8594E-02
XA1	.9311E-05	.9311E-05	.9311E-05	.9311E-05	.9311E-05	.9311E-05
XA2	.9450E-05	.9540E-05	.9497E-05	.9378E-05	.9426E-05	.1001E-04
XA3	.7123E-05	.6425E-05	.7682E-05	.8948E-05	.8837E-05	.8054E-05
Separation	0.2350	0.3100	0.1750	0.0390	0.0510	0.1350
Pore Blocking	0.0300	0.0212	0.0147	0.0179	0.0128	0.0092

Table C-31

Data for Experiment Number 128

Solute: BENZENE
Pressure: 690. kPa
Feed Concentration: 138.2 ppm
Feed Flow Rate: 400.0 mL/min

Membrane	1	2	3	4	5	6
Water Flux	.9579E-03	.1222E-02	.1683E-02	.2670E-02	.3492E-02	.3579E-02
Solution Flux	.8544E-03	.1110E-02	.1551E-02	.2494E-02	.3315E-02	.3454E-02
XA1	.3189E-04	.3189E-04	.3189E-04	.3189E-04	.3189E-04	.3189E-04
XA2	.3224E-04	.3231E-04	.3233E-04	.3239E-04	.3251E-04	.3332E-04
XA3	.1610E-04	.1773E-04	.2133E-04	.2442E-04	.2500E-04	.2452E-04
Separation	0.4950	0.4440	0.3310	0.2340	0.2160	0.2310
Pore Blocking	0.1080	0.0922	0.0780	0.0660	0.0507	0.0347

Table C-32

Data for Experiment Number 129

Solute: BENZENE
Pressure: 690. kPa
Feed Concentration: 53.4 ppm
Feed Flow Rate: 400.0 mL/min

Membrane	1	2	3	4	5	6
Water Flux	.9490E-03	.1211E-02	.1666E-02	.2641E-02	.3465E-02	.3552E-02
Solution Flux	.9105E-03	.1170E-02	.1622E-02	.2585E-02	.3398E-02	.3500E-02
XA1	.1233E-04	.1233E-04	.1233E-04	.1233E-04	.1233E-04	.1233E-04
XA2	.1247E-04	.1251E-04	.1255E-04	.1251E-04	.1263E-04	.1285E-04
XA3	.6584E-05	.6559E-05	.7188E-05	.9703E-05	.9111E-05	.9691E-05
Separation	0.4660	0.4680	0.4170	0.2130	0.2610	0.2140
Pore Blocking	0.0406	0.0336	0.0264	0.0214	0.0194	0.0146

Table C-33

Data for Experiment Number 133

Solute: BENZENE
Pressure: 690. kPa
Feed Concentration: 116.7 ppm
Feed Flow Rate: 400.0 mL/min

Membrane	1	2	3	4	5	6
Water Flux	.9342E-03	.1192E-02	.1628E-02	.2603E-02	.3398E-02	.3498E-02
Solution Flux	.8391E-03	.1086E-02	.1511E-02	.2431E-02	.3227E-02	.3370E-02
XA1	.2693E-04	.2693E-04	.2693E-04	.2693E-04	.2693E-04	.2693E-04
XA2	.2730E-04	.2732E-04	.2730E-04	.2724E-04	.2736E-04	.2784E-04
XA3	.1018E-04	.1319E-04	.1769E-04	.2219E-04	.2202E-04	.2211E-04
Separation	0.6220	0.5100	0.3430	0.1760	0.1820	0.1790
Pore Blocking	0.1018	0.0886	0.0720	0.0659	0.0503	0.0366

Table C-34

Data for Experiment Number 134

Solute: BENZENE
Pressure: 1725. kPa
Feed Concentration: 24.2 ppm
Feed Flow Rate: 400.0 mL/min

Membrane	1	2	3	4	5	6
Water Flux	.2397E-02	.2980E-02	.4100E-02	.6481E-02	.8301E-02	.8686E-02
Solution Flux	.2362E-02	.2953E-02	.4070E-02	.6450E-02	.8281E-02	.8640E-02
XA1	.5588E-05	.5588E-05	.5588E-05	.5588E-05	.5588E-05	.5588E-05
XA2	.5715E-05	.5725E-05	.5713E-05	.5791E-05	.5784E-05	.5989E-05
XA3	.3610E-05	.3883E-05	.4476E-05	.4487E-05	.4783E-05	.4872E-05
Separation	0.3540	0.3050	0.1990	0.1970	0.1440	0.1280
Pore Blocking	0.0143	0.0089	0.0075	0.0048	0.0024	0.0053

Table C-35

Data for Experiment Number 136

Solute: BENZENE
Pressure: 690. kPa
Feed Concentration: 259.5 ppm
Feed Flow Rate: 400.0 mL/min

Membrane	1	2	3	4	5	6
Water Flux	.9388E-03	.1197E-02	.1637E-02	.2604E-02	.3403E-02	.3496E-02
Solution Flux	.7743E-03	.1016E-02	.1430E-02	.2334E-02	.3122E-02	.3291E-02
XA1	.5988E-04	.5988E-04	.5988E-04	.5988E-04	.5988E-04	.5988E-04
XA2	.6055E-04	.6070E-04	.6079E-04	.6096E-04	.6161E-04	.6227E-04
XA3	.2713E-04	.2952E-04	.3605E-04	.4287E-04	.3970E-04	.4695E-04
Separation	0.5470	0.5070	0.3980	0.2840	0.3370	0.2160
Pore Blocking	0.1752	0.1516	0.1261	0.1038	0.0828	0.0585

Table C-36

Data for Experiment Number 138

Solute: TOLUENE
Pressure: 3450. kPa
Feed Concentration: 136.7 ppm
Feed Flow Rate: 400.0 mL/min

Membrane	1	2	3	4	5	6
Water Flux	.4657E-02	.5765E-02	.7889E-02	.1233E-01	.1545E-01	.1644E-01
Solution Flux	.3778E-02	.4867E-02	.6835E-02	.1095E-01	.1416E-01	.1541E-01
XA1	.2674E-04	.2674E-04	.2674E-04	.2674E-04	.2674E-04	.2674E-04
XA2	.2742E-04	.2733E-04	.2737E-04	.2721E-04	.2722E-04	.3034E-04
XA3	.2072E-04	.2281E-04	.2382E-04	.2545E-04	.2578E-04	.2412E-04
Separation	0.2250	0.1470	0.1090	0.0480	0.0360	0.0980
Pore Blocking	0.1886	0.1558	0.1336	0.1116	0.0837	0.0623

Table C-37

Data for Experiment Number 139

Solute: TOLUENE
Pressure: 3450. kPa
Feed Concentration: 51.6 ppm
Feed Flow Rate: 400.0 mL/min

Membrane	1	2	3	4	5	6
Water Flux	.4641E-02	.5758E-02	.7896E-02	.1236E-01	.1551E-01	.1651E-01
Solution Flux	.4264E-02	.5356E-02	.7452E-02	.1176E-01	.1490E-01	.1600E-01
XA1	.1009E-04	.1009E-04	.1009E-04	.1009E-04	.1009E-04	.1009E-04
XA2	.1038E-04	.1037E-04	.1026E-04	.1048E-04	.1051E-04	.1061E-04
XA3	.7847E-05	.8392E-05	.9370E-05	.9098E-05	.9279E-05	.9723E-05
Separation	0.2220	0.1680	0.0710	0.0980	0.0800	0.0360
Pore Blocking	0.0813	0.0697	0.0563	0.0487	0.0396	0.0311

Table C-38

Data for Experiment Number 140

Solute: CUMENE
Pressure: 6900. kPa
Feed Concentration: 24.6 ppm
Feed Flow Rate: 400.0 mL/min

Membrane	1	2	3	4	5	6
Water Flux	.8803E-02	.1089E-01	.1480E-01	.2258E-01	.2751E-01	.3018E-01
Solution Flux	.7626E-02	.9658E-02	.1348E-01	.2095E-01	.2598E-01	.2895E-01
XA1	.3682E-05	.3682E-05	.3682E-05	.3682E-05	.3682E-05	.3682E-05
XA2	.4021E-05	.3840E-05	.3484E-05	.3571E-05	.4131E-05	.5054E-05
XA3	.2478E-05	.3255E-05	.4043E-05	.3796E-05	.3343E-05	.3424E-05
Separation	0.3270	0.1160	-.0980	-.0310	0.0920	0.0700
Pore Blocking	0.1337	0.1131	0.0891	0.0724	0.0558	0.0406

Table C-39

Data for Experiment Number 142

Solute: CUMENE
Pressure: 6900. kPa
Feed Concentration: 12.7 ppm
Feed Flow Rate: 400.0 mL/min

Membrane	1	2	3	4	5	6
Water Flux	.8774E-02	.1085E-01	.1470E-01	.2239E-01	.2725E-01	.2980E-01
Solution Flux	.8181E-02	.1023E-01	.1406E-01	.2165E-01	.2660E-01	.2929E-01
XA1	.1900E-05	.1900E-05	.1900E-05	.1900E-05	.1900E-05	.1900E-05
XA2	.1945E-05	.1944E-05	.1825E-05	.1826E-05	.1863E-05	.2646E-05
XA3	.1749E-05	.1787E-05	.2029E-05	.1972E-05	.1926E-05	.1763E-05
Separation	0.0790	0.0590	-.0680	-.0380	-.0140	0.0720
Pore Blocking	0.0676	0.0568	0.0440	0.0334	0.0238	0.0172

Table C-40

Data for Experiment Number 143

Solute: CUMENE
Pressure: 6900. kPa
Feed Concentration: 8.1 ppm
Feed Flow Rate: 400.0 mL/min

Membrane	1	2	3	4	5	6
Water Flux	.8786E-02	.1084E-01	.1475E-01	.2236E-01	.2722E-01	.2979E-01
Solution Flux	.8421E-02	.1051E-01	.1428E-01	.2185E-01	.2684E-01	.2932E-01
XA1	.1210E-05	.1210E-05	.1210E-05	.1210E-05	.1210E-05	.1210E-05
XA2	.1239E-05	.1212E-05	.1181E-05	.1284E-05	.1254E-05	.1534E-05
XA3	.1118E-05	.1204E-05	.1258E-05	.1138E-05	.1178E-05	.1151E-05
Separation	0.0760	0.0050	-.0400	0.0590	0.0260	0.0490
Pore Blocking	0.0415	0.0301	0.0321	0.0232	0.0138	0.0157

Table C-41

Data for Experiment Number 144

Solute: CUMENE
Pressure: 6900. kPa
Feed Concentration: 4.5 ppm
Feed Flow Rate: 400.0 mL/min

Membrane	1	2	3	4	5	6
Water Flux	.8772E-02	.1083E-01	.1469E-01	.2234E-01	.2720E-01	.2978E-01
Solution Flux	.8476E-02	.1068E-01	.1443E-01	.2196E-01	.2688E-01	.2949E-01
XA1	.6731E-06	.6731E-06	.6731E-06	.6731E-06	.6731E-06	.6731E-06
XA2	.7073E-06	.7055E-06	.7066E-06	.7538E-06	.8188E-06	.1315E-05
XA3	.5654E-06	.5950E-06	.6173E-06	.5957E-06	.5688E-06	.5574E-06
Separation	0.1600	0.1160	0.0830	0.1150	0.1550	0.1720
Pore Blocking	0.0338	0.0136	0.0177	0.0170	0.0119	0.0096

Table C-42

Data for Experiment Number 146

Solute: CUMENE
Pressure: 3450. kPa
Feed Concentration: 26.5 ppm
Feed Flow Rate: 400.0 mL/min

Membrane	1	2	3	4	5	6
Water Flux	.4572E-02	.5717E-02	.7804E-02	.1217E-01	.1517E-01	.1620E-01
Solution Flux	.4063E-02	.5086E-02	.7064E-02	.1125E-01	.1439E-01	.1553E-01
XA1	.3967E-05	.3967E-05	.3967E-05	.3967E-05	.3967E-05	.3967E-05
XA2	.4293E-05	.4225E-05	.4172E-05	.4210E-05	.4241E-05	.4643E-05
XA3	.1658E-05	.2531E-05	.3174E-05	.3416E-05	.3507E-05	.3566E-05
Separation	0.5820	0.3620	0.2000	0.1390	0.1160	0.1010
Pore Blocking	0.1114	0.1104	0.0948	0.0756	0.0515	0.0412

Table C-43

Data for Experiment Number 147

Solute: CUMENE
Pressure: 3450. kPa
Feed Concentration: 16.0 ppm
Feed Flow Rate: 400.0 mL/min

Membrane	1	2	3	4	5	6
Water Flux	.4562E-02	.5687E-02	.7760E-02	.1211E-01	.1521E-01	.1614E-01
Solution Flux	.4277E-02	.5398E-02	.7430E-02	.1169E-01	.1478E-01	.1587E-01
XA1	.2396E-05	.2396E-05	.2396E-05	.2396E-05	.2396E-05	.2396E-05
XA2	.2619E-05	.2551E-05	.2627E-05	.2501E-05	.2551E-05	.3288E-05
XA3	.9008E-06	.1588E-05	.1550E-05	.2168E-05	.2144E-05	.1885E-05
Separation	0.6240	0.3370	0.3530	0.0950	0.1050	0.2130
Pore Blocking	0.0625	0.0507	0.0425	0.0354	0.0283	0.0165

Table C-44

Data for Experiment Number 148

Solute: CUMENE
Pressure: 3450. kPa
Feed Concentration: 10.2 ppm
Feed Flow Rate: 400.0 mL/min

Membrane	1	2	3	4	5	6
Water Flux	.4529E-02	.5694E-02	.7725E-02	.1206E-01	.1512E-01	.1604E-01
Solution Flux	.4335E-02	.5444E-02	.7409E-02	.1174E-01	.1480E-01	.1579E-01
XA1	.1532E-05	.1532E-05	.1532E-05	.1532E-05	.1532E-05	.1532E-05
XA2	.1676E-05	.1666E-05	.1623E-05	.1610E-05	.1688E-05	.1925E-05
XA3	.5838E-06	.8427E-06	.1197E-05	.1365E-05	.1279E-05	.1305E-05
Separation	0.6190	0.4500	0.2190	0.1090	0.1650	0.1480
Pore Blocking	0.0430	0.0440	0.0409	0.0271	0.0215	0.0155

Table C-45

Data for Experiment Number 150

Solute: CUMENE
Pressure: 3450. kPa
Feed Concentration: 7.7 ppm
Feed Flow Rate: 400.0 mL/min

Membrane	1	2	3	4	5	6
Water Flux	.4595E-02	.5742E-02	.7812E-02	.1223E-01	.1532E-01	.1624E-01
Solution Flux	.4446E-02	.5574E-02	.7632E-02	.1199E-01	.1508E-01	.1607E-01
XA1	.1159E-05	.1159E-05	.1159E-05	.1159E-05	.1159E-05	.1159E-05
XA2	.1265E-05	.1234E-05	.1241E-05	.1211E-05	.1255E-05	.1547E-05
XA3	.4763E-06	.7788E-06	.8657E-06	.1050E-05	.1007E-05	.9410E-06
Separation	0.5890	0.3280	0.2530	0.0940	0.1310	0.1880
Pore Blocking	0.0324	0.0293	0.0230	0.0199	0.0154	0.0104

Table C-46

Data for Experiment Number 151

Solute: CUMENE
Pressure: 690. kPa
Feed Concentration: 17.3 ppm
Feed Flow Rate: 400.0 mL/min

Membrane	1	2	3	4	5	6
Water Flux	.9614E-03	.1228E-02	.1669E-02	.2660E-02	.3473E-02	.3579E-02
Solution Flux	.8436E-03	.1097E-02	.1524E-02	.2466E-02	.3287E-02	.3440E-02
XA1	.2589E-05	.2589E-05	.2589E-05	.2589E-05	.2589E-05	.2589E-05
XA2	.2651E-05	.2648E-05	.2644E-05	.2657E-05	.2671E-05	.2724E-05
XA3	.3444E-06	.9813E-06	.1504E-05	.1771E-05	.1864E-05	.2040E-05
Separation	0.8670	0.6210	0.4190	0.3160	0.2800	0.2120
Pore Blocking	0.1225	0.1073	0.0866	0.0730	0.0535	0.0388

Table C-47

Data for Experiment Number 152

Solute: CUMENE
Pressure: 690. kPa
Feed Concentration: 15.9 ppm
Feed Flow Rate: 400.0 mL/min

Membrane	1	2	3	4	5	6
Water Flux	.9600E-03	.1222E-02	.1666E-02	.2651E-02	.3455E-02	.3575E-02
Solution Flux	.8628E-03	.1123E-02	.1556E-02	.2510E-02	.3323E-02	.3473E-02
XA1	.2378E-05	.2378E-05	.2378E-05	.2378E-05	.2378E-05	.2378E-05
XA2	.2432E-05	.2439E-05	.2445E-05	.2461E-05	.2462E-05	.2674E-05
XA3	.4755E-06	.7181E-06	.1079E-05	.1396E-05	.1636E-05	.1179E-05
Separation	0.8000	0.6980	0.5460	0.4130	0.3120	0.5040
Pore Blocking	0.1013	0.0810	0.0660	0.0531	0.0384	0.0284

Table C-48

Data for Experiment Number 153

Solute: CUMENE
Pressure: 690. kPa
Feed Concentration: 8.1 ppm
Feed Flow Rate: 400.0 mL/min

Membrane	1	2	3	4	5	6
Water Flux	.9492E-03	.1216E-02	.1654E-02	.2639E-02	.3438E-02	.3540E-02
Solution Flux	.9118E-03	.1180E-02	.1623E-02	.2581E-02	.3396E-02	.3519E-02
XA1	.1207E-05	.1207E-05	.1207E-05	.1207E-05	.1207E-05	.1207E-05
XA2	.1239E-05	.1244E-05	.1250E-05	.1264E-05	.1271E-05	.1361E-05
XA3	.1340E-06	.2462E-06	.4067E-06	.5503E-06	.6541E-06	.5925E-06
Separation	0.8890	0.7960	0.6630	0.5440	0.4580	0.5090
Pore Blocking	0.0394	0.0291	0.0188	0.0221	0.0123	0.0059

Table C-49

Data for Experiment Number 154

Solute: CUMENE
Pressure: 690. kPa
Feed Concentration: 6.8 ppm
Feed Flow Rate: 400.0 mL/min

Membrane	1	2	3	4	5	6
Water Flux	.9481E-03	.1221E-02	.1659E-02	.2641E-02	.3444E-02	.3550E-02
Solution Flux	.9163E-03	.1184E-02	.1622E-02	.2584E-02	.3403E-02	.3526E-02
XA1	.1025E-05	.1025E-05	.1025E-05	.1025E-05	.1025E-05	.1025E-05
XA2	.1048E-05	.1052E-05	.1056E-05	.1067E-05	.1075E-05	.1134E-05
XA3	.2357E-06	.3177E-06	.4416E-06	.5369E-06	.5984E-06	.5892E-06
Separation	0.7700	0.6900	0.5690	0.4760	0.4160	0.4250
Pore Blocking	0.0335	0.0299	0.0225	0.0215	0.0119	0.0068

Table C-50

Data for Experiment Number 156

Solute: CUMENE
Pressure: 1725. kPa
Feed Concentration: 25.9 ppm
Feed Flow Rate: 400.0 mL/min

Membrane	1	2	3	4	5	6
Water Flux	.2354E-02	.2974E-02	.4052E-02	.6420E-02	.8225E-02	.8572E-02
Solution Flux	.2076E-02	.2650E-02	.3690E-02	.5949E-02	.7730E-02	.8251E-02
XA1	.3877E-05	.3877E-05	.3877E-05	.3877E-05	.3877E-05	.3877E-05
XA2	.4100E-05	.4090E-05	.4060E-05	.4088E-05	.4104E-05	.4531E-05
XA3	.6823E-06	.1504E-05	.2439E-05	.2888E-05	.3082E-05	.2931E-05
Separation	0.8240	0.6120	0.3710	0.2550	0.2050	0.2440
Pore Blocking	0.1181	0.1089	0.0894	0.0733	0.0602	0.0374

Table C-51

Data for Experiment Number 157

Solute: CUMENE
Pressure: 1725. kPa
Feed Concentration: 16.1 ppm
Feed Flow Rate: 400.0 mL/min

Membrane	1	2	3	4	5	6
Water Flux	.2368E-02	.2970E-02	.4056E-02	.6441E-02	.8212E-02	.8568E-02
Solution Flux	.2187E-02	.2781E-02	.3839E-02	.6166E-02	.7962E-02	.8407E-02
XA1	.2421E-05	.2421E-05	.2421E-05	.2421E-05	.2421E-05	.2421E-05
XA2	.2566E-05	.2574E-05	.2582E-05	.2609E-05	.2618E-05	.3039E-05
XA3	.4600E-06	.8111E-06	.1213E-05	.1576E-05	.1755E-05	.1550E-05
Separation	0.8100	0.6650	0.4990	0.3490	0.2750	0.3600
Pore Blocking	0.0763	0.0638	0.0534	0.0427	0.0304	0.0188

Table C-52

Data for Experiment Number 158

Solute: CUMENE
Pressure: 1725. kPa
Feed Concentration: 12.2 ppm
Feed Flow Rate: 400.0 mL/min

Membrane	1	2	3	4	5	6
Water Flux	.2368E-02	.2980E-02	.4056E-02	.6437E-02	.8225E-02	.8576E-02
Solution Flux	.2241E-02	.2838E-02	.3883E-02	.6213E-02	.8018E-02	.8427E-02
XA1	.1832E-05	.1832E-05	.1832E-05	.1832E-05	.1832E-05	.1832E-05
XA2	.1925E-05	.1927E-05	.1933E-05	.1969E-05	.1972E-05	.2230E-05
XA3	.5991E-06	.8519E-06	.1085E-05	.1220E-05	.1363E-05	.1271E-05
Separation	0.6730	0.5350	0.4080	0.3340	0.2560	0.3060
Pore Blocking	0.0535	0.0476	0.0427	0.0349	0.0252	0.0174

Table C-53

Data for Experiment Number 159

Solute: CUMENE
Pressure: 1725. kPa
Feed Concentration: 9.9 ppm
Feed Flow Rate: 400.0 mL/min

Membrane	1	2	3	4	5	6
Water Flux	.2339E-02	.2957E-02	.4012E-02	.6360E-02	.8147E-02	.8489E-02
Solution Flux	.2258E-02	.2857E-02	.3919E-02	.6229E-02	.8041E-02	.8420E-02
XA1	.1490E-05	.1490E-05	.1490E-05	.1490E-05	.1490E-05	.1490E-05
XA2	.1574E-05	.1574E-05	.1578E-05	.1595E-05	.1605E-05	.1836E-05
XA3	.3859E-06	.6273E-06	.8419E-06	.1021E-05	.1104E-05	.1003E-05
Separation	0.7410	0.5790	0.4350	0.3150	0.2590	0.3270
Pore Blocking	0.0345	0.0336	0.0232	0.0206	0.0130	0.0082

APPENDIX D

Integration of the Flux Equation in the z-direction for the Surface Force-Pore Flow Model

The purpose of this appendix is to illustrate the integration of Equation (91) with respect to z to yield Equation (95). In this analysis the effect of pressure induced solute transport is added to the surface force-pore flow model. The integration, although relatively straightforward, is significantly different than the original version (49) and is therefore presented here in detail.

It is required to integrate Equation (91):

$$N_A(r) = \left| -\frac{RT}{X_{AB}} \frac{\partial C_{AM}(r,z)}{\partial z} + \frac{V_A C_{AM}(r,z)\,\Delta P(r)}{X_{AB}\,\iota} + C_{AM}(r,z)\,u_B(r) \right| / b(r) \tag{91}$$

with the boundary conditions (49):

$$C_{AM}(r,0) = C_{A2}\, e^{-\phi(r)} \tag{92}$$

and

$$C_{AM}(r,\iota) = C_{A3}(r)\, e^{-\phi(r)} \tag{93}$$

Noting that:

$$C_{A3}(r) = N_A(r)/u_B(r) \tag{94}$$

and substituting Equation (94) into Equation (91) gives:

$$C_{A3}(r)\,u_B(r)\,b(r) = -\frac{RT}{X_{AB}} \frac{\partial C_{AM}(r,z)}{\partial z} + \frac{V_A C_{AM}(r,z)\,\Delta P(r)}{X_{AB}\,\iota} + C_{AM}(r,z)\,u_B(r) \tag{D-1}$$

which can be arranged as:

$$\frac{\partial C_{AM}(r,z)}{\partial z} = \frac{\partial C_{AM}(r,z)\,u_B(r)\,X_{AB}}{RT} + \frac{V_A C_{AM}(r,z)\,\Delta P(r)}{RT\,\iota} - \frac{C_{A3}(r)\,u_B(r)\,b(r)\,X_{AB}}{RT} \tag{D-2}$$

Collecting $C_{AM}(r,z)$ terms:

$$\frac{\partial C_{AM}(r,z)}{\partial z} = C_{AM}\left| \frac{u_B(r)\,X_{AB}}{RT} + \frac{V_A\,\Delta P(r)}{RT\,\iota} \right| - \frac{C_{A3}(r)\,u_B(r)\,b(r)\,X_{AB}}{RT} \tag{D-3}$$

and moving them to the left hand side gives:

$$\frac{\partial C_{AM}(r,z)}{\partial z} - \frac{X_{AB}}{RT}\left[u_B(r) + \frac{V_A\,\Delta P(r)}{X_{AB}\,\iota}\right] C_{AM}(r,z) = -\frac{X_{AB}}{RT}\,C_{A3}(r)\,u_B(r)\,b(r) \tag{D-4}$$

Defining:

$$Y(z) = C_{AM}(r,z) \tag{D-5}$$

$$Y'(z) = \frac{\partial C_{AM}(r,z)}{\partial z} \tag{D-6}$$

$$B_1 = \frac{X_{AB}}{RT}\left[u_B(r) + \frac{V_A\,\Delta P(r)}{X_{AB}\,\iota}\right] \tag{D-7}$$

$$B_2 = -\frac{X_{AB}}{RT}\,C_{A3}(r)\,u_B(r)\,b(r) \tag{D-8}$$

allows Equation (D-4) to be rewritten as:

$$Y'(z) - B_1\,Y(z) = B_2 \tag{D-9}$$

which is a first order linear nonhomogeneous differential equation. B_1 and B_2 are functions of r only and may be considered as constants when integrating with respect to z. The boundary conditions, Equation (92) and (93), can be rewritten as:

$$\text{at } z = 0, \quad Y(0) = C_{A2}\,e^{-\phi(r)} \tag{D-10}$$

$$\text{at } z = \iota, \quad Y(\iota) = C_{A3}(r)\,e^{-\phi(r)} \tag{D-11}$$

Equation (D-9) can be solved by multiplying through by the integration factor $\exp(-B_1 z)$:

$$Y'(z)e^{-B_1 z} - B_1 e^{-B_1 z}\,Y(z) = B_2 e^{-B_1 z} \tag{D-12}$$

which is equivalent to:

$$\frac{d}{dz}\left(Y(z)e^{-B_1 z}\right) = B_2 e^{-B_1 z} \tag{D-13}$$

Integration from $z = 0$ to $z = \iota$ gives:

$$Y(z)e^{-B_1 z}\Big|_{Y(0)e^{-B_1(0)}}^{Y(\iota)e^{-B_1 \iota}} = -\frac{B_2}{B_1}\,e^{-B_1 z}\Big|_{z=0}^{z=\iota} \tag{D-14}$$

which can be rearranged as:

$$Y(t)e^{-B_1 t} - Y(0) = -\frac{B_2}{B_1}\left(e^{-B_1 t} - 1\right) \tag{D-15}$$

Multiplying by $\exp(B_1 t)/Y(0)$ gives:

$$\frac{Y(t)}{Y(0)} = e^{B_1 t} - \frac{B_2}{Y(0)\,B_1}\left(1 - e^{B_1 t}\right) \tag{D-16}$$

Substituting Equations (D-7), (D-8), (D-10) and (D-11) into Equation (D-16) gives:

$$\frac{C_{A3}(r)}{C_{A2}} = e^{B_1 t} + \frac{C_{A3}(r)\,u_B(r)\,b(r)}{C_{A2}\,e^{-\phi(r)}\left(u_B(r) + \dfrac{V_A\,\Delta P(r)}{X_{AB}\,t}\right)}\left(1 - e^{B_1 t}\right) \tag{D-17}$$

Collecting $C_{A3}(r)/C_{A2}$ terms gives:

$$\frac{C_{A3}(r)}{C_{A2}} = \frac{e^{B_1 t}}{1 - \dfrac{b(r)}{\exp(-\phi(r))}\left(\dfrac{u_B(r)}{u_B(r) + \dfrac{V_A\,\Delta P}{X_{AB}\,t}}\right)\left(1 - e^{B_1 t}\right)} \tag{D-18}$$

and substitution for B_1 and rearrangement produces:

$$\frac{C_{A3}(r)}{C_{A2}} = \frac{\exp\left|\dfrac{X_{AB}\,t}{RT}\left(u_B(r) + \dfrac{V_A\,\Delta P}{X_{AB}\,t}\right)\right|}{1 + \dfrac{b(r)}{\exp(-\phi(r))}\left(\dfrac{u_B(r)}{u_B(r) + \dfrac{V_A\,\Delta P}{X_{AB}\,t}}\right)\left(\exp\left|\dfrac{X_{AB}\,t}{RT}\left(u_B(r) + \dfrac{V_A\,\Delta P}{X_{AB}\,t}\right)\right| - 1\right)} \tag{95}$$

which is the desired solution of Equation (91) integrated with respect to z and the appropriate boundary conditions.

REFERENCES

1. Sourirajan, S.; Matsuura, T. In "Reverse Osmosis and Synthetic Membranes", Sourirajan, S., Ed.; National Research Council Canada: Ottawa, 1977; Chapters 2, 3.

2. Matsuura, T.; Sourirajan, S. J. Appl. Polymer Sci. 1973, 17, 3683-3708.

3. Matsuura, T; Dickson, J.M.; Sourirajan, S. Ind. Eng. Chem. Process Des. Dev. 1976, 15, 149-161.

4. Small, P.A. J. Appl. Chem. 1953, 3, 71-80.

5. Verschueren, K. "Handbook of Environmental Data on Organic Chemicals"; Van Nostrand Reinhold: New York, 1977.

6. Reid, R.C.; Sherwood, T.K. "The Properties of Gases and Liquids"; 2nd Edition; McGraw-Hill: New York, 1966.

7. Lonsdale, H.K.; Merten, U.; Tagami, M. J. Appl. Polymer Sci. 1967, 11, 1807-1820.

8. Wilke, C.R.; Chang, P. AIChE J. 1955, 1, 264-270.

9. Blunk, R. Report WRCC-88, University of California, Los Angeles Water Resources Center, 1964.

10. Keilin, B. Research and Development Progress Report No. 117, Office of Saline Water, Aerojet-General Corp., 1964.

11. Lonsdale, H.K.; Cross, B.P.; Graber, F.M.; Milstead, C.E., J. Macromol. Sci.-Phys. 1971, 85, 167-188.

12. Merten, U.; Lonsdale, H.K.; Riley, R.L.; Tagami, M. In "Proc. NATO Advanced Study Inst. Synthetic Polymer Membranes"; Ravello, Italy, September 1966.

13. Matsuura, T.; Sourirajan, S. J. Appl. Polymer Sci. 1971, 15, 2905-2927.

14. Matsuura, T.; Sourirajan, S. J. Appl. Polymer Sci. 1972, 16, 2531-2554.

15. Matsuura, T.; Sourirajan, S. J. Appl. Polymer Sci. 1973, 17, 1043-1071.

16. Pusch, W.; Burghoff, H.-G.; Staude, E. Proc. 5th International Symposium on Fresh Water from the Sea 1976, 4, 143-156.

17. Burghoff, H.-G.; Lee, K.L.; Pusch, W. J. Appl. Polymer Sci. 1980, 25, 323-347.

18. Anderson, J.E.; Hoffman, S.J.; Peters, C.R. J. Phys. Chem. 1972, 76, 4006-4011.

19. Chian, E.S.K.; Fang, H.H.P. In "Water-1976: I. Physical Chemical Wastewater Treatment"; AIChE Symposium Series, 1976; p. 152-161.

20. Jonsson, G. Desalination 1978, 24, 19-37.

21. Dickson, J.M.; Matsuura, T.; Sourirajan, S. Ind. Eng. Chem. Process Des. Dev. 1979, 18, 641-647.

22. Dickson, J.M.; Lloyd, D.R. In "Synthetic Membranes"; Turbak, A.F., Ed.; ACS Symposium Series: Washington, D.C., 1981.

23. Dickson, J.M.; Babai-Pirouz, M.; Lloyd, D.R. Ind. Eng. Chem. Process Des. Dev. 1983, 22, 625-632.

24. Lloyd, D.R.; Babai-Pirouz, M.; Dickson, J.M. J. Sep. Process Tech. 1982, 3, 21-28.

25. Matsuura, T.; Blais, P.; Dickson, J.M.; Sourirajan, S. J. Appl. Polymer Sci. 1974, 18, 3671-3684.

26. Rozelle, L.T.; Cadotte, J.E.; Cobian, K.E.; Kopp, C.V., Jr. In "Reverse Osmosis and Synthetic Membranes"; Sourirajan, S., Ed.; National Research Council Canada: Ottawa, 1977; Chapter 12.

27. Jonsson, G. Desalination 1980, 35, 21-38.

28. Soltanieh, M.; Gill, W.N. Chem. Eng. Commun. 1981, 12, 279-363.

29. Bird, R.B.; Stewart, W.E.; Lightfoot, E.N. "Transport Phenomena"; John Wiley and Sons: New York, 1960; Chapter 17.

30. Sourirajan, S. "Reverse Osmosis"; Academic Press: New York, 1970; (a) Chapter 2, (b) Chapter 3.

31. Kimura, S.; Sourirajan, S. AIChE J. 1967, 13, 497-503.

32. Matsuura, T.; Bednas, M.E.; Sourirajan, S. J. Appl. Polymer Sci. 1974, 18, 567-588.

33. Brian, P.L.T. In "Desalination by Reverse Osmosis"; Merten, U., Ed.; M.I.T. Press: Cambridge, Mass., 1966; pp. 161-202.

34. Jonsson, G.; Boesen, C.E. Desalination 1975, 17, 145-165.

35. Gill, W.N.; Derzansky, L.; Doshi, M.R. In "Surface and Colloid Science IV"; John Wiley and Sons: 1971; pp. 261-360.

36. Castellan, G.W. "Physical Chemistry"; 2nd Edition; Addison-Wesley: London, 1971; pp. 297-301.

37. Kesting, R.E. "Synthetic Polymeric Membranes"; McGraw-Hill: New York, 1971.

38. Matsuura, T.; Pageau, L.; Sourirajan, S. J. Appl. Polymer Sci. 1975, 19, 179-198.

39. Kedem, O.; Katchalsky, A. Biochem. Biophys. Acta 1958, 27, 229-246.

40. Onsager, L. Phys. Rev. 1931, 37, 405-425.

41. Staverman, A.J. Recueil Trav. Chim. Pays-Bas 1951, 70, 344-352.

42. Pusch, W. Ber. Bunsenges. Phys. Chem. 1977, 81, 269-276.

43. Spiegler, K.S.; Kedem, O. Desalination 1966, 1, 311-326.

44. Lonsdale, H.K.; Merten, U.; Riley, R.L. J. Appl. Polymer Sci. 1965, 9, 1341-1362.

45. Merten, U., Ed., In "Desalination by Reverse Osmosis"; M.I.T. Press: Cambridge, Mass., 1966; p. 15-54.

46. Sherwood, T.K.; Brian, P.L.T.; Fisher, R.E. Ind. Eng. Chem. Fundamentals 1967, 6, 2-12.

47. Sourirajan, S. Ind. Eng. Chem. Fundamentals 1963, 2, 51-55.

48. Spiegler, K.S. Trans. Faraday Soc. 1958, 54, 1408-1428.

49. Matsuura, T.; Sourirajan, S. Ind. Eng. Chem. Process Des. Dev. 1981, 20, 273-282.

50. Matsuura, T.; Taketani, Y.; Sourirajan, S. In "Synthetic Membranes"; Turbak, A.F., Ed.; ACS Symposium Series: Washington, D.C., 1981; Chapter 19.

51. Prausnitz, J.M. "Molecular Thermodynamics of Fluid-Phase Equilibria"; Prentice-Hall: New Jersey, 1969.

52. Faxen, H. Arkiv. Mat. Astron. Fys. 1923, 17, No. 27.

53. Bohlin, T. Trans. Roy. Inst. Technol. (Stockholm) 1959, No. 155.

54. Faxen, H. Kolloid Z. 1959, 167, 146.

55. Lane, J.A.; Riggle, J.W. Chem. Eng. Progr. Symposium Ser. 1959, 55, 127-143.

56. Bean, C.P. In "Membranes - A Series of Advances"; Eisenman, G., Ed.; Marcel-Dekker, Inc.: New York, 1972.

57. Famularo, J. D. Eng. Sci. Thesis New York University; New York, 1962.

58. Satterfield, C.N.; Colton, C.K.; Pitcher, W.H., Jr. AIChE J. 1973, 19, 628-635.

59. Anderson, J.L.; Quinn, J.A. Biophys. J. 1974, 14, 130-150.

60. Chan, K.; Matsuura, T.; Sourirajan, S. Ind. Eng. Chem. Prod. Res. Dev. 1982, 21, 605-612.

61. Deen, W.M.; Bohrer, M.P.; Epstein, N.B. AIChE J. 1981, 27, 952-959.

62. Beck, R.E.; Schultz, J.S. Biochim. Biophys. Acta 1972, 255, 273-303.

63. Munch, W.D.; Zestar, L.P.; Anderson, J.L. J. Memb. Sci. 1979, 5, 77-102.

64. Ferry, J.D. J. Gen. Physiol. 1936, 20, 95-104.

65. Ackers, G.K. Adv. Prot. Chem. 1970, 24, 343-446.

66. Renkin, E.M. J. Gen. Physiol. 1954, 38, 225-243.

67. Barrow, G.M. "Physical Chemistry"; 2nd Edition; McGraw-Hill: New York, 1966; pp. 432-434, 529-530.

68. Lowry, T.H.; Richardson, K.S. "Mechanism and Theory in Organic Chemistry"; Harper and Row: New York, 1976; pp. 85-88.

69. Weast, R.C. "Handbook of Chemistry and Physics"; 54th Edition: CRC Press: Cleveland, Ohio, 1973.

70. Babai-Pirouz, M. M.Sc. Thesis University of Texas at Austin, Austin, TX, 1983.

71. Pageau, L.; Sourirajan, S. J. Appl. Polymer Sci. 1972, 16, 3185-3206.

72. Dickson, J.M.; Babai-Pirouz, M.; Lloyd, D.R. Operating Manual for a Reverse Osmosis Radial Flow Test Cell System University of Texas at Austin, Austin, TX, 1981.

73. Kunst, B.; Sourirajan, S. J. Appl. Polymer Sci. 1970, 14, 2559-2568.

74. Draper, N.R.; Smith, H. "Applied Regression Analysis"; J. Wiley and Sons: New York; 1966.

75. International Mathematics and Statistics Library (ISML), Reference Manual, Houston, TX (1982).

76. Levenberg, K. Quart. Appl. Math. 1944, 2, 164-168.

77. Marquardt, D.W. J. SIAM 1963, 11, 431-441.

78. Lasdon, L.S. "Generalized Reduced Gradient Software for Linearly and Nonlinearly Constrained Problems", Working Paper 77-85, Graduate School of Business, University of Texas at Austin, Austin, Texas 78712. Proceedings NATO advanced study institute on "Design and Implementation of Optimization Software", Sijthoff and Noordhoff, Publishers (197).

79. Lasdon, L.S.; Waren, A.D.; Jain, A.; Ratner, M. ACM Transactions on Mathematical Software 1978, 4, 34-50.

80. Paul, D.R. Sep. and Purif. Methods 1976, 5, 33-50.

81. Matsuura, T.; Sourirajan, S. Ind. Eng. Chem. Process Des. Dev. 1978, 17, 419-428.

82. Glueckauf, E. Proceedings, First International Symposium on Water Desalination Washington, D.C. 1965, published by the Office of Saline Water 1, 143-156.

83. Morris, J.L. "Computerized Methods in Elementary Numerical Analysis"; John Wiley and Sons: New York, 1983; pp. 388-400.

84. Stark, P.A. "Introduction to Numerical Methods"; MacMillan: London, 1970; pp. 194-202.

85. Matsuura, T. Personal Communication, 1981.

86. Tone, S.; Demiya, M.; Shinohara, K.; Otake, T., J. Memb. Sci. 1984, 17, 275-288.

87. Tone, S.; Shinohara, K.; Igarashi, Y.; Otake, T., J. Memb. Sci. 1984, 19, 195-208.

88. Lloyd, D.R., Ed., "Material Science of Synthetic Membranes"; ACS Symposium Series No. 269: Washington, D.C., 1985.

89. Staverman, A.J. J. Memb. Sci. 1983, 16, 7-20.

90. Babai-Pirouz, M.; Thiel, S.W.; Lloyd, D.R.; Dickson, J.M. J. Memb. Sci. 1984, 21, 21-33.

91. Thiel, S.W.; Lloyd, D.R.; Dickson, J.M., In "Reverse Osmosis and Ultrafiltration", Sourirajan, S., Ed.; ACS Symposium Series, in press.

92. Thiel, S.W.; Lloyd, D.R.; Dickson, J.M., In "Reverse Osmosis and Ultrafiltration", Sourirajan, S., Ed.; ACS Symposium Series, in press.

The vita has been removed from the scanned document